

IMAGE LICENSED BY INGRAM PUBLISHING

# Retrospective Cost Adaptive Control

## POLE PLACEMENT, FREQUENCY RESPONSE, AND CONNECTIONS WITH LQG CONTROL

YOUSAF RAHMAN, ANTAI XIE, and DENNIS S. BERNSTEIN

**A**vast range of technological systems—from aerospace vehicles to chemical processes to Segways—depend on feedback control. These applications typically rely on a combination of classical and modern control techniques, logic for mode switching, and diagnostics for fault detection to ensure safety and reliability, all of

which are validated and verified through simulation and testing. A feedback control system is the quintessential cyber-physical system, in which real-time digital computing elements interact bidirectionally with the full complexity of the real world through noisy transducers and limited communication channels [1]. In many applications, the control system is crucial to safe operation, and the potential benefits of new ideas and techniques for feedback control must be weighed against the risk of unanticipated response and/or failure.

*Digital Object Identifier 10.1109/MCS.2017.2718825*  
*Date of publication: 18 September 2017*

A successful application of feedback control depends first and foremost on the availability of reliable and affordable sensors and actuators that can monitor the response of the plant and modify its behavior. An autopilot for an aircraft is a classical example, where inertial and noninertial sensors provide measurements of position, velocity, attitude, and angular rates, while thrust and aerodynamic surfaces provide forces and moments. In other applications, such as controlled combustion [2], flow control [3]–[5], and controlled fusion [6], the development of sensing and actuation strategies presents a challenge. Control research is typically concerned with applications for which effective sensing and actuation technologies are available, and the goal is to use this technology reliably and efficiently to achieve stabilization, command following, and disturbance rejection.

Despite these successes, many applications of feedback control remain beyond the reach of modern tools and techniques. These applications may be highly undersensed and underactuated relative to the order of their significant dynamics; they may be difficult to model due to complex, unknown, or unpredictably changing physics; and they may require reliable high-performance control systems that must be engineered within tight deadlines and budgets. Adaptive control offers a viable approach to these applications.

The underlying motivation for research in adaptive control is to develop control algorithms that can accommodate sensor and actuator limitations; respect communication constraints; account for complex, uncertain, and unpredictably changing dynamics; and operate robustly in the presence of noise and reliably in the event of sensor/actuator failure. The promise of adaptive control is the ability to account for all of these effects with minimal prior modeling, tuning, and analysis for applications that are beyond the reach of fixed-gain and fixed-logic model-based control laws.

Adaptive control is different from robust control, which also accounts for uncertainty. In particular, robust control views uncertainty as static and seeks to trade performance for robustness to the assumed level of uncertainty. In contrast, adaptive control strives to learn about the plant during operation, either explicitly or implicitly, to overcome prior uncertainty. Consequently, by tuning itself to the actual plant, an adaptive controller transcends the performance/robustness tradeoff of robust control. To illustrate this point, consider a plant subject to a harmonic disturbance whose frequency is  $\omega$ . If  $\omega$  is known, then a stabilizing controller based on the internal model principle can be used to apply infinite gain at the disturbance frequency to asymptotically reject the disturbance. If, however,  $\omega$  is unknown, then a robust controller must apply high but finite gain across a bandwidth of possible disturbance frequencies, thus sacrificing asymptotic disturbance rejection and unnecessarily amplifying sensor noise. In contrast, an adaptive controller can tune itself to the actual disturbance frequency and thereby asymptotically reject the disturbance. The same principle applies to the case of a plant with a lightly damped mode subject

to broadband disturbances. If the modal frequency is uncertain, then the  $H_\infty$  distance between possible plants is large. Consequently, a robust controller based on an  $H_\infty$  uncertainty metric must account for a large set of uncertain plants. In contrast, an adaptive controller can tune itself to the actual modal frequency.

Plants that are inherently difficult to control due to achievability constraints on closed-loop performance [7] pose a potentially severe challenge to adaptive control, as articulated in [8]:

Control engineers grounded in classical control know it is possible to formulate control design problems which in practical terms are not possible to solve. An inverted pendulum with more than two rods is a well-known example; again, a plant with nonminimum phase zeros well inside the passband and unstable poles may be near impossible to control, unless additional inputs or outputs are used; another famous example was provided in [9] and so on. When the plant is initially known, as well as the control objective, it will generally become clear at some point in the design process, if not *ab initio*, that the control objective is impractical.

Now what happens in adaptive control? The catch is that a full description of the plant is lacking. There may be no way to decide on the basis of the a priori information that the projected design task is or is not practical. So what will happen if an adaptive control algorithm is run in such a case? At the least, the algorithm will not converge. At worst, an unstable closed loop will be established.

This article focuses on retrospective cost adaptive control (RCAC), which is a direct, discrete-time adaptive control technique for stabilization, command following, and disturbance rejection. As a discrete-time approach, RCAC is motivated by the desire to implement control algorithms that operate at a fixed measurement sampling rate without the need for controller discretization. This discretization also means that the required modeling information can be estimated based on data sampled at the same rate as the control update. Adaptive control algorithms for continuous-time plants are developed in [10]–[18] and for discrete-time plants in [19]–[30], and the ability to handle plants with nonminimum-phase (NMP) zeros, that is, zeros outside of the open unit disk, is demonstrated in [20]–[23].

RCAC was motivated by the concept of retrospectively optimized control, where past controller coefficients used to generate past control inputs are reoptimized in the sense that, if the reoptimized coefficients had been used over a previous window of operation, then the performance would have been better. However, unlike signal processing applications such as estimation and identification, it is impossible to change past control inputs, and thus the reoptimized controller coefficients are used only to generate the next control input. Since RCAC depends heavily on

data for the controller update, this technique is similar to data-driven control [31]–[36].

RCAC was originally developed within the context of active noise-control experiments [37]. The algorithm used in [37] is gradient based, where the direction and step size are derived from different cost functions. In subsequent work [38], the gradient algorithm was replaced by batch least-squares optimization. In both [37] and [38], the modeling information is given by Markov parameters (impulse-response coefficients) of the open-loop transfer function  $G_{zu}$  from the control input  $u$  to the performance variable  $z$ . More recently, in [39], a recursive least-squares (RLS) algorithm is used along with knowledge of the NMP zeros of  $G_{zu}$ . The approaches in [37]–[39] are closely related in the sense that all of the NMP zeros outside of the spectral radius of  $G_{zu}$  are approximate roots of a polynomial whose coefficients are Markov parameters of  $G_{zu}$ ; this polynomial is the numerator of a truncated Laurent expansion of  $G_{zu}$  about infinity. The truncated Laurent expansion serves as the transfer function  $G_f$  that defines the retrospective cost by filtering the difference between the actual past control inputs and the reoptimized control inputs. A key contribution of this article is to show that  $G_f$  serves as a target model for a specific closed-loop transfer function, as explained below. To construct  $G_f$ , Markov parameters are used in [37] and [38], and NMP zeros are used in [39].

RCAC is applied to Rohrs’s counterexamples [40] in [41], broadband disturbance rejection in [42], decentralized control in [43], sampled-data plants with aliasing in [44], multi-input, multi-output (MIMO) plants in [45], and Hammerstein plants in [46]–[48]. Numerical simulation studies are given in [49] and [50] for flow control; in [51] for noncolocated control of a linkage; in [42], [43], [52], and [53] for vibration control; in [54] for engine control; in [55]–[59] for aircraft control; in [60] for spacecraft control; in [61] for quadrotor control; in [62] for missile control; in [63] for scramjet control; and in [48], [64], and [65] for control of plants with hysteresis and hysteretic friction. Laboratory experiments are reported in [37], [66], and [67] for noise control; in [68] for control of a ducted flame; and in [69] for control of a six-degree-of-freedom shaker table.

This article has several objectives. The first objective is to present the RCAC algorithm in sufficient detail that readers can grasp all of the key steps. This version of the algorithm is based on RLS optimization. The algorithm is presented within the context of the adaptive standard problem, which includes command-following and disturbance-rejection problems with and without feedforward control as special cases; several of these problems are presented as special cases of the adaptive servo problem. The adaptive standard problem and the adaptive servo problem are stated for vector signals, and thus the RCAC algorithm is fully MIMO.

The next contribution of this article concerns the modeling data used by RCAC as incorporated in  $G_f$ . In particular, it is shown that  $G_f$  serves as a target model for a closed-loop

transfer function  $\tilde{G}_{z\tilde{u},k}$  whose zeros include the zeros of  $G_{zu}$ . The special closed-loop transfer function  $\tilde{G}_{z\tilde{u},k}$  arises from the way in which RCAC updates the controller coefficients. This controller update can be interpreted as a virtual external control perturbation  $\tilde{u}$  that is injected internally to the control update, which is called *intercalated injection*.

Intercalated injection of the virtual external control perturbation  $\tilde{u}$  gives rise to the closed-loop transfer function  $\tilde{G}_{z\tilde{u},k}$ . At the same time, minimization of the retrospective cost updates the controller coefficients so as to fit  $\tilde{G}_{z\tilde{u},k}$  to the target model  $G_f$ . With this insight, it immediately becomes clear why RCAC requires knowledge of the NMP zeros of  $G_{zu}$ . Specifically, if an NMP zero of  $G_{zu}$  is *not* included in  $G_f$ , then RCAC cancels the zero through feedback to match  $\tilde{G}_{z\tilde{u},k}$  to  $G_f$ . Although the RCAC algorithm is presented in the fully MIMO case, the construction of  $G_f$  in the present article is confined to the case where the control input and performance variable are scalar signals.

Since RCAC updates the controller so as to match  $\tilde{G}_{z\tilde{u},k}$  to the target model  $G_f$ , it is straightforward to use  $G_f$  to place the closed-loop poles, that is, for adaptive pole placement. Pole placement aside, RCAC also matches the frequency response of  $\tilde{G}_{z\tilde{u},k}$  to the frequency response of  $G_f$ . What is, perhaps, more surprising is that, if  $G_f$  is chosen to be a finite impulse response (FIR) target model and the controller order is chosen to be sufficiently large, then RCAC yields a controller whose closed-loop frequency response matches the frequency response of the closed-loop system given by high-authority linear-quadratic-Gaussian (LQG) synthesis, that is, LQG with zero control weighting and zero measurement-noise covariance. This connection is surprising because LQG uses a complete and exact plant model, whereas RCAC uses extremely limited modeling information.

In addition to presenting a self-contained description of the RCAC algorithm, a further goal of this article is to illustrate RCAC and investigate the role of  $G_f$  through examples. These examples include plants with various types of stability (asymptotically stable, Lyapunov stable, and unstable), various types of control architectures [feedback, feedforward, model reference adaptive control (MRAC), and proportional-integral-derivative (PID)], various problem objectives (stabilization, command following, and disturbance rejection), and various types of exogenous signals, including step, ramp, and harmonic commands as well as step, ramp, harmonic, and stochastic sensor noise and disturbances. In addition, RCAC is applied to linear plants with magnitude and rate control saturation and tested on nonlinear oscillators. Many of these examples go beyond the theory presented in [39], which is confined to feedback control of linear plants in the absence of sensor noise and with exogenous signals generated by Lyapunov-stable exogenous dynamics. Neither broadband disturbances nor saturation are considered in [39]. Consequently, these examples provide insight into the performance of RCAC in

situations that lie outside the current theory. To this end, for several examples, the problem data are varied to make the problems progressively more difficult until RCAC fails. These trends highlight the strengths and weaknesses of RCAC and provide guidelines for applications.

The contents of this article are as follows. The next section presents the standard and servo control problems, followed by a definition of the adaptive standard and servo problems. The RCAC algorithm is then presented with a discussion of the construction of the target model  $G_t$ , which incorporates the modeling information required by RCAC. Several examples of adaptive pole placement and adaptive control for harmonic commands and disturbances are then presented. Stochastic exogenous signals are also considered, and RCAC is compared to high-authority LQG. The final sections investigate the effect of sensor noise and modeling errors, in particular, erroneous and unmodeled NMP zeros, erroneous relative degree, unmodeled time delay, and erroneous plant gain.

## STANDARD PROBLEM

Consider the standard problem consisting of the discrete-time, linear, time-invariant plant

$$x(k+1) = Ax(k) + Bu(k) + D_1w(k), \quad (1)$$

$$y(k) = Cx(k) + D_0u(k) + D_2w(k), \quad (2)$$

$$z(k) = E_1x(k) + E_2u(k) + E_0w(k), \quad (3)$$

where  $x(k) \in \mathbb{R}^n$  is the state,  $y(k) \in \mathbb{R}^{l_y}$  is the measurement,  $u(k) \in \mathbb{R}^{l_u}$  is the control input,  $w(k) \in \mathbb{R}^{l_w}$  is the exogenous input, and  $z(k) \in \mathbb{R}^{l_z}$  is the performance variable. The plant (1)–(3) may represent a continuous-time, linear time-invariant plant sampled at a fixed rate. The goal is to develop a feedback or feedforward controller that operates on  $y$  to minimize  $z$  in the presence of the exogenous signal  $w$ . The components of  $w$  can represent either a command signal  $r$  to be followed, an external disturbance  $d$  to be rejected, and/or sensor noise  $v$  that corrupts the measurement as determined by the choice of  $D_1$ ,  $D_2$ , and  $E_0$ . Depending on the application, components of  $w$  may or may not be measured, and, for feedforward control, the measured components of  $w$  can be included in  $y$  by suitable choice of  $C$  and  $D_2$ . For fixed-gain control,  $z$  need not be measured. For adaptive control, however,  $z$  is assumed to be measured.

Using the forward-shift operator  $\mathbf{q}$ , (1)–(3) can be rewritten as

$$z(k) = G_{zw}(\mathbf{q})w(k) + G_{zu}(\mathbf{q})u(k), \quad (4)$$

$$y(k) = G_{yw}(\mathbf{q})w(k) + G_{yu}(\mathbf{q})u(k), \quad (5)$$

where

$$G_{zw}(\mathbf{q}) \triangleq E_1(\mathbf{q}I - A)^{-1}D_1 + E_0, \quad (6)$$

$$G_{zu}(\mathbf{q}) \triangleq E_1(\mathbf{q}I - A)^{-1}B + E_2, \quad (7)$$

$$\begin{aligned} G_{yw}(\mathbf{q}) &\triangleq C(\mathbf{q}I - A)^{-1}D_1 + D_2, \\ G_{yu}(\mathbf{q}) &\triangleq C(\mathbf{q}I - A)^{-1}B + D_0. \end{aligned} \quad (8)$$

Furthermore, the discrete-time, linear, time-invariant controller has the form

$$u(k) = G_c(\mathbf{q})y(k). \quad (9)$$

Note that  $\mathbf{q}$  is a time-domain operator that accounts for initial conditions, and, although (6) and (7) are written as transfer functions, these expressions are convenient representations of time-domain dynamics. For pole-zero analysis,  $\mathbf{q}$  can be replaced by the Z-transform complex variable  $z$ , in which case (4), (5), and (8) do not account for the initial conditions. Figures 1 and 2 illustrate (4)–(8).

The closed-loop transfer function from the exogenous signal  $w$  to the performance variable  $z$  is

$$\tilde{G}_{zw} \triangleq G_{zw} + G_{zu}G_c(I - G_{yu}G_c)^{-1}G_{yw}. \quad (9)$$

The poles of  $\tilde{G}_{zw}$  are referred to as the closed-loop poles, and the transmission zeros of  $\tilde{G}_{zw}$  are the closed-loop zeros. In the case where  $y$ ,  $z$ ,  $u$ , and  $w$  are scalar signals, (6), (7), and (9) can be written as

$$G_{zw} = \frac{N_{zw}}{D}, \quad G_{zu} = \frac{N_{zu}}{D}, \quad G_{yw} = \frac{N_{yw}}{D}, \quad G_{yu} = \frac{N_{yu}}{D}, \quad (10)$$

$$\tilde{G}_{zw} = \frac{\tilde{N}_{zw}}{\tilde{D}_{zw}} = \frac{N_{zu}N_{yw}N_c + N_{zw}(DD_c - N_{yu}N_c)}{D(DD_c - N_{yu}N_c)}, \quad (11)$$

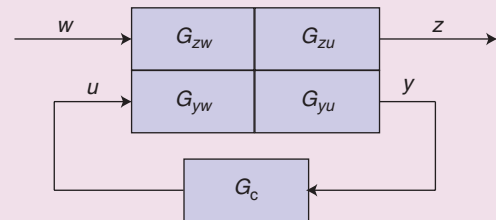


FIGURE 1 A block diagram representation of the standard problem with the controller  $G_c$ .

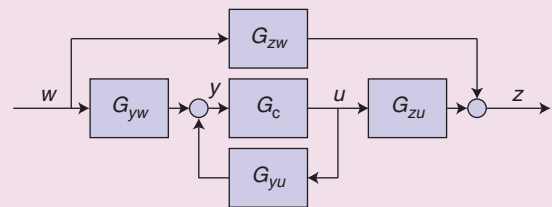


FIGURE 2 An equivalent block diagram representation of the standard problem with the controller  $G_c$ .

**This article focuses on retrospective cost adaptive control, which is a direct, discrete-time, adaptive control technique for stabilization, command following, and disturbance rejection.**

where

$$G_c = \frac{N_c}{D_c}. \quad (12)$$

It is assumed that  $D$  and  $D_c$  are monic. In the case where  $y = z$ , that is,  $C = E_1$ ,  $D_0 = E_2$ , and  $D_2 = E_0$ , (10) and (11) can be written as

$$G_{zw} = G_{yw} = \frac{N_w}{D}, \quad G_{zu} = G_{yu} = \frac{N_u}{D}, \quad \tilde{G}_{zw} = \frac{N_w D_c}{D D_c - N_u N_c}. \quad (13)$$

In the case where  $w$  is matched with  $u$ , that is,  $B = D_1$ ,  $E_0 = E_2$ , and  $D_0 = D_2$ , (10) and (11) can be written as

$$G_{zw} = G_{zu} = \frac{N_z}{D}, \quad G_{yw} = G_{yu} = \frac{N_y}{D}, \quad \tilde{G}_{zw} = \frac{N_z D_c}{D D_c - N_y N_c}. \quad (14)$$

In the case where  $y = z$  and  $w$  is matched with  $u$ , (10) and (11) can be written as

$$G \triangleq G_{zw} = G_{yw} = G_{zu} = G_{yu} = \frac{N}{D}, \quad \tilde{G}_{zw} = \frac{N D_c}{D D_c - N N_c}. \quad (15)$$

For examples where  $y = z$  and  $w$  is matched with  $u$ ,  $G$  is used to define the plant (1)–(3); otherwise, the state-space representation is used.

### SERVO PROBLEM

As a special case of the standard problem, consider the discrete-time, linear, time-invariant plant

$$x(k+1) = Ax(k) + Bu(k) + \bar{D}_1 d(k), \quad (16)$$

$$y_0(k) = \bar{C}x(k) + \bar{D}_0 u(k), \quad (17)$$

$$y_n(k) = y_0(k) + v(k), \quad (18)$$

$$e_0(k) = r(k) - y_0(k), \quad (19)$$

$$e_n(k) = r(k) - y_n(k), \quad (20)$$

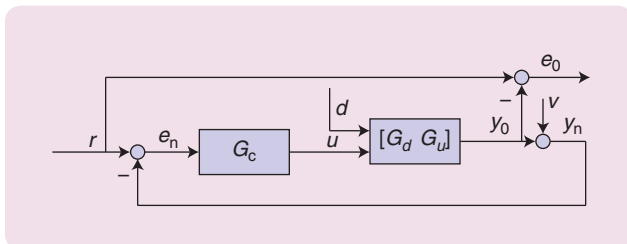


**FIGURE 3** A block diagram representation of the servo problem.  $e_n$  is the measured error, and  $e_0$  is the true error.

where  $x(k) \in \mathbb{R}^n$  is the state,  $y_n(k) \in \mathbb{R}^{l_y}$  is the measurement,  $u(k) \in \mathbb{R}^{l_u}$  is the control input,  $d(k) \in \mathbb{R}^{l_d}$  is the disturbance,  $r(k) \in \mathbb{R}^{l_y}$  is the command,  $v(k) \in \mathbb{R}^{l_y}$  is the sensor noise, and  $e_n(k) \in \mathbb{R}^{l_y}$  is the performance variable. Equation (17) can be rewritten in terms of  $\mathbf{q}$  as

$$y_0(k) = G_u(\mathbf{q})u(k) + G_d(\mathbf{q})d(k), \quad (21)$$

where

$$G_u(\mathbf{q}) \triangleq \bar{C}(\mathbf{q}I - A)^{-1}B + \bar{D}_0, \quad G_d(\mathbf{q}) \triangleq \bar{C}(\mathbf{q}I - A)^{-1}\bar{D}_1. \quad (22)$$

Furthermore, the linear, time-invariant controller has the form

$$u(k) = G_c(\mathbf{q})e_n(k). \quad (23)$$

The measured error signal  $e_n$  is the difference between the command  $r$  and the measurement  $y_n$ , which may be corrupted by noise. Since only the measured error is available for feedback,  $e_n$  serves as the performance variable within RCAC. However, the true error signal  $e_0$ , which is the difference between the command  $r$  and the plant output  $y_0$ , provides a true measure of the command-following performance. Since this signal is not available for feedback, it is used only as a diagnostic. If, however, the sensor noise  $v$  is absent, then  $e_n$  and  $e_0$  are identical. Figure 3 illustrates (21)–(23). The servo problem is a special case of the standard problem with

$$w = \begin{bmatrix} r \\ d \\ v \end{bmatrix}, \quad y = e_n, \quad z = e_n, \quad (24)$$

and

$$D_1 = [0 \quad \bar{D}_1 \quad 0], \quad C = E_1 = -\bar{C}, \quad D_0 = E_2 = -\bar{D}_0, \quad (25)$$

$$D_2 = [I_{l_y} \quad 0 \quad -I_{l_y}], \quad E_0 = [I_{l_y} \quad 0 \quad 0], \quad (26)$$

$$G_{zw} = [I_{l_y} \quad -G_d \quad 0], \quad G_{zu} = -G_u, \quad (27)$$

$$G_{yw} = [I_{l_y} \quad -G_d \quad -I_{l_y}], \quad G_{yu} = -G_u. \quad (28)$$

In the case where  $d$  and  $u$  are collocated, it follows that  $\bar{D}_1 = B$  and  $\bar{D}_0 = 0$ , and thus  $G_d = G_u$ . In this case, define  $\hat{G} \triangleq G_d = G_u$ . However,  $w$  is not necessarily matched with  $u$ . Moreover, if  $r = v = 0$  and  $d$  and  $u$  are collocated, then  $w$  is matched with  $u$ . For examples where  $d$  and  $u$  are

colocated,  $G$  is used to define the plant (16)–(20); otherwise, the state-space representation is used.

## RETROSPECTIVE COST ADAPTIVE CONTROL ALGORITHM

### Adaptive Standard and Servo Problems

Figure 4 shows the adaptive standard problem, which is the standard problem with an adaptive controller, while Figure 5 shows the adaptive servo problem, which is the servo problem with an adaptive controller. Note that, for the adaptive servo problem, it is desirable to minimize the true error  $e_0$ . However, since  $e_0$  is not available, RCAC minimizes the measured error  $e_n$ , which may be corrupted by noise, as shown in Figure 3. For the adaptive standard problem,  $z = e_n$ .

### Controller Structure

Define the dynamic compensator

$$u(k) = \sum_{i=1}^{n_c} P_i(k)u(k-i) + \sum_{i=k_c}^{n_c} Q_i(k)y(k-i), \quad (29)$$

where  $P_i(k) \in \mathbb{R}^{l_u \times l_u}$  and  $Q_i(k) \in \mathbb{R}^{l_u \times l_y}$  are the controller coefficient matrices and  $k_c \geq 0$ . For controller startup, (29) is implemented as

$$u(k) = \begin{cases} 0, & k < k_w, \\ \Phi(k)\theta(k), & k \geq k_w, \end{cases} \quad (30)$$

where the regressor matrix  $\Phi(k)$  is

$$\Phi(k) \triangleq \begin{bmatrix} u(k-1) \\ \vdots \\ u(k-n_c) \\ y(k-k_c) \\ \vdots \\ y(k-n_c) \end{bmatrix}^T \otimes I_{l_u} \in \mathbb{R}^{l_u \times l_\theta}, \quad (31)$$

where  $k_w \geq n_c$  is an initial waiting period during which  $\Phi(k)$  is populated with data. The controller coefficient vector  $\theta(k)$  is

$$\theta(k) \triangleq \text{vec}[P_1(k) \ \cdots \ P_{n_c}(k) \ Q_{k_c}(k) \ \cdots \ Q_{n_c}(k)]^T \in \mathbb{R}^{l_\theta}, \quad (32)$$

where  $l_\theta \triangleq l_u^2 n_c + l_u l_y (n_c + 1 - k_c)$ , “ $\otimes$ ” is the Kronecker product, and “ $\text{vec}$ ” is the column-stacking operator. Note that  $k_c = 0$  allows an exactly proper controller, whereas  $k_c \geq 1$  yields a strictly proper controller of relative degree of at least  $k_c$ . All examples in this article use  $k_c = 1$ , and, unless specified otherwise,  $k_w = n_c$ . In terms of  $\mathbf{q}$ , the time-domain transfer function of the controller from  $y$  to  $u$  is given by

$$G_{c,k}(\mathbf{q}) = (I_{l_u} \mathbf{q}^{n_c} - P_1(k) \mathbf{q}^{n_c-1} - \cdots - P_{n_c}(k))^{-1} \cdot (Q_{k_c}(k) \mathbf{q}^{n_c-k_c} + \cdots + Q_{n_c}(k)). \quad (33)$$

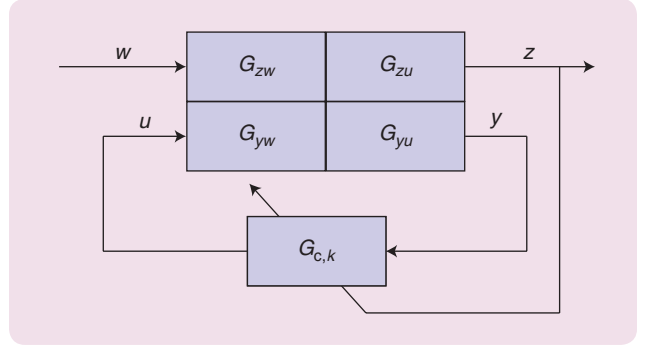


FIGURE 4 A block diagram representation of the adaptive standard problem with the adaptive controller  $G_{c,k}$ .

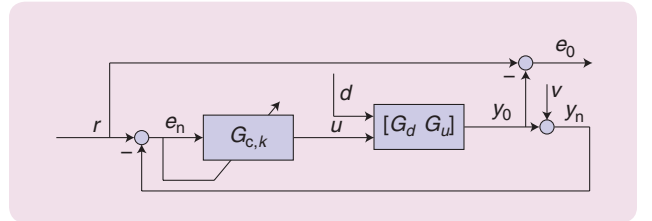


FIGURE 5 A block diagram representation of the adaptive servo problem with the adaptive controller  $G_{c,k}$ .

Note that the coefficients of  $G_{c,k}$  are given by the components of  $\theta(k)$ , which are time dependent, and thus  $G_{c,k}$  is a linear, time-varying controller. Also, note that (33) is expressed in terms of the forward-shift operator  $\mathbf{q}$  rather than the Z-transform variable  $\mathbf{z}$ . Consequently, although (33) is written as a transfer function, this expression is merely a convenient representation of the time-domain operator represented by (29). If  $y$  and  $u$  are scalar signals, then  $G_{c,k}$  is single-input, single-output (SISO), and (33) can be written as

$$G_{c,k}(\mathbf{q}) = \frac{Q_{k_c}(k) \mathbf{q}^{n_c-k_c} + \cdots + Q_{n_c}(k)}{\mathbf{q}^{n_c} - P_1(k) \mathbf{q}^{n_c-1} - \cdots - P_{n_c}(k)}. \quad (34)$$

Note that (33) is an infinite impulse response (IIR) controller. By removing  $u(k-1), \dots, u(k-n_c)$  from (29) and  $\Phi(k)$ , and by modifying the structure of  $\theta$ , an FIR controller structure can be enforced, where

$$u(k) = \sum_{i=k_c}^{n_c} Q_i(k)y(k-i). \quad (35)$$

In this case, (33) becomes

$$G_{c,k}(\mathbf{q}) = \frac{1}{\mathbf{q}^{n_c}} [Q_{k_c}(k) \mathbf{q}^{n_c-k_c} + \cdots + Q_{n_c}(k)]. \quad (36)$$

### Retrospective Performance Variable

The retrospective performance variable is defined as

$$\hat{z}(k, \hat{\theta}) \triangleq z(k) + G_r(\mathbf{q})[\Phi(k)\hat{\theta} - u(k)], \quad (37)$$

where  $\hat{\theta} \in \mathbb{R}^{l_\theta}$  and  $G_f$  is an  $n_z \times n_u$  filter specified below. The rationale underlying (37) is to replace the control  $u(k)$  with  $\Phi(k)\hat{\theta}^*$ , where  $\hat{\theta}^*$  is the retrospectively optimized controller coefficient vector obtained by optimization below. The updated controller thus has the coefficients  $\theta(k+1) = \hat{\theta}^*$ . Consequently, the implemented control at step  $k+1$  is given by

$$u(k+1) = \Phi(k+1)\theta(k+1). \quad (38)$$

The filter  $G_f$  is constructed in the ‘‘Virtual External Control Perturbation and Target Model  $G_f$ ’’ section based on the required modeling information. This filter has the form

$$G_f \triangleq D_f^{-1}N_f, \quad (39)$$

where  $D_f$  is an  $l_z \times l_z$  polynomial matrix with leading coefficient  $I_{l_z}$ , and  $N_f$  is an  $l_z \times l_u$  polynomial matrix.  $G_f$  is referred to as the *target model* for reasons given below. By defining the filtered versions  $\Phi_f(k) \in \mathbb{R}^{l_z \times l_\theta}$  and  $u_f(k) \in \mathbb{R}^{l_z}$  of  $\Phi(k)$  and  $u(k)$ , respectively, (37) can be written as

$$\hat{z}(k, \hat{\theta}) = z(k) + \Phi_f(k)\hat{\theta} - u_f(k), \quad (40)$$

where

$$\Phi_f(k) \triangleq G_f(\mathbf{q})\Phi(k), \quad u_f(k) \triangleq G_f(\mathbf{q})u(k). \quad (41)$$

Note that implementation requires  $k_w \geq \max(n_c, n_i)$ , where  $n_i$  is the McMillan degree of  $G_f$ .

### Retrospective Cost

Using the retrospective performance variable  $\hat{z}(k, \hat{\theta})$  defined by (37), the cumulative retrospective cost function is defined as

$$J(k, \hat{\theta}) \triangleq \sum_{i=1}^k \lambda^{k-i} [z^T(i, \hat{\theta})R_z(i)\hat{z}(i, \hat{\theta}) + (\Phi_f(i)\hat{\theta})^T R_u(i)\Phi_f(i)\hat{\theta}] + \lambda^k (\hat{\theta} - \theta(0))^T R_\theta (\hat{\theta} - \theta(0)), \quad (42)$$

where  $\lambda \in (0, 1]$  is the forgetting factor,  $R_\theta \in \mathbb{R}^{l_\theta \times l_\theta}$  is positive definite, and, for all  $i \geq 1$ ,  $R_z(i) \in \mathbb{R}^{l_z \times l_z}$  is positive definite and  $R_u(i) \in \mathbb{R}^{l_z \times l_z}$  is positive semidefinite. The performance-variable and control-input weighting matrices  $R_z(i)$  and  $R_u(i)$  are time dependent and thus may depend on present and past values of  $y, z$ , and  $u$ . For example, choosing  $R_u(i)$  to be a function of  $z(i)^T z(i)$  can help prevent unstable pole-zero cancellation in the case of unmodeled NMP zeros [70]. The recursive minimization of (42) is used to update the controller coefficient vector  $\hat{\theta}$ . The following result uses recursive least squares to obtain the minimizer of (42).

### Proposition

Let  $P(0) = R_\theta^{-1}$ , and, for all  $k \geq 1$ , let  $\hat{\theta}^*$  be the unique global minimizer of the retrospective cost function (42). Then,  $\hat{\theta}^*$  is given by

$$\hat{\theta}^* = \theta(k) - P(k)\Phi_f^T(k)\Upsilon^{-1}(k) \cdot [\Phi_f(k)\theta(k) + (R_z(k) + R_u(k))^{-1}R_z(k)(z(k) - u_f(k))], \quad (43)$$

where

$$P(k+1) = \frac{1}{\lambda}P(k) - \frac{1}{\lambda}P(k)\Phi_f^T(k)\Upsilon^{-1}(k)\Phi_f(k)P(k) \quad (44)$$

and

$$\Upsilon(k) \triangleq \lambda[R_z(k) + R_u(k)]^{-1} + \Phi_f(k)P(k)\Phi_f^T(k). \quad (45)$$

Setting  $\theta(k+1) = \hat{\theta}^*$ , (43) yields the recursive controller-coefficient update equation

$$\theta(k+1) = \theta(k) - P(k)\Phi_f^T(k)\Upsilon^{-1}(k) \cdot [\Phi_f(k)\theta(k) + (R_z(k) + R_u(k))^{-1}R_z(k)(z(k) - u_f(k))]. \quad (46)$$

If  $\lambda = 1$ , then the covariance  $P(k)$  decreases monotonically, and thus the rate of adaptation decreases. To maintain adaptation in cases where the plant or exogenous signals are changing, the covariance can be reset using suitable logic. Alternatively, choosing the forgetting factor  $\lambda < 1$  prevents monotonic decrease of  $P(k)$  but can lead to instability in the presence of noise and in the absence of persistency [71], [72]. Yet another approach is to include an additional positive-semidefinite term  $Q(k)$  on the right-hand side of (44) of the form

$$P(k+1) = P(k) - P(k)\Phi_f^T(k)\Upsilon^{-1}(k)\Phi_f(k)P(k) + Q(k), \quad (47)$$

where  $\lambda = 1$  in (45). Note that (47) is the discrete-time Kalman predictor, Riccati error-covariance update equation with the dynamics matrix  $A = I_{l_\theta}$ , output matrix  $C(k) = \Phi_f(k)$ , process-noise covariance  $Q(k)$ , and sensor-noise covariance  $R(k) = [R_z(k) + R_u(k)]^{-1}$  [73]. Consequently, persistency in (47) is determined by the observability of the time-varying pair  $(I_{l_\theta}, \Phi_f)$ , and the corresponding state-estimate update is given by (43). An alternative is to use the discrete-time Kalman filter, Riccati error-covariance update equation

$$P(k+1) = P(k) - P(k)\Phi_f^T(k+1)\Upsilon^{-1}(k)\Phi_f(k+1)P(k) + Q(k), \quad (48)$$

where the corresponding state-estimate update is

$$\theta(k+1) = \theta(k) - P(k)\Phi_f^T(k+1)\Upsilon^{-1}(k+1) \cdot [\Phi_f(k+1)\theta(k) + (R_z(k) + R_u(k))^{-1} \cdot R_z(k)(z(k+1) - u_f(k+1))]. \quad (49)$$

Note that, in (49), the estimate  $\theta(k+1)$  depends on  $z(k+1)$ . Therefore, implementation of (49) requires instantaneous update of the controller coefficient vector.

In contrast, in (46),  $\theta(k+1)$  depends on  $z(k)$ , and thus (46) is implementable.

In practice,  $\theta(0)$  can be chosen based on an initial design, if one is available. However, for all examples in this article, the initialization  $\theta(0) = 0$  is used to reflect the absence of additional prior modeling information. Furthermore, for all  $i \geq 1$ ,  $R_z(i) = I_{L_z}$ . Note that RCAC can use batch least-squares optimization instead of recursive minimization.

## VIRTUAL EXTERNAL CONTROL PERTURBATION AND TARGET MODEL $G_f$

The target model  $G_f$  is a key feature of RCAC. In [38],  $G_f$  is viewed as a model of  $G_{zu}$  that captures the sign of the leading coefficient of  $N_{zu}$  along with the NMP zeros of  $G_{zu}$ . In [39], the analysis of RCAC involves an ideal filter  $\tilde{G}_f$ , which is a closed-loop transfer function involving an ideal feedback controller  $\tilde{G}_c$ . These insights lead to an alternative interpretation of  $G_f$  as a target model for a specific closed-loop transfer function, as demonstrated below.

Using (30), the retrospective performance variable (37) can be written as

$$\hat{z}(k, \hat{\theta}) = z(k) - G_f(\mathbf{q})[u(k) - \Phi(k)\hat{\theta}]. \quad (50)$$

It can be seen from (50) that minimizing the cumulative retrospective cost function (42) determines the controller coefficient vector  $\hat{\theta}$  that best fits  $G_f(\mathbf{q})[u(k) - \Phi(k)\hat{\theta}]$  to the performance data  $z(k)$ . In terms of the optimal controller coefficient vector  $\hat{\theta}^*$ , (50) can be written as

$$\hat{z}(k, \hat{\theta}^*) = z(k) - G_f(\mathbf{q})[u(k) - \Phi(k)\hat{\theta}^*]. \quad (51)$$

For convenience, define

$$u^*(k) \triangleq \Phi(k)\hat{\theta}^*, \quad (52)$$

$$\tilde{u}(k) \triangleq u(k) - u^*(k), \quad (53)$$

so that

$$u(k) = u^*(k) + \tilde{u}(k). \quad (54)$$

With this notation, (51) can be written as

$$\hat{z}(k, \hat{\theta}^*) = z(k) - G_f(\mathbf{q})\tilde{u}(k). \quad (55)$$

Using (54) to replace  $u$  in  $\Phi$  by  $u^* + \tilde{u}$ , it follows from (29)–(31) and (52) that  $u^*$  satisfies

$$u^*(k) = \sum_{i=1}^{n_c} P_i^* u^*(k-i) + \sum_{i=1}^{n_c} P_i^* \tilde{u}(k-i) + \sum_{i=k_c}^{n_c} Q_i^* y(k-i). \quad (56)$$

Note that the actual input to the plant at step  $k$  is  $u(k)$ , which, in (54), is written as the sum of the *pseudocontrol input*  $u^*(k)$  and the *virtual external control perturbation*  $\tilde{u}(k)$ . Although the signals  $u^*$  and  $\tilde{u}$  are not explicitly used by RCAC, it is now shown that they are crucial to understanding the role of  $G_f$ . From (56) it follows that

$$u^*(k) = D_c^{*-1}(\mathbf{q})[(\mathbf{q}^{n_c} I_u - D_c^*(\mathbf{q}))\tilde{u}(k) + N_c^*(\mathbf{q})y(k)], \quad (57)$$

where

$$D_c^*(\mathbf{q}) \triangleq \mathbf{q}^{n_c} I_u - \mathbf{q}^{n_c-1} P_1^* - \dots - P_{n_c}^* \quad (58)$$

$$N_c^*(\mathbf{q}) \triangleq \mathbf{q}^{n_c-k_c} Q_{k_c}^* + \dots + Q_{n_c}^* \quad (59)$$

$$G_c^* \triangleq D_c^{*-1} N_c^*. \quad (60)$$

The special closed-loop transfer function from  $\tilde{u}$  to  $z$  arises from the way in which RCAC updates the controller coefficients. This controller update can be interpreted as a virtual external control perturbation  $\tilde{u}$  that is injected internally to the control update, which is called *intercalated injection*. Figures 6 and 7 show the equivalent transfer function representations of (54) and (57) with  $\tilde{u}$  represented as an external input. Figure 6 illustrates the intercalated injection of  $\tilde{u}$  inside the control update.

It follows from (4), (5), (54), and (57) that

$$z(k) = G_{zw}(\mathbf{q})w(k) + G_{zu}(\mathbf{q}) \cdot [D_c^{*-1}(\mathbf{q})[(\mathbf{q}^{n_c} I_u - D_c^*(\mathbf{q}))\tilde{u}(k) + N_c^*(\mathbf{q})y(k)] + \tilde{u}(k)], \quad (61)$$

$$y(k) = G_{yw}(\mathbf{q})w(k) + G_{yu}(\mathbf{q}) \cdot [D_c^{*-1}(\mathbf{q})[(\mathbf{q}^{n_c} I_u - D_c^*(\mathbf{q}))\tilde{u}(k) + N_c^*(\mathbf{q})y(k)] + \tilde{u}(k)]. \quad (62)$$

Solving (62) for  $y(k)$  and substituting  $y(k)$  into (61) yields

$$z(k) = \tilde{G}_{zw}^*(\mathbf{q})w(k) + \tilde{G}_{zu}^*(\mathbf{q})\tilde{u}(k), \quad (63)$$

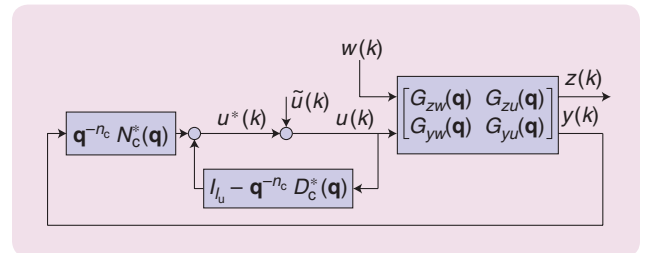


**FIGURE 6** A block diagram representation of (54) and (57) with the virtual external control perturbation  $\tilde{u}$  represented as an external input. The inner feedback loop, which represents (57), illustrates the intercalated injection of  $\tilde{u}$  inside the control update.

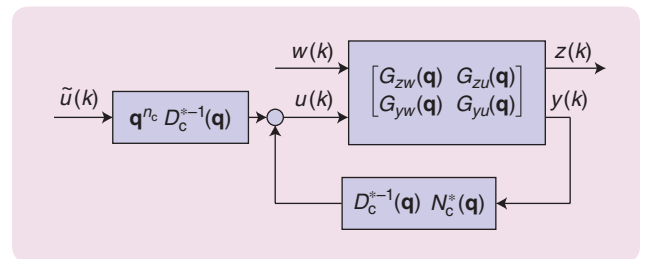


**FIGURE 7** An equivalent block diagram representation of (54) and (57) with  $\tilde{u}$  represented as an external input. In this representation, the inner feedback loop in Figure 6 is replaced by a prefilter.

where  $\tilde{G}_{zu}^*$  is given by (9) with  $G_c$  replaced by  $G_c^*$ , that is,

$$\tilde{G}_{zu}^* \triangleq G_{zu} + G_{zu} G_c^* (I - G_{yu} G_c^*)^{-1} G_{yw}, \quad (64)$$

and where

$$\tilde{G}_{zu}^*(\mathbf{q}) \triangleq \mathbf{q}^{n_c} G_{zu}(\mathbf{q}) [D_c^{*-1}(\mathbf{q}) + G_c^*(\mathbf{q}) \cdot [I_y - G_{yu}(\mathbf{q}) G_c^*(\mathbf{q})]^{-1} G_{yu}(\mathbf{q}) D_c^{*-1}(\mathbf{q})]. \quad (65)$$

Now assume that  $y$ ,  $z$ , and  $u$  are scalar signals. Using the notation in (10), (65) can be written as

$$\tilde{G}_{zu}^*(\mathbf{q}) = \frac{N_{zu}(\mathbf{q}) \mathbf{q}^{n_c}}{D(\mathbf{q}) D_c^*(\mathbf{q})} + \frac{N_{zu}(\mathbf{q}) N_c^*(\mathbf{q}) N_{yu}(\mathbf{q}) \mathbf{q}^{n_c}}{D(\mathbf{q}) D_c^*(\mathbf{q}) [D(\mathbf{q}) D_c^*(\mathbf{q}) - N_{yu}(\mathbf{q}) N_c^*(\mathbf{q})]} \quad (66)$$

$$= \frac{N_{zu}(\mathbf{q}) \mathbf{q}^{n_c}}{D(\mathbf{q}) D_c^*(\mathbf{q}) - N_{yu}(\mathbf{q}) N_c^*(\mathbf{q})}. \quad (67)$$

It can be seen from (55) that  $\hat{z}(k, \hat{\theta}^*) = z(k) - G_f(\mathbf{q}) \tilde{u}(k)$  is the residual of the fit between  $z$  and the output of the target model  $G_f$  with input  $\tilde{u}$ . However, (63) shows that  $\tilde{G}_{zu}^*$ , whose coefficients are given by  $\hat{\theta}^*$ , is the actual transfer function from  $\tilde{u}(k)$  to  $z(k)$ . Therefore, minimizing the retrospective cost function (42) yields the value  $\theta(k+1) = \hat{\theta}^*$  of  $\hat{\theta}$ , and thus the controller  $G_{c,k+1}$ , that provides the best fit of  $G_f$  by the transfer function  $\tilde{G}_{zu,k+1}$  from  $\tilde{u}$  to  $z$ . In other words, RCAC determines  $G_{c,k+1}$  so as to optimally fit  $\tilde{G}_{zu,k+1}$  to  $G_f$ .

The intercalated closed-loop transfer function  $\tilde{G}_{zu,k+1}$  is distinct from the closed-loop transfer function  $G_{zu,k}$  from an external control-input perturbation  $\tilde{u}$  to the performance variable  $z$ . In the case where  $y$ ,  $z$ , and  $u$  are scalar signals,  $G_{zu,k}$  is given by

$$G_{zu,k} = \frac{N_{zu} D_{c,k}}{D D_{c,k} - N_{yu} N_{c,k}}. \quad (68)$$

The difference between (67) and (68) is that the numerator of (67) has the fixed polynomial  $\mathbf{q}^{n_c}$  in place of the time-varying polynomial  $D_{c,k}$  in the numerator of (68). This distinction implies that the only NMP zeros in (67) are those arising from  $G_{zu}$ , unlike (68), which includes "time-varying" zeros arising from  $D_{c,k}$ .

## MODELING INFORMATION REQUIRED FOR $G_f$

This section specifies the modeling information required by RCAC. For the standard problem, this information includes the relative degree, the leading numerator coefficient, and all of the NMP zeros of  $G_{zu}$ . For the adaptive servo problem, it follows from (28) that this information is obtained from  $G_u = -G_{zu}$ . The discussion in this section is confined to the case where  $z$  and  $u$  are scalar signals. Note, however, that  $y$  may be a vector signal, and thus the controllers based on  $G_f$  as specified below may be multiple input, single output.

## Relative Degree

Since  $\tilde{G}_{zu,k+1}$  approximates  $G_f$ , it is advantageous to choose the relative degree of  $G_f$  to be equal to the relative degree of  $\tilde{G}_{zu,k+1}$ . It follows from (67) that the relative degree of  $\tilde{G}_{zu,k+1}$  is equal to the relative degree of  $G_{zu}$ . The relative degree of  $G_f$  is thus chosen to be equal to the relative degree of  $G_{zu}$ . This choice requires knowledge of the relative degree  $d_{zu}$  of  $G_{zu}$  [39].

## Nonminimum-Phase Zeros

In [39], the target model  $G_f$  is chosen such that the roots of  $N_f$  include the NMP zeros of  $G_{zu}$ . As can be seen from (67), a key feature of  $\tilde{G}_{zu,k+1}$  is the factor  $N_{zu}$  in its numerator. This means that, since RCAC adapts  $G_{c,k}$  so as to match  $\tilde{G}_{zu,k+1}$  to  $G_f$ , RCAC may cancel NMP zeros of  $G_{zu}$  that are not included in the roots of  $N_f$  to remove them from  $\tilde{G}_{zu,k+1}$ . This observation motivates the need to include all of the NMP zeros of  $G_{zu}$  in  $N_f$ . As an aside, Example PP1 shows that RCAC cancels all of the minimum-phase zeros of  $G_{zu}$  that are not included in the roots of  $N_f$  to remove them from  $\tilde{G}_{zu,k+1}$ .

## Markov Parameters

In [37] and [38],  $G_f$  is based on the Markov parameters of  $G_{zu}$ . In particular, for each complex number  $\mathbf{z}$  whose absolute value is greater than the spectral radius of  $A$ , it follows that  $G_{zu}$  has the Laurent expansion

$$G_{zu}(\mathbf{z}) = E_1 (\mathbf{z}I - A)^{-1} B = \sum_{i=d_{zu}}^{\infty} \frac{H_i}{\mathbf{z}^i}, \quad (69)$$

where  $H_0 \triangleq E_2$  and, for all  $i \geq 1$ , the  $i$ th Markov parameter of  $G_{zu}$  is given by

$$H_i \triangleq E_1 A^{i-1} B. \quad (70)$$

As shown in [38], a sufficiently large number  $\bar{n} > d_{zu}$  of Markov parameters in a truncation of (69) yields an FIR target model  $G_f(\mathbf{z}) = \sum_{i=d_{zu}}^{\bar{n}} (H_i / \mathbf{z}^i)$  whose zeros approximate the NMP zeros of  $G_{zu}$  with absolute value greater than the spectral radius of  $A$ . In addition, every truncation of (69) with  $\bar{n} \geq d_{zu}$  has the correct relative degree, that is, the relative degree of  $G_{zu}$ . Note that, since  $G_{zu} = N_{zu}/D$  and  $D$  is monic,  $H_{d_{zu}}$  is the leading numerator coefficient of  $G_{zu}$ .

## Finite Impulse Response Target Model

In the case where  $G_{zu}$  is minimum phase, the FIR target model is defined to be

$$G_f(\mathbf{q}) \triangleq \frac{H_{d_{zu}}}{\mathbf{q}^{d_{zu}}}. \quad (71)$$

This choice of  $G_f$  requires knowledge of the relative degree  $d_{zu}$  of  $G_{zu}$  and the first nonzero Markov parameter  $H_{d_{zu}}$  of  $G_{zu}$ . Note that, for the adaptive servo problem, since  $G_{zu} = -G_u$ , it follows that  $H_{d_{zu}} = -H_{d_u}$ , where  $H_{d_u}$  is the first nonzero Markov parameter of  $G_u$ .

In the case where  $G_{zu}$  is NMP, the FIR target model is defined to be

$$G_f(\mathbf{q}) \triangleq \frac{H_{d_{zu}} N_{zu,u}(\mathbf{q})}{\mathbf{q}^{d_{zu} + \deg(N_{zu,u})}}, \quad (72)$$

where the roots of the monic polynomial  $N_{zu,u}$  are the NMP zeros of  $G_{zu}$ . This choice of  $G_f$  requires knowledge of the relative degree  $d_{zu}$  of  $G_{zu}$ , the first nonzero Markov parameter  $H_{d_{zu}}$  of  $G_{zu}$ , and the NMP zeros of  $G_{zu}$ . In both cases, the relative degree of  $G_f$  is equal to the relative degree of  $G_{zu}$ .

### ADAPTIVE POLE PLACEMENT

This section considers adaptive pole placement for the adaptive standard problem and the adaptive servo problem using RCAC. The first step is to define the IIR target model for pole placement.

#### Infinite Impulse Response Target Model for Pole Placement

Since  $\tilde{G}_{z\tilde{u}}$  approximates  $G_f$ , RCAC attempts to place the poles of  $\tilde{G}_{z\tilde{u}}$  at the locations of the poles of  $G_f$ . It can be seen from (11) and (67) that the denominator of  $\tilde{G}_{z\tilde{u}}$  is equal to the denominator of the closed-loop transfer function  $\tilde{G}_{zw}$ . Consequently, RCAC attempts to place the closed-loop poles at the locations of the poles of  $G_f$ . To use  $G_f$  for pole placement, let  $D_p$  be a monic polynomial of degree  $n_p$  whose roots are the desired closed-loop pole locations. Then, in the case where  $G_{zu}$  is minimum phase, the IIR target model is defined to be

$$G_f(\mathbf{q}) \triangleq \frac{H_{d_{zu}} \mathbf{q}^{n_p - d_{zu}}}{D_p(\mathbf{q})}, \quad (73)$$

and, in the case where  $G_{zu}$  is NMP, the IIR target model is defined to be

$$G_f(\mathbf{q}) \triangleq \frac{H_{d_{zu}} \mathbf{q}^{n_p - d_{zu} - \deg(N_{zu,u})} N_{zu,u}(\mathbf{q})}{D_p(\mathbf{q})}. \quad (74)$$

The target models (71) and (73) for minimum-phase  $G_{zu}$  along with the target models (72) and (74) for NMP  $G_{zu}$  represent the modeling information required by RCAC.

In the case where  $n_p < n + n_c$ , RCAC attempts to place  $n_p$  closed-loop poles at the locations of the poles of  $G_f$ . The remaining  $n + n_c - n_p$  closed-loop poles are placed either at the locations of the minimum-phase zeros of  $G_{zu}$  that are not included in the roots of  $N_f$  so that  $\tilde{G}_{z\tilde{u}}$  approximates  $G_f$  or at zero.

#### Example PP1: Pole Placement for the Adaptive Servo Problem

Consider the unstable, minimum-phase plant

$$G(\mathbf{q}) = \frac{\mathbf{q}^2 - 1.4\mathbf{q} + 0.85}{(\mathbf{q} - 1.05)(\mathbf{q}^2 - 1.6\mathbf{q} + 0.89)}. \quad (75)$$

Let  $r$  be a unit step command, and let  $d = v = 0$ . To place five closed-loop poles at 0.3, 0.4, 0.6, and  $\pm 0.1j$ , the IIR target model (73) is used with

$$D_p(\mathbf{q}) = (\mathbf{q} - 0.3)(\mathbf{q} - 0.4)(\mathbf{q} - 0.6)(\mathbf{q}^2 + 0.01). \quad (76)$$

Let  $R_\theta = 10^{-20} I_{l_\theta}$ ,  $R_u = 0$ , and  $n_c = 4$ . RCAC asymptotically follows the step command and places five closed-loop poles near the locations of the roots of  $D_p$ , as shown in Figure 8. Note that the remaining two closed-loop poles cancel the

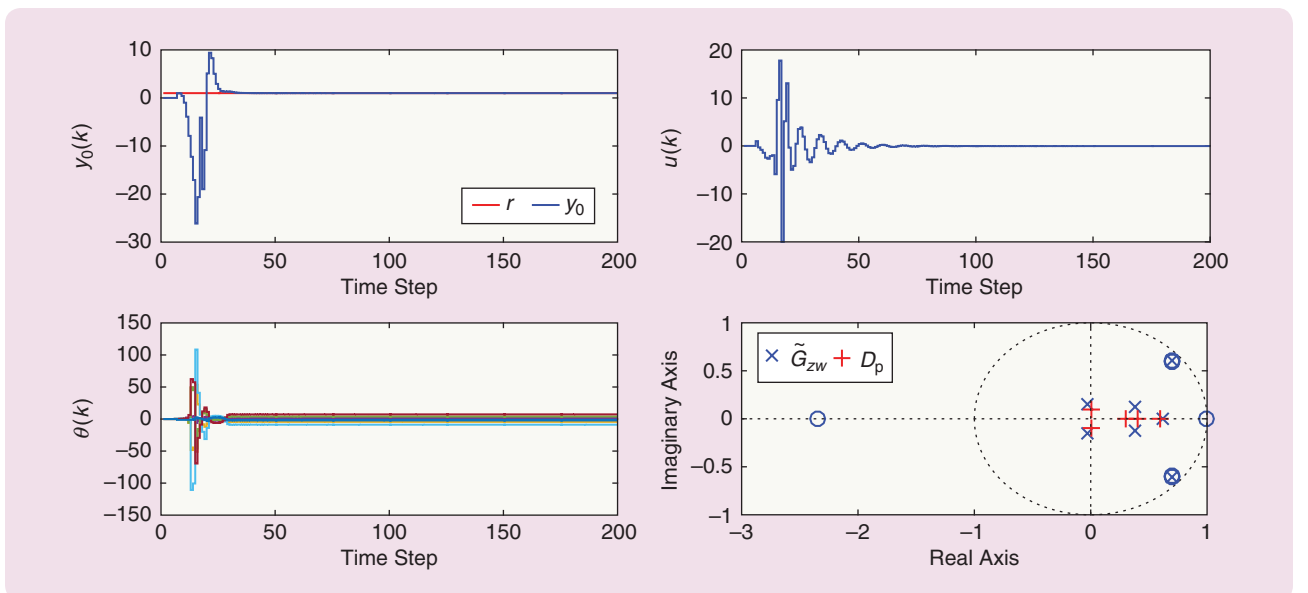


**FIGURE 8** Example PP1: Pole placement for the adaptive servo problem. With  $R_\theta = 10^{-20} I_{l_\theta}$ , retrospective cost adaptive control places five closed-loop poles near the locations of the roots of  $D_p$ . The closed-loop poles and zeros are shown at step  $k = 100$ .

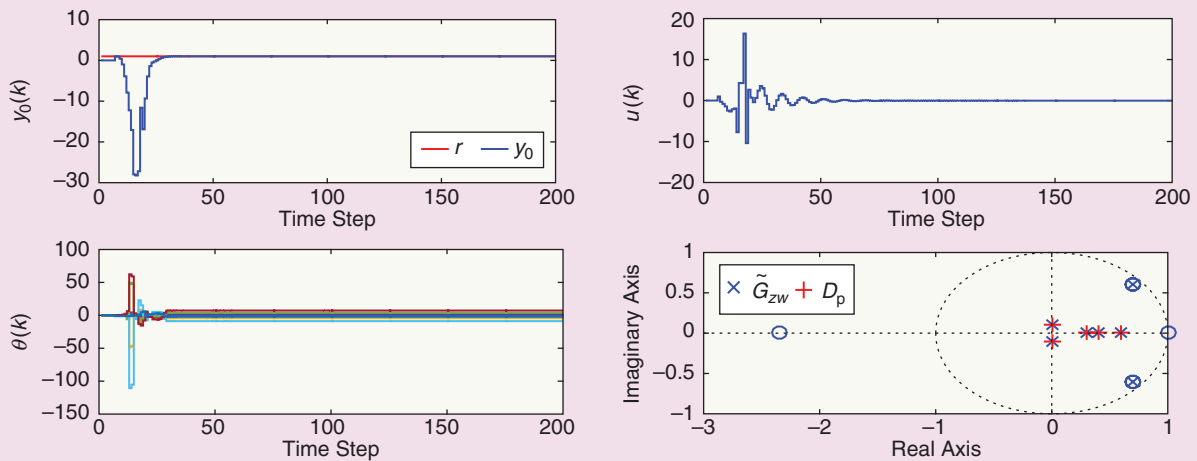


**FIGURE 9** Example PP1: Pole placement for the adaptive servo problem. With  $R_\theta = 10^{-40}I_{l_\theta}$ , retrospective cost adaptive control places the closed-loop poles closer to the target locations than in Figure 8.

minimum-phase zeros of  $G$ , which are not included in the target model (73).

Next set  $R_\theta = 10^{-40}I_{l_\theta}$ . Figure 9 shows the locations of the closed-loop poles. Note that RCAC places the closed-loop poles closer to the desired locations because  $R_\theta$  is decreased and thus  $P(0)$  is increased. ■

**Example PP2: Pole Placement for the Adaptive Standard Problem**  
Consider the unstable NMP plant

$$G(\mathbf{q}) = \frac{\mathbf{q} - 1.2}{(\mathbf{q} - 1.1)(\mathbf{q} - 2)}. \quad (77)$$

Let  $w$  be a unit step. RCAC is applied with  $R_\theta = 10^{-30}I_{l_\theta}$ ,  $R_u = 0$ , and  $n_c = 3$ . To place five closed-loop poles at 0.1, 0.3, 0.5, and  $\pm 0.75j$ , the IIR target model (74) is used with

$$D_p(\mathbf{q}) = (\mathbf{q} - 0.1)(\mathbf{q} - 0.3)(\mathbf{q} - 0.5)(\mathbf{q}^2 + 0.5625). \quad (78)$$

Note that the NMP zero of (77) lies between the two unstable poles. It follows from root-locus analysis and the parity interlacing property [74] that stabilization of (77) requires the controller to be unstable [21]. RCAC places five closed-loop poles near the locations of the roots of  $D_p$ , as shown in Figure 10. As expected,  $G_{c,k}$  converges to an unstable controller. ■

The examples in this section show how RCAC can be used to assign a subset of the closed-loop poles, which can be viewed as partial pole placement. Example PP2 demonstrates this objective for an unstable plant that requires an unstable controller for stabilization. The “Effect of Sensor

Noise” section investigates the effect of sensor noise on the ability to achieve pole placement.

### ADAPTIVE HARMONIC COMMAND FOLLOWING AND DISTURBANCE REJECTION

This section demonstrates the ability of RCAC to develop internal models of commands and disturbances by considering two examples of adaptive harmonic command following and disturbance rejection. In the first example, RCAC is used to follow harmonic commands with an IIR feedback controller as well as with combined feedback-feedforward control. Next, for harmonic disturbance rejection, the ability of RCAC to readapt to changing disturbance frequencies is investigated.

**Example H1: Harmonic Command Following for the Adaptive Servo Problem**

Consider the asymptotically stable, minimum-phase plant

$$G(\mathbf{q}) = \frac{\mathbf{q} - 0.8}{(\mathbf{q} - 0.95)(\mathbf{q} - 0.99)}. \quad (79)$$

Let  $r$  be the harmonic command  $r(k) = \cos \omega k$ , where  $\omega = 0.5$  rad/sample, and let  $d = v = 0$ . RCAC is applied with  $R_\theta = 0.2I_{l_\theta}$ ,  $R_u = 0$ ,  $n_c = 5$ , and the FIR target model (71).  $G_{c,k}$  is restricted to be an FIR controller of the form (35) and (36). Since RCAC cannot develop an internal model of the command  $r$  due to the FIR structure of  $G_{c,k}$ , the command-following performance is severely restricted, as shown in Figure 11. The closed-loop system is instantaneously unstable at most time steps up to  $k = 500$ .

Next,  $G_{c,k}$  is an IIR controller of the form (29) and (34). In this case, RCAC automatically develops an internal model

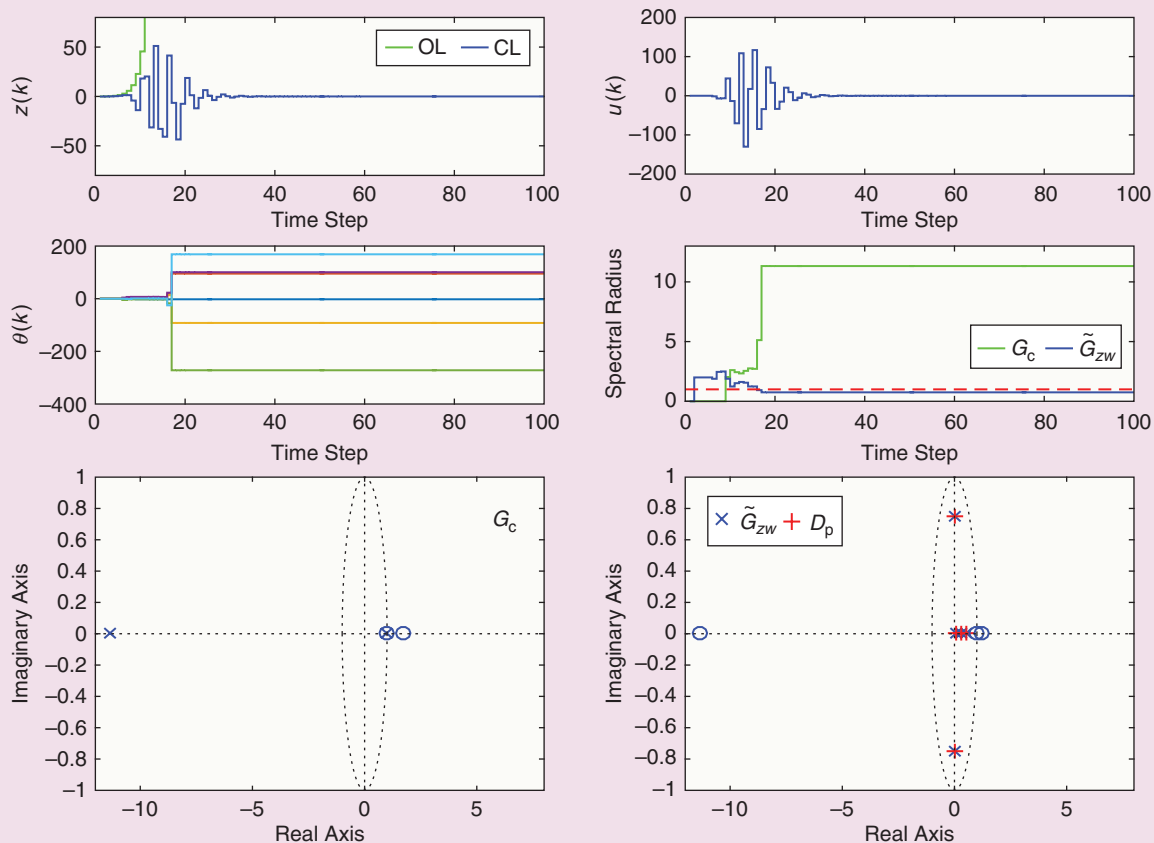


**FIGURE 10** Example PP2: Pole placement for the adaptive standard problem. Retrospective cost adaptive control places five closed-loop poles near the locations of the roots of  $D_p$ . Note that the controller becomes unstable after a few steps, and the closed-loop system is stabilized at step  $k = 16$ . The closed-loop poles and zeros are shown at step  $k = 100$ .

in the form of controller poles located on the unit circle at the command frequency  $\omega$  and asymptotically follows the harmonic command, as shown in Figure 12.

Finally, the feedback-feedforward control is combined with decentralized adaptation, as shown in Figure 13, where the feedback controller is FIR and the feedforward controller is IIR. Both controllers are of order  $n_c = 5$ . In this case, since the controller is feedback-feedforward, RCAC asymptotically follows the harmonic command without developing an internal model, as shown in Figure 14. ■

**Example H2: Two-Tone Harmonic Disturbance Rejection for the Adaptive Servo Problem Using an IIR Controller**  
Consider the asymptotically stable plant

$$A = \begin{bmatrix} 0.9 & -0.5625 & 0 \\ 1 & 0 & 0 \\ 0 & 1 & 0 \end{bmatrix}, \quad B = \begin{bmatrix} 1 \\ 0 \\ 0 \end{bmatrix}, \quad \bar{D}_1 = \begin{bmatrix} 0 & 0 \\ 1 & 0 \\ 0 & 1 \end{bmatrix}, \quad (80)$$

$$\bar{C} = [0.78 \quad -1.18 \quad 1], \quad \bar{D}_0 = 0, \quad (81)$$

where  $G_u$  is NMP. Let  $r = v = 0$  and  $d(k) = [\cos \omega_1 k \quad \cos \omega_2 k]^T$ , where  $\omega_1 = (\pi/8)$  rad/sample and  $\omega_2 = (\pi/12)$  rad/sample. RCAC is applied with  $k_w = 50$ ,  $R_\theta = 0.01I_{10}$ ,  $R_u = 0$ ,  $n_c = 12$ , and the FIR target model (72) with an IIR controller. RCAC automatically develops an internal model of the harmonic disturbance and thus rejects the harmonic disturbance, as shown in Figure 15.

Next, let  $r(k) = \cos \omega_1 k$ ,  $v = 0$ , and  $d(k) = [\cos \omega_2 k \quad 1]^T$ , where  $\omega_1 = (\pi/15)$  rad/sample and  $\omega_2 = (\pi/5)$  rad/sample for  $1 \leq k \leq 2000$ , and where  $\omega_2 = (\pi/8)$  rad/sample for  $2000 < k \leq 4000$ . RCAC automatically develops internal models of the command and disturbance and thus asymptotically follows the harmonic command and rejects the step and harmonic disturbances, as shown in Figure 16. Note that, after the disturbance frequency changes at step  $k = 2000$ , RCAC readapts and rejects the disturbance. ■

The examples in this section show that, for harmonic command following and harmonic disturbance rejection, RCAC has the ability to automatically develop an internal model of the command and disturbance without knowledge

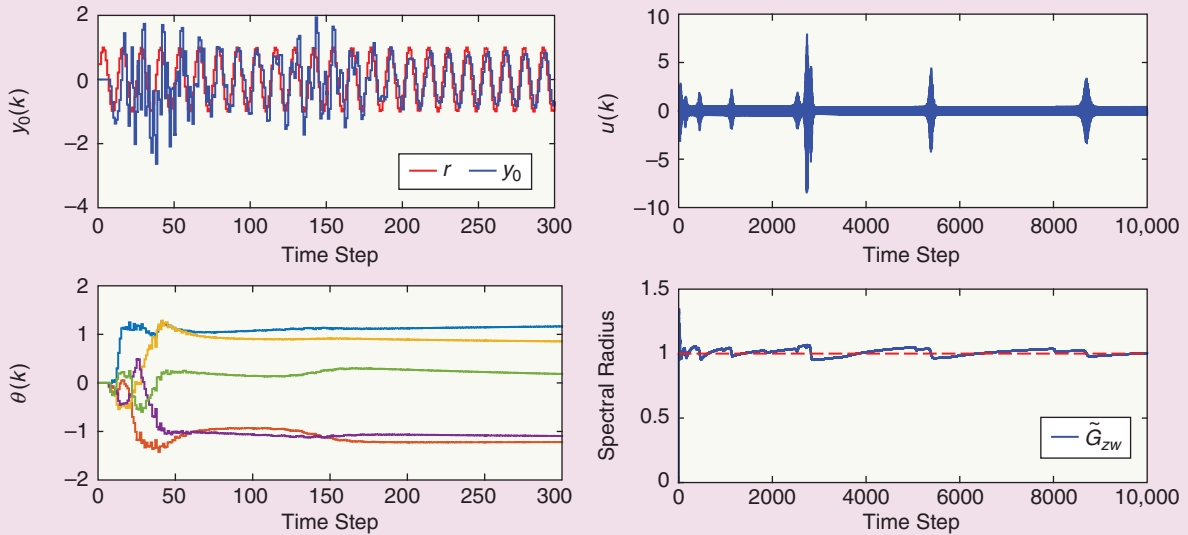


**FIGURE 11** Example H1: Harmonic command following for the adaptive servo problem using a finite impulse response (FIR) controller. Since retrospective cost adaptive control cannot develop an internal model of the command  $r$  due to the FIR structure of  $G_{c,k}$ , the command-following performance is severely restricted. Note that the controller coefficients do not converge, and the closed-loop system alternates between asymptotic stability and instability.

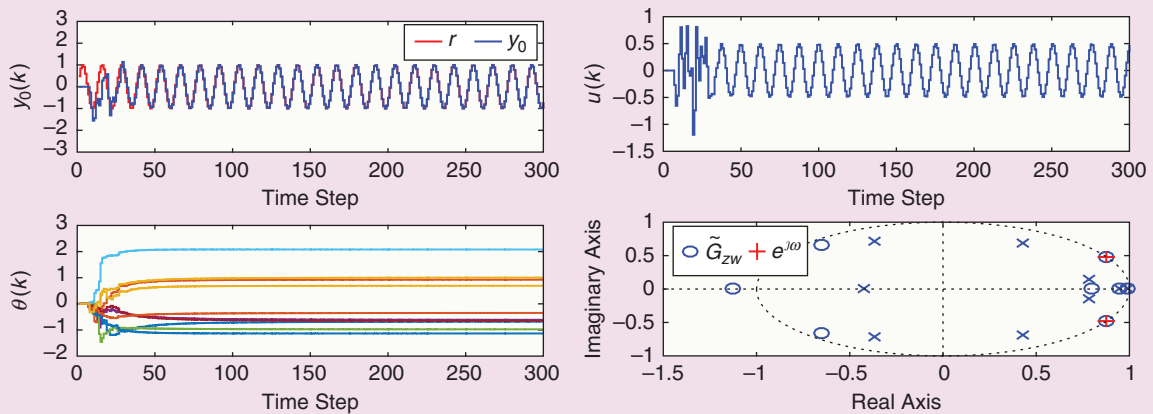


**FIGURE 12** Example H1: Harmonic command following for the adaptive servo problem. With an infinite impulse response controller structure, retrospective cost adaptive control achieves an internal model of the harmonic command signal by placing controller poles on the unit circle at the command frequency. The internal-model poles of the controller are evident in the form of two closed-loop zeros on the unit circle, which are shown by the red plus signs. The closed-loop poles and zeros are shown at step  $k = 300$ .

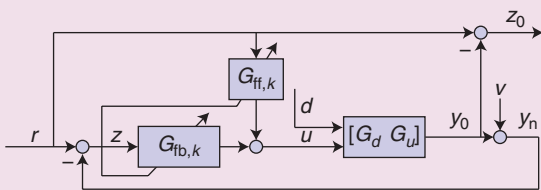


**FIGURE 13** A block diagram representation of combined feedback-feedforward control with decentralized adaptation for the adaptive servo problem.

of the spectrum of these signals. In “Adaptive PID Control,” RCAC is applied to step-command following using an adaptively tuned PID controller. In “RCAC for Model Reference Adaptive Control,” RCAC is compared to a continuous-time MRAC method for minimum-phase and NMP plants.

#### ADAPTIVE CONTROL WITH STOCHASTIC $w$ AND $d$

RCAC is applied to the adaptive standard problem in the case where the exogenous signal  $w$  is stochastic as well as to the adaptive servo problem in the case where the disturbance  $d$  is stochastic. The closed-loop frequency

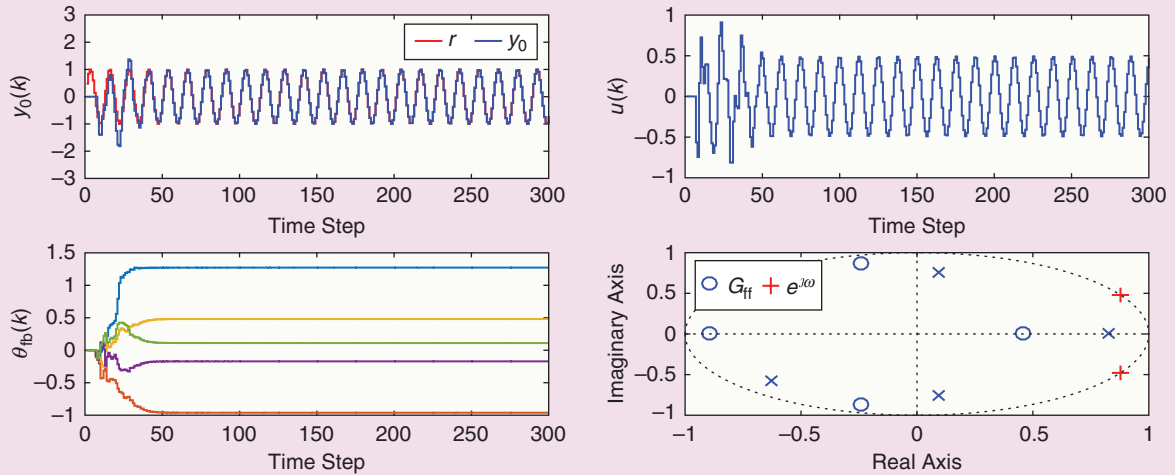


**FIGURE 14** Example H1: Harmonic command following for the adaptive servo problem using feedback-feedforward control with decentralized adaptation. Retrospective cost adaptive control asymptotically follows the command without developing an internal model.

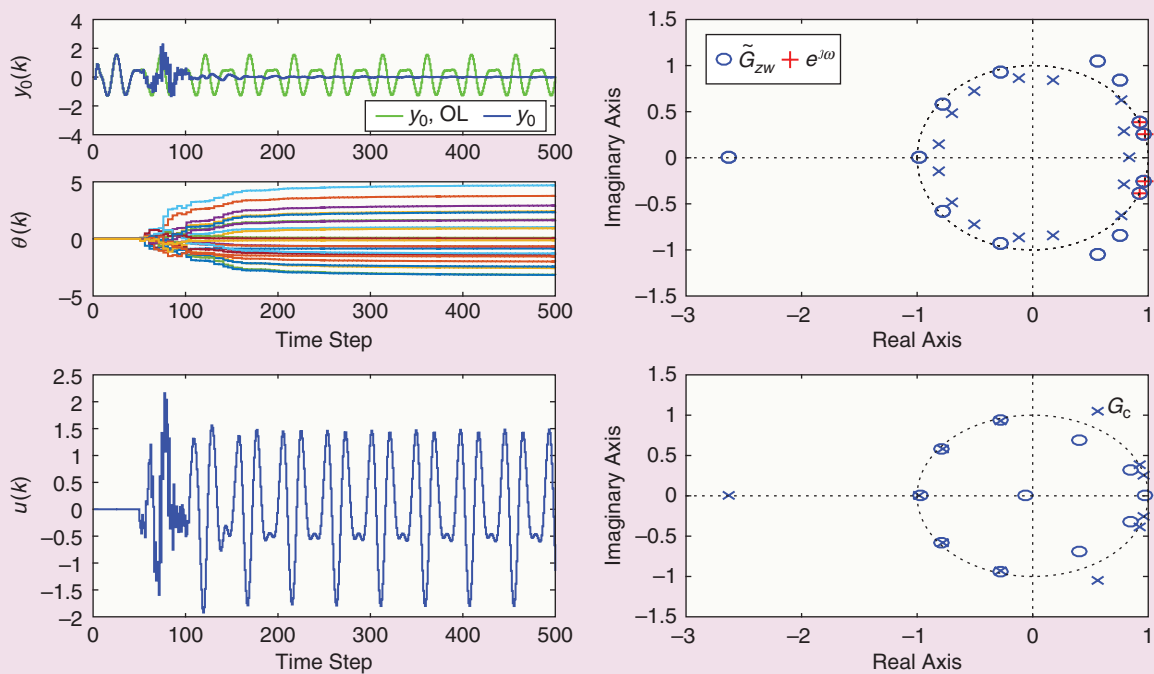


**FIGURE 15** Example H2: Two-tone harmonic disturbance rejection for the adaptive servo problem using an infinite impulse response controller.  $y_{0,OL}$  indicates the open-loop response. Retrospective cost adaptive control automatically develops an internal model of the two-tone harmonic disturbance by placing controller poles at the two disturbance frequencies. The internal-model poles of the controller are evident in the form of four closed-loop zeros on the unit circle, which are shown by the red plus signs. The closed-loop poles and zeros are shown at step  $k = 10^4$ .

response and the  $H_2$  cost of RCAC are compared to high-authority LQG, presented in “Discrete-Time LQG Control.”

### $H_2$ Cost of Strictly Proper Controllers

For the plant (1)–(3), the  $H_2$  cost of an arbitrary stabilizing strictly proper controller

$$G_c \sim \begin{bmatrix} A_c & B_c \\ C_c & 0 \end{bmatrix}$$

is computed by first defining

$$\tilde{D} \triangleq \begin{bmatrix} D_1 \\ B_c D_2 \end{bmatrix}, \quad \tilde{V} = \tilde{D} \tilde{D}^T. \quad (82)$$

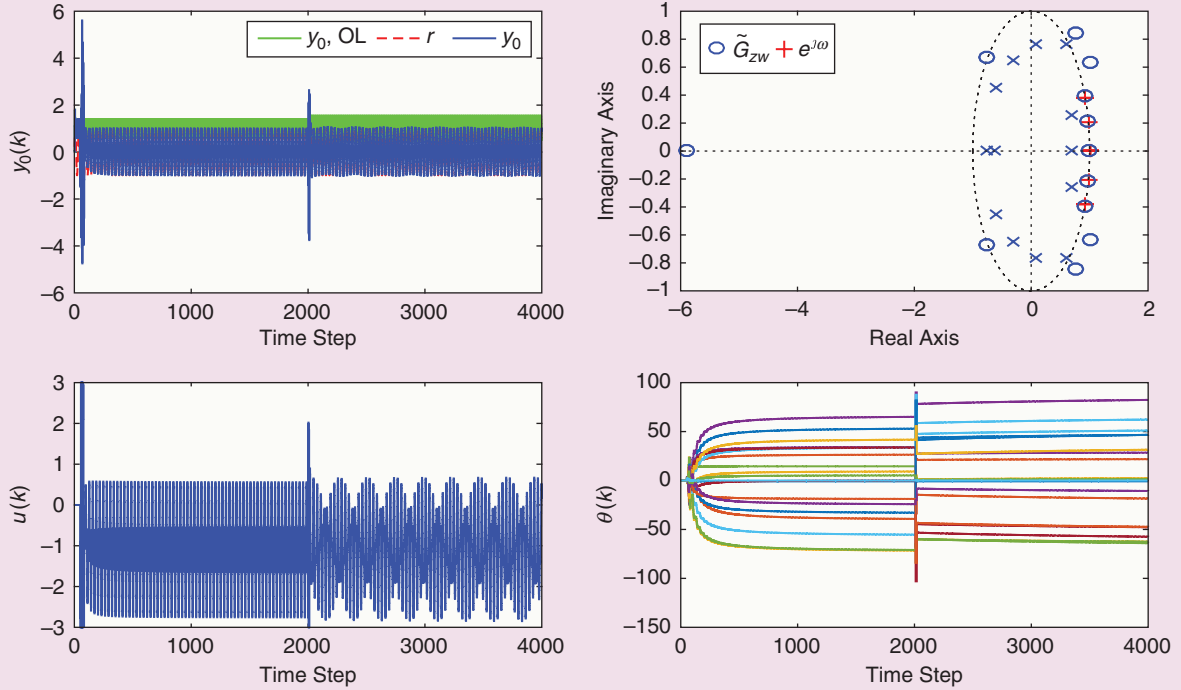


**FIGURE 16** Example H2: Harmonic command following and step-plus-harmonic disturbance rejection for the adaptive servo problem. Note that, after the disturbance frequency changes at step  $k = 2000$ , retrospective cost adaptive control (RCAC) readapts and rejects the disturbance. RCAC automatically develops an internal model of the command and disturbance signals by placing controller poles on the unit circle at the command frequency and the two disturbance frequencies. The internal-model poles of the controller are evident in the form of five closed-loop zeros on the unit circle, which are shown by the red plus signs. The closed-loop poles and zeros are shown at step  $k = 10^5$ .

Then, the  $H_2$  cost is given by

$$J(A_c, B_c, C_c) = \text{tr}(Q_1 R_1) + \text{tr}(Q_2 C_c^T R_2 C_c). \quad (83)$$

$Q_1 \in \mathbb{R}^{n \times n}$ ,  $Q_2 \in \mathbb{R}^{n_c \times n_c}$  satisfy

$$\tilde{Q} = \begin{bmatrix} Q_1 & Q_{12} \\ Q_{12}^T & Q_2 \end{bmatrix} \quad (84)$$

and  $\tilde{Q} \in \mathbb{R}^{(n+n_c) \times (n+n_c)}$  is the solution of the discrete-time Lyapunov equation

$$\tilde{Q} = \tilde{A} \tilde{Q} \tilde{A}^T + \tilde{V}, \quad (85)$$

where  $\tilde{A}$  is defined in (S24).

### High-Authority LQG Target Model

Since RCAC tends to match  $\tilde{G}_{zu}$  to  $G_f$ ,  $G_f$  is chosen with the numerator  $N_{zu}(\mathbf{q})\mathbf{q}^{n_c}$  and the closed-loop denominator  $\tilde{D}_{HA}$  of high-authority LQG to construct the high-authority LQG target model

$$G_f(\mathbf{q}) = \frac{N_{zu}(\mathbf{q})\mathbf{q}^{n_c}}{\tilde{D}_{HA}(\mathbf{q})} = \frac{H_{d_{zu}}\mathbf{q}^m N_{zu,u}(\mathbf{q})}{N_{zu,u}(\mathbf{q}^{-1})N_{yw,s}(\mathbf{q})N_{yw,u}(\mathbf{q}^{-1})} \quad (86)$$

where  $m \triangleq n_c - d_{zu} - d_{yu}$ . Note that  $m$  may be negative. The target model (86) is based on (S29). By choosing (86), the

goal is to compare the performance of RCAC with the performance of high-authority LQG in the case  $n_c = n$ . Note that using (86) as the target model requires knowledge of  $\tilde{D}_{HA}$  in addition to the modeling information required by (71) and (72). The use of (86) is thus only for conceptual illustration. To avoid using knowledge of  $\tilde{D}_{HA}$ , the following uses the FIR target models (71) and (72), but with  $n_c > n$ .

All examples in this section, unless specified otherwise, use  $R_\theta = 10^{-10}I_{l_\theta}$ ,  $k_w = 50$ , and  $R_u = 0$ .

### Example SD1: Adaptive Control with Stochastic $w$ for the Adaptive Standard Problem

Consider the asymptotically stable plant

$$A = \begin{bmatrix} 0.855 & 1 & 0 & 0 & 0 \\ -0.1715 & 0.855 & -0.4266 & -0.3607 & 0.4952 \\ 0 & 0 & 0.5 & -0.5072 & 0.6964 \\ 0 & 0 & 0 & 0.6716 & 1 \\ 0 & 0 & 0 & -0.4514 & 0.6716 \end{bmatrix}, \quad (87)$$

$$B = \begin{bmatrix} 0 \\ 0 \\ 0 \\ 0 \\ 1 \end{bmatrix}, \quad D_1 = \begin{bmatrix} -0.6269 \\ 0.3985 \\ -0.3306 \\ 0.4415 \\ 0.3794 \end{bmatrix}$$

## Adaptive PID Control

Proportional-integral-derivative (PID) control is likely the most widely used feedback control technique [S1]–[S3]. Adaptive PID control is considered in [S4]. This sidebar considers the discrete-time PID controller structure

$$u(k) = u_P(k) + u_I(k) + u_D(k), \quad (S1)$$

where

$$u_P(k) = K_P(k)y(k-1), \quad (S2)$$

$$u_I(k) = K_I(k)\gamma(k-1), \quad (S3)$$

$$u_D(k) = K_D(k)[y(k-1) - y(k-2)], \quad (S4)$$

and the integrator state  $\gamma$  satisfies

$$\gamma(k) = \gamma(k-1) + y(k-1). \quad (S5)$$

Note that the PID controller (S1)–(S5) is strictly proper. RCAC is used to adaptively tune  $K_P$ ,  $K_I$ , and  $K_D$ .

### Example PID1: Step Command Following for the Adaptive Servo Problem Using Adaptive PID Control

Consider the asymptotically stable, NMP plant

$$G(q) = \frac{(q - 0.975)(q - 1.2)}{(q - 0.99)(q^2 - 1.6q + 0.965)}, \quad (S6)$$

let  $r$  be a step command with height two, let  $d$  be a step disturbance with height  $-1.1$ , and let  $v = 0$ . RCAC is applied to the adaptive PID controller (S1)–(S5) with  $R_\theta = 10^4 I_\theta$  and  $R_u = 0$ . RCAC rejects the step disturbance and asymptotically follows the step command, as shown in Figure S1. ■

### REFERENCES

- [S1] K. J. Astrom and T. Hagglund, *Advanced PID Control*. Research Triangle Park, NC: Instrumentation, Systems, and Automation Society, 2006.  
 [S2] Y. Li, K. H. Ang, and G. C. Y. Chong, "PID control system analysis and design: problems, remedies, and future directions," *IEEE Control Syst. Mag.*, vol. 26, pp. 32–41, 2006.  
 [S3] A. O'Dwyer, *Handbook of PI and PID Controller Tuning Rules*. London: Imperial College Press, 2009.  
 [S4] V. Bobal, J. Bohm, J. Fessl, and J. Machacek, *Digital Self-tuning Controllers*. New York: Springer-Verlag, 2005.

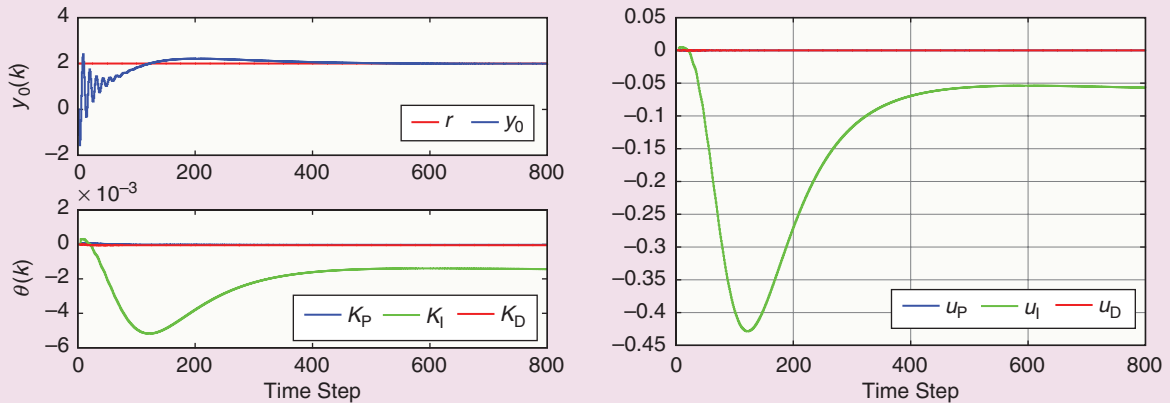


**FIGURE S1** Example PID1: Step command following for the adaptive servo problem using adaptive proportional-integral-derivative control. Retrospective cost adaptive control rejects the disturbance and asymptotically follows the step command.

$$C = [0.7298 \quad -0.3954 \quad -0.3605 \quad 0.4003 \quad 0.1447], \quad (88)$$

$$D_0 = 0, \quad D_2 = 0,$$

$$E_1 = [0.1717 \quad 0.3351 \quad -0.5294 \quad -0.4476 \quad 0.6145], \quad (89)$$

$$E_0 = 0, \quad E_2 = 0,$$

where  $G_{zu}$ ,  $G_{zw}$ ,  $G_{yu}$ , and  $G_{yw}$  are NMP. The  $H_2$  cost of the LQG controller is 1.059. The exogenous signal  $w$  is zero-mean Gaussian white noise with standard deviation 0.1. RCAC is applied with  $n_c = n$  and the high-authority LQG target model (86). RCAC places the closed-loop poles near the high-authority LQG closed-loop poles and approxi-

mates the closed-loop frequency response of high-authority LQG, as shown in Figure 17. The  $H_2$  cost of the RCAC controller is 1.0591.

The next example shows that, for sufficiently large  $n_c > n$ , RCAC approximates the performance of the high-authority LQG controller using the FIR target model (72), which uses knowledge of  $d_{zu}$ ,  $H_{d_{zu}}$  and the NMP zeros of  $G_{zu}$  but no other modeling data and no knowledge of  $\tilde{D}_{HA}$ . RCAC is applied with  $n_c = 4n = 20$ . In this case, RCAC approximates the closed-loop frequency response of high-authority LQG, as shown in Figure 18, and the  $H_2$  cost of the RCAC controller is 1.061. ■

## RCAC for Model Reference Adaptive Control

The model reference adaptive control (MRAC) problem is shown in Figure S2. This problem is a special case of the adaptive standard problem with

$$w = \begin{bmatrix} r \\ d \\ v \end{bmatrix}, \quad y = \begin{bmatrix} r \\ y_n \end{bmatrix}, \quad y_m = G_m r, \quad z = y_m - y_n, \quad (S7)$$

$$G_{zw} = [G_m \quad -G_d \quad -I_z], \quad G_{zu} = -G_u, \\ G_{yw} = \begin{bmatrix} I_r & 0 & 0 \\ 0 & G_d & I_z \end{bmatrix}, \quad G_{yu} = G_u, \quad (S8)$$

where  $r \in \mathbb{R}^{l_r}$  and  $G_m$  is the reference model. Since  $y$  includes the command  $r$ , the controller includes both feedback and feedforward action. Note that the role of the target model  $G_r$  used by RCAC is distinct from the role of the reference model  $G_m$  used in MRAC.

The MRAC problem is widely studied, and numerous techniques have been developed [11], [12], [14], [17], [78]. The MRAC controllers in [11, pp. 343–371] are compared below to RCAC for continuous-time plants. These controllers require knowledge of the relative degree of the plant as well as the

leading coefficient of the plant numerator. The form of the controller depends on the relative degree of the plant, and the approach is confined to minimum-phase plants. An extension to NMP plants is given in [12].

### Example MRAC1: MRAC for a Minimum-Phase Plant

Consider the continuous-time unstable, minimum-phase triple integrator

$$\bar{G}(s) = \frac{s+0.1}{s^3}. \quad (S9)$$

Let  $r$  be an alternating sequence of step commands with heights  $\pm 1$ , let  $d = v = 0$ , and let  $\bar{G}_m$  be the continuous-time reference model  $\bar{G}_m(s) = 1/(s+1)$ . The MRAC algorithm is the one given in [11, p. 355] for plants with relative degree two. Figure S3 shows the closed-loop response. Next, the plant (S9) and reference model  $\bar{G}_m$  are discretized with the sampling period  $h = 0.01$  s, yielding

$$G(\mathbf{q}) = \frac{10^{-5}(5\mathbf{q}^2 + 0.0067\mathbf{q} - 5)}{(\mathbf{q} - 1)^3}, \quad G_m(\mathbf{q}) = \frac{0.01}{\mathbf{q} - 0.99}. \quad (S10)$$

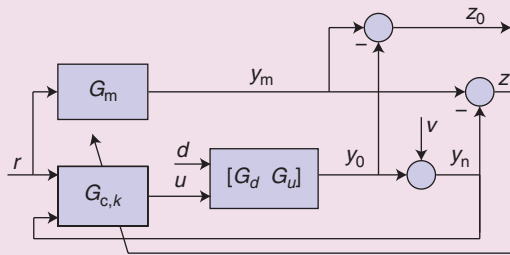


FIGURE S2 A block diagram representation of the model reference adaptive control problem with the adaptive controller  $G_{c,k}$ .

TABLE S1 The performance metric  $\epsilon$  for the model reference adaptive controller given in [11, p. 355] and retrospective cost adaptive control (RCAC). Note that RCAC yields better performance in the case where  $d = 0$  as well as in the presence of a constant disturbance.

Method	$d$	$\epsilon$
[11, p. 355]	0	216
RCAC	0	132
[11, p. 355]	-0.2	3667
RCAC	-0.2	153

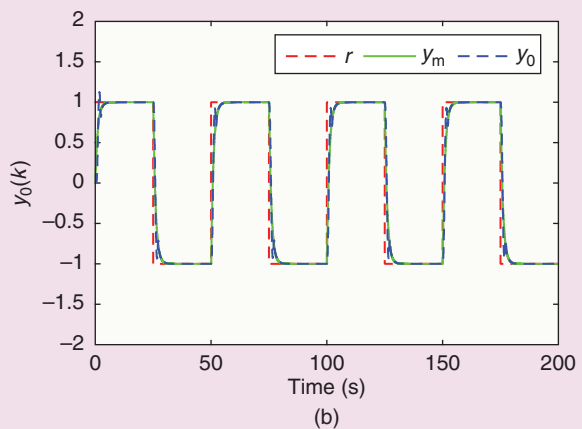
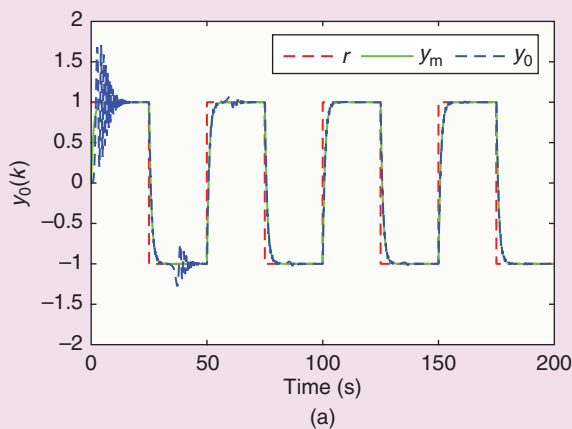
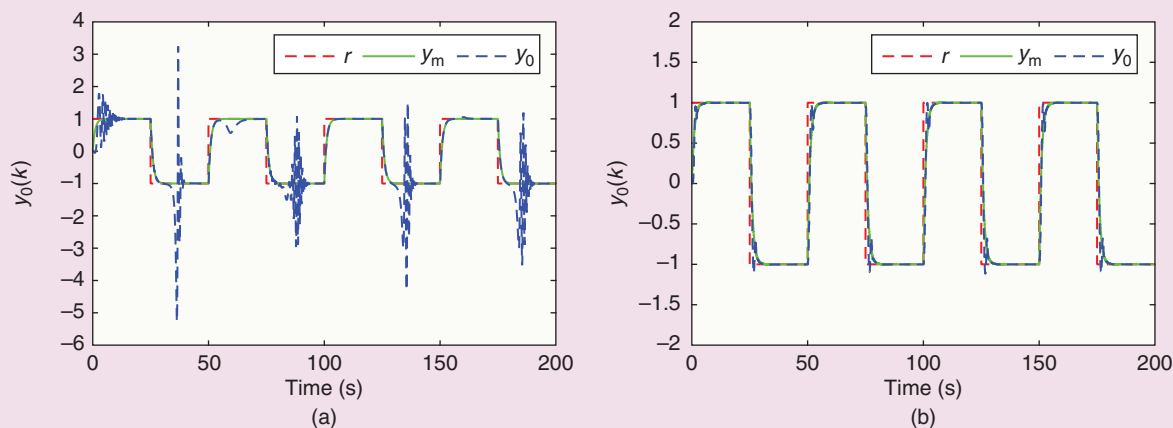
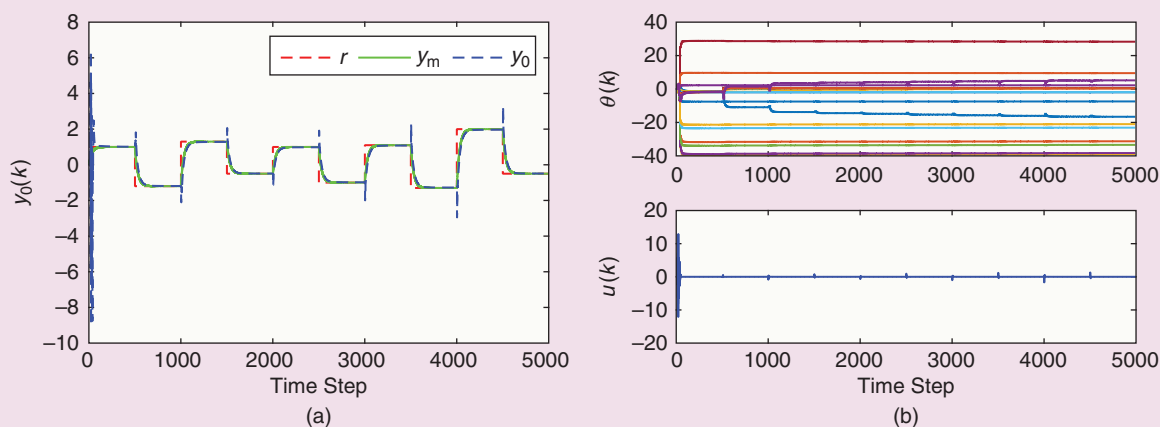


FIGURE S3 Example MRAC1: Application of retrospective cost adaptive control (RCAC) to the model reference adaptive control (MRAC) problem for the minimum-phase triple integrator (S9). (a) shows the MRAC controller from [11, p. 355], and (b) shows the RCAC controller; both follow the output of the reference model.



**FIGURE S4** Example MRAC1: Application of retrospective cost adaptive control (RCAC) to the model reference adaptive control (MRAC) problem for the minimum-phase triple integrator (S9) in the presence of a step disturbance. (a) shows the response of the MRAC controller from [11, p. 355], and (b) shows the response of RCAC.



**FIGURE S5** Example MRAC2: Application of retrospective cost adaptive control (RCAC) to the model reference adaptive control problem for the nonminimum-phase double integrator (S12). (a) shows that RCAC asymptotically follows the output of the reference model, and (b) shows the controller coefficient vector  $\theta$  and the control  $u$ .

RCAC is applied to the MRAC problem with  $R_\theta = 10^{-10}I_{16}$ ,  $R_u = 0$ , and  $n_c = 10$ . Twenty Markov parameters are used to construct the target model. RCAC asymptotically follows the output of the reference model, as shown in Figure S3. Table S1 shows the value of the performance metric  $\varepsilon \triangleq \sum_{k=1}^{20000} z^2(k)$  for the MRAC controller given in [11, p. 355] and for RCAC.

Finally, let the disturbance  $d$  be a step with height  $-0.2$ . Figure S4 shows the command-following performance for the MRAC controller given in [11, p. 355] and RCAC. Table S1 shows the value of the performance metric for the MRAC controller and RCAC. ■

#### Example MRAC2: MRAC for an NMP Plant

Consider the continuous-time unstable, NMP double integrator

$$\bar{G}(s) = \frac{s - 0.0952}{s^2}. \quad (\text{S11})$$

Let  $r$  be a sequence of step commands with sign-alternating heights, let  $d = v = 0$ , and let  $\bar{G}_m$  be the continuous-time reference model  $\bar{G}_m(s) = (s - 0.0952)/(s^2 + 30s + 1)$ . Note that  $\bar{G}$  and  $\bar{G}_m$  have the same NMP zero. Attempting to use the MRAC algorithm given in [11, p. 345] yields an unstable closed-loop system (not shown). The plant (S9) and the reference model  $\bar{G}_m(s) = 1/(s^2 + 30s + 1)$  are discretized with the sampling period  $h = 1$  s, yielding

$$G(\mathbf{q}) = \frac{\mathbf{q} - 1.1}{(\mathbf{q} - 1)^2}, \quad G_m(\mathbf{q}) = \frac{0.03174\mathbf{q} + 0.001078}{\mathbf{q}^2 - 0.9672\mathbf{q}}. \quad (\text{S12})$$

RCAC is applied to the MRAC problem with  $R_\theta = 0.002I_{16}$ ,  $R_u = 0$ ,  $n_c = 6$ , and the FIR target model (72). RCAC asymptotically follows the output of the reference model, as shown in Figure S5. ■

## Discrete-Time LQG Control

Discrete-time linear-quadratic-Gaussian (LQG) is not as widely used as the continuous-time version [S5], [S6]; the relevant equations for discrete-time LQG can be found in [79, p. 878], and a complete derivation in a more general context is given in [S7]. Solutions of the discrete-time Riccati equations are discussed in [S8]. Here the focus is on the high-authority LQG solution.

For the standard problem (1)–(3), define

$$R_1 \triangleq E_1^T E_1 \in \mathbb{R}^{n \times n}, \quad R_{12} \triangleq E_1^T E_2 \in \mathbb{R}^{n \times l_2}, \quad R_2 \triangleq E_2^T E_2 \in \mathbb{R}^{l_2 \times l_2}, \quad (S13)$$

$$V_1 \triangleq D_1 D_1^T \in \mathbb{R}^{n \times n}, \quad V_{12} \triangleq D_1 D_2^T \in \mathbb{R}^{n \times l_2}, \quad V_2 \triangleq D_2 D_2^T \in \mathbb{R}^{l_2 \times l_2}. \quad (S14)$$

Assuming that  $w$  is zero-mean Gaussian white noise with covariance  $I_w$ , the  $n$ th-order strictly proper LQG controller  $G_c \sim \begin{bmatrix} A_c & B_c \\ C_c & 0 \end{bmatrix}$  minimizes

$$J(A_c, B_c, C_c) \triangleq \lim_{k \rightarrow \infty} \mathbb{E} \left[ \frac{1}{k} \sum_{i=0}^k z^T(i) z(i) \right] \quad (S15)$$

and is given by

$$A_c = A + BC_c - B_c C - B_c D_0 C_c, \quad (S16)$$

$$B_c = (AQC^T + V_{12})(V_2 + CQC^T)^{-1}, \quad (S17)$$

$$C_c = -(R_2 + B^T P B)^{-1}(R_{12}^T + B^T P A), \quad (S18)$$

where the positive-semidefinite matrices  $P \in \mathbb{R}^{n \times n}$  and  $Q \in \mathbb{R}^{n \times n}$  are solutions of the discrete-time algebraic Riccati equations

$$P = \hat{A}_R^T P \hat{A}_R - \hat{A}_R^T P B (R_2 + B^T P B)^{-1} B^T P \hat{A}_R + \hat{R}_1, \quad (S19)$$

$$Q = \hat{A}_E Q \hat{A}_E^T - \hat{A}_E Q C^T (V_2 + CQC^T)^{-1} C Q \hat{A}_E^T + \hat{V}_1, \quad (S20)$$

where

$$\hat{A}_R \triangleq A - BR_2^{-1} R_{12}^T, \quad \hat{R}_1 \triangleq R_1 - R_{12} R_2^{-1} R_{12}^T, \quad (S21)$$

$$\hat{A}_E \triangleq A - V_{12} V_2^{-1} C, \quad \hat{V}_1 \triangleq V_1 - V_{12} V_2^{-1} V_{12}^T. \quad (S22)$$

The eigenvalues of the closed-loop system are given by

$$\text{mspec}(\tilde{A}) = \text{mspec}(A + BC_c) \cup \text{mspec}(A - B_c C), \quad (S23)$$

where

$$\tilde{A} \triangleq \begin{bmatrix} A & BC_c \\ B_c C & A_c + B_c D_0 C_c \end{bmatrix} \quad (S24)$$

and “mspec” denotes the spectrum of a matrix including eigenvalue multiplicity. Under the assumptions

- $(A, B)$  is stabilizable
- $(\hat{A}_R, \hat{R}_1)$  has no unobservable eigenvalues on the unit circle
- $(A, C)$  is detectable
- $(\hat{A}_E, \hat{V}_1)$  has no uncontrollable eigenvalues on the unit circle,

it then follows that (S19) and (S20) have unique positive-semidefinite solutions  $P$  and  $Q$ , and, furthermore,  $\tilde{A}$  is asymptotically stable.

Note that the LQG controller is independent of  $E_0$ . This is because, since LQG is based on the assumption that  $w$  is zero-mean Gaussian white noise, the contribution of  $E_0 w$  to  $J(A_c, B_c, C_c)$  is not affected by the choice of  $A_c$ ,  $B_c$ , and  $C_c$ . However, for the servo problem shown in Figure 3,  $E_0$  is not zero, and the command  $r$ , which is a component of  $w$ , is not Gaussian white noise. Likewise, in some applications, the disturbance  $d$  in the servo problem is not Gaussian white noise, and thus the exogenous signal  $w$  in the standard problem is not Gaussian white noise. Therefore, in these cases, the LQG controller is not necessarily optimal. Nevertheless, the LQG controller is used for comparison with RCAC in these cases without modification. Examples SD1–SD3 compare the closed-loop frequency response and  $H_2$  cost of RCAC to high-authority LQG.

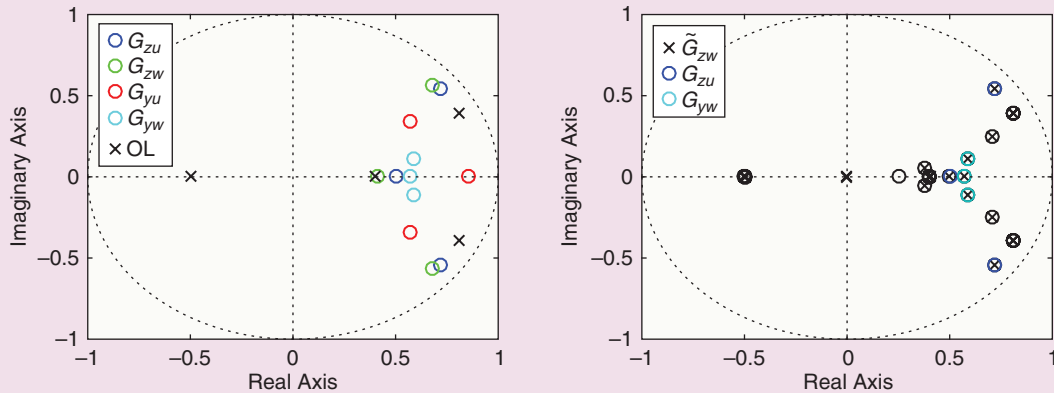


**FIGURE S6** Example LQG1: The closed-loop transfer function  $\tilde{G}_{zw}$  has one pole at each zero of  $G_{zu}$  and  $G_{yw}$  as well as two poles at zero.

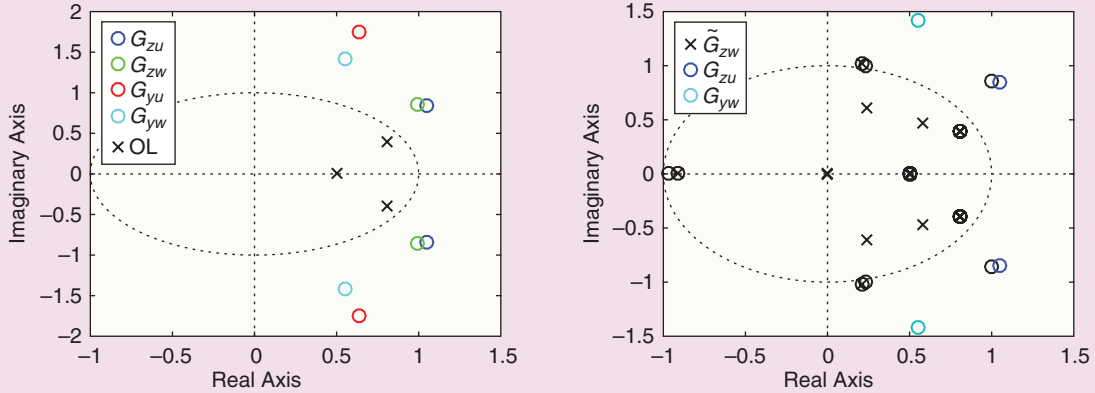


**FIGURE S7** Example LQG2: The closed-loop transfer function  $\tilde{G}_{zw}$  has one pole at the reciprocal of each NMP zero of  $G_{zu}$  and  $G_{yw}$  as well as two poles at zero.

### Properties of Discrete-Time High-Authority LQG

This section reviews properties of high-authority LQG, that is, the case where  $R_2 = 0$  and  $V_2 = 0$ . In this case,  $\hat{A}_R = A$ ,  $\hat{R}_1 = R_1$ ,  $\hat{A}_E = A$ , and  $\hat{V}_1 = V_1$ . The properties of discrete-time high-authority LQG are analogous to the properties of continuous-time high-authority LQG given in [S5, pp. 281–289].

For simplicity, assume that  $y$ ,  $z$ ,  $u$ , and  $w$  are scalar signals. Consider the factorizations of the numerators  $N_{zu}$  and  $N_{yw}$  of  $G_{zu}$  and  $G_{yw}$ , respectively, given by

$$N_{zu} = H_{d_{zu}} N_{zu,s} N_{zu,u}, \quad (\text{S25})$$

$$N_{yw} = H_{d_{yw}} N_{yw,s} N_{yw,u}, \quad (\text{S26})$$

where  $d_{zu} \geq 0$  is the relative degree of  $G_{zu}$ ,  $H_{d_{zu}}$  is the first nonzero Markov parameter of  $G_{zu}$ ,  $d_{yw} \geq 0$  is the relative degree of  $G_{yw}$ ,  $H_{d_{yw}}$  is the first nonzero Markov parameter of  $G_{yw}$ , the roots of the monic polynomials  $N_{zu,s}$  and  $N_{yw,s}$  are the minimum-phase zeros of  $G_{zu}$  and  $G_{yw}$ , respectively, and the roots of the monic polynomials  $N_{zu,u}$  and  $N_{yw,u}$  are the NMP zeros of  $G_{zu}$  and  $G_{yw}$ , respectively. Note that  $H_{d_{zu}}$  is the leading nonzero coefficient of  $N_{zu}$ , and  $H_{d_{yw}}$  is the leading nonzero coefficient of  $N_{yw}$ . With this notation it follows that

$$\text{mspec}(A + BC_c) = \text{mzeros}(z^{d_{zu}} N_{zu,s}(z) N_{zu,u}(z^{-1})), \quad (\text{S27})$$

$$\text{mspec}(A - B_c C) = \text{mzeros}(z^{d_{yw}} N_{yw,s}(z) N_{yw,u}(z^{-1})), \quad (\text{S28})$$

where  $\text{mzeros}$  denotes the multiset of zeros of a rational function including multiplicity. Note that the zeros of  $N_{zu,u}(z^{-1})$  are the reflections across the unit circle (that is, the reciprocals) of the NMP zeros of  $G_{zu}$ . For example, if  $N_{zu,u}(z) = z - 1.2$ , then  $N_{zu,u}(z^{-1}) = (1 - 1.2z)/z$ . It follows from (S27) and (S28) that the closed-loop poles of high-authority LQG control are the zeros of

$$\tilde{D}_{\text{HA}}(z) = z^{d_{zu} + d_{yw}} N_{zu,s}(z) N_{zu,u}(z^{-1}) N_{yw,s}(z) N_{yw,u}(z^{-1}). \quad (\text{S29})$$

It thus follows from (S23) that  $\text{mspec}(\tilde{A}) = \text{mzeros}(\tilde{D}_{\text{HA}})$ . Similar observations are made for continuous-time systems in [S5] and for discrete-time systems in [42]. A surprising aspect of high-authority LQG control is that the poles and zeros of  $G_{yu}$ , which is present in the feedback loop and thus determines the gain and phase margins, do not affect the locations of the closed-loop poles.

### Example LQG1: High-Authority LQG Control for the Standard Problem with $y \neq z$ , with Stochastic $w$ Not Matched with $u$ , and with Minimum-Phase $G_{zu}$ , $G_{zw}$ , $G_{yu}$ , and $G_{yw}$

Consider the asymptotically stable, minimum-phase plant

$$A = \begin{bmatrix} 0.4 & 0.0958 & 0.1183 & 0.3162 \\ 0 & 0.81 & 1 & 0 \\ 0 & -0.1539 & 0.81 & 0.4813 \\ 0 & 0 & 0 & -0.5 \end{bmatrix}, \quad B = \begin{bmatrix} 0 \\ 0 \\ 0 \\ 1 \end{bmatrix}, \quad D_1 = \begin{bmatrix} -0.3807 \\ -0.2039 \\ 0.1771 \\ 0.8844 \end{bmatrix}, \quad (\text{S30})$$

$$C = [0.4456 \quad 0.0832 \quad -0.332 \quad -0.8272], \quad D_0 = 0, \quad D_2 = 0, \quad (\text{S31})$$

$$E_1 = [-0.274 \quad 0.2625 \quad 0.3241 \quad 0.8666], \quad E_0 = 0, \quad E_2 = 0. \quad (\text{S32})$$

The open- and closed-loop poles are shown in Figure S6. Note that  $\text{mspec}(A + BC_c)$  consists of the zeros of  $G_{zu}$  as well as zero with multiplicity one, while  $\text{mspec}(A - B_c C)$  consists of the zeros of  $G_{yw}$  as well as zero with multiplicity one. This example illustrates (S27) and (S28), which relate the closed-loop spectrum to the zeros of  $G_{zu}$  and  $G_{yw}$ . ■

### Example LQG2: High-Authority LQG Control for the Standard Problem with $y=z$ , with Stochastic $w$ Not Matched with $u$ , and with NMP $G_{zu}$ , $G_{zw}$ , $G_{yu}$ , and $G_{yw}$ , All of Which Have Different NMP Zeros

(continued)

## Discrete-Time LQG Control (Continued)

Consider the asymptotically stable, NMP plant

$$A = \begin{bmatrix} 0.81 & 1 & 0 \\ -0.1539 & 0.81 & 0.6998 \\ 0 & 0 & 0.5 \end{bmatrix}, \quad B = \begin{bmatrix} 0 \\ 0 \\ 1 \end{bmatrix}, \quad D_1 = \begin{bmatrix} 0.1841 \\ 0.1074 \\ 0.9770 \end{bmatrix}, \quad (S33)$$

$$C = [0.9280 \quad 0.1102 \quad 0.3558], \quad D_0 = 0, \quad D_2 = 0, \quad (S34)$$

$$E_1 = [0.4531 \quad -0.3513 \quad 0.8193], \quad E_0 = 0, \quad E_2 = 0. \quad (S35)$$

The open- and closed-loop poles are shown in Figure S7. Note that  $\text{mspec}(A + BC_c)$  consists of the reciprocals of the NMP zeros of  $G_{zu}$  as well as zero with multiplicity one, while  $\text{mspec}(A - B_c C)$  consists of the reciprocals of the NMP zeros of  $G_{yw}$  as well as zero with multiplicity one. This example illustrates

(S27) and (S28) in the case where both  $G_{yu}$  and  $G_{zw}$  are NMP. This example also shows that the NMP zeros of  $G_{zw}$  and  $G_{yu}$  have no effect on the closed-loop poles. ■

### REFERENCES

- [S5] H. Kwakernaak and R. Sivan, *Linear Optimal Control Systems*. New York: Wiley, 1972.
- [S6] K. Zhou, J. C. Doyle, and K. Glover, *Robust and Optimal Control*. Englewood Cliffs, NJ: Prentice Hall, 1996.
- [S7] W. M. Haddad, V. Kapila, and E. G. Collins, Jr., "Optimality conditions for reduced-order modeling, estimation, and control for discrete-time linear periodic plants," *J. Math. Syst. Est. Control*, vol. 6, pp. 437–460, 1996.
- [S8] V. Ionescu, C. Oara, and M. Weiss, *Generalized Riccati Theory and Robust Control*. New York: Wiley, 1999.

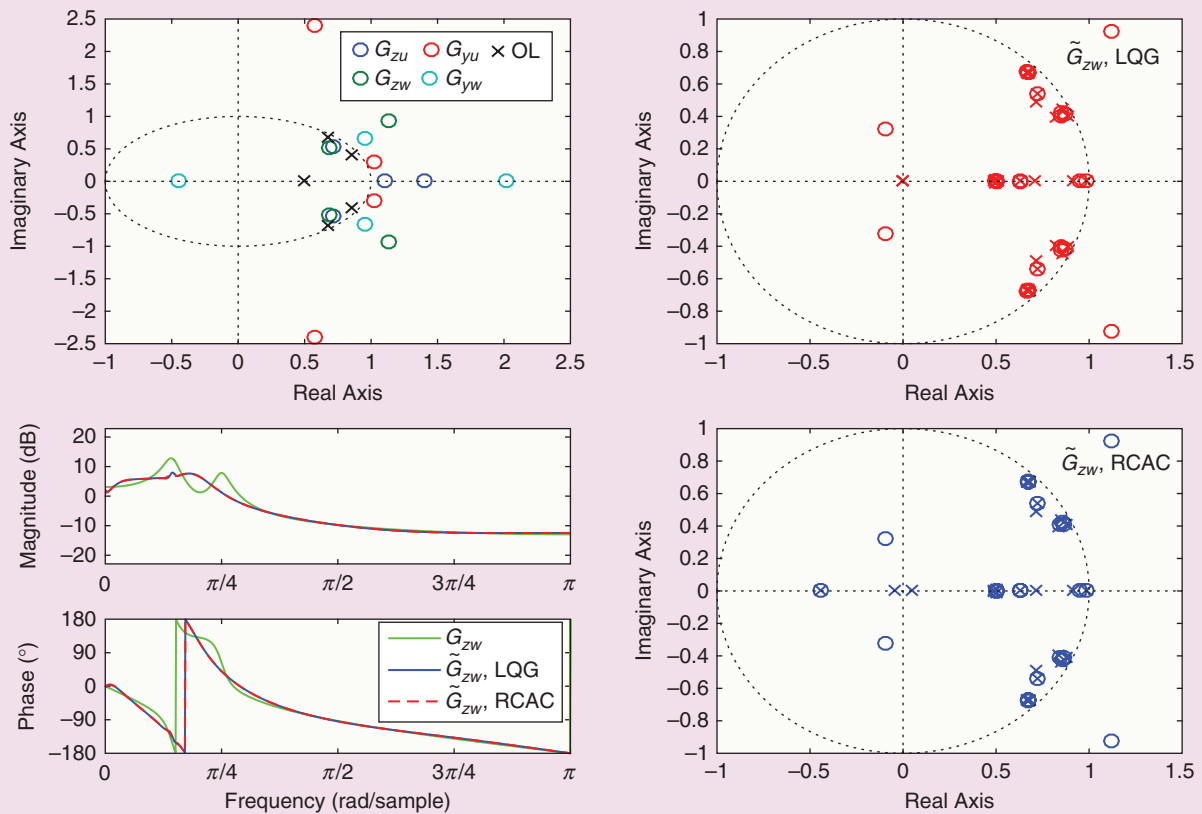


**FIGURE 17** Example SD1: Adaptive standard problem, with the high-authority linear-quadratic-Gaussian (LQG) target model (86). Retrospective cost adaptive control places the closed-loop poles near the high-authority LQG closed-loop poles and approximates the closed-loop frequency response of high-authority LQG. The frequency-response plots and closed-loop poles and zeros are shown at step  $k = 10^5$ .

**Example SD2: Adaptive Control with Nonzero-Mean, Stochastic  $w$  for the Adaptive Standard Problem**  
Consider the Lyapunov-stable, NMP plant

$$G(q) = \frac{(q - 0.5)(q^2 - 1.92q + 1.44)}{(q - 1)(q - 0.9)(q^2 - 1.62q + 0.81)}, \quad (90)$$

and let  $w$  be Gaussian white noise with mean 0.1 and standard deviation 0.05. The  $H_2$  cost of the LQG controller is 28.96. RCAC is applied with  $n_c = 5n = 20$  and the FIR target model (72), which uses no knowledge of  $\tilde{D}_{HA}$ . RCAC approximates the closed-loop frequency response of high-authority LQG except for the internal model of the disturbance bias, which has the form of a notch at dc, as shown in Figure 19.

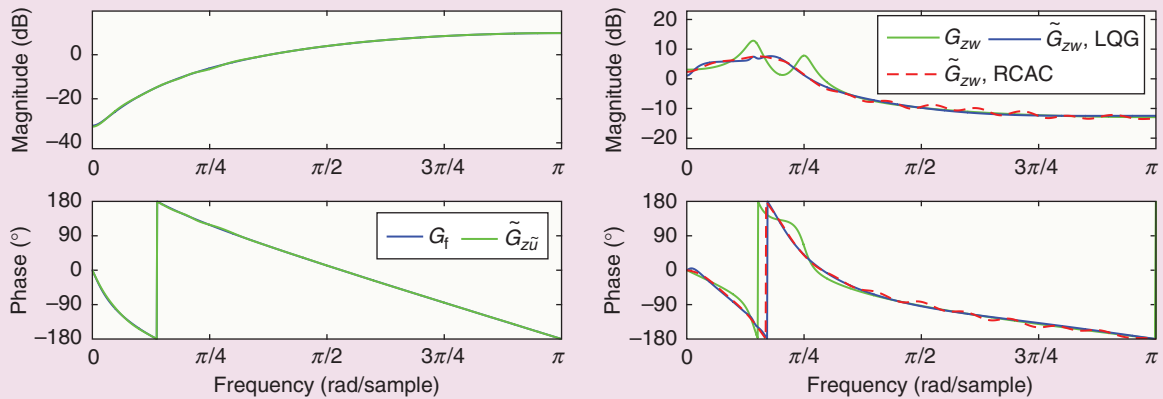


**FIGURE 18** Example SD1: Adaptive standard problem with  $n_c = 20$ . Retrospective cost adaptive control approximates the closed-loop frequency response of the high-authority linear-quadratic-Gaussian controller. In addition, the frequency response of  $\tilde{G}_{z\bar{u},k}$  approximates the frequency response of  $G_f$ . The frequency-response plots are shown at step  $k = 10^5$ .

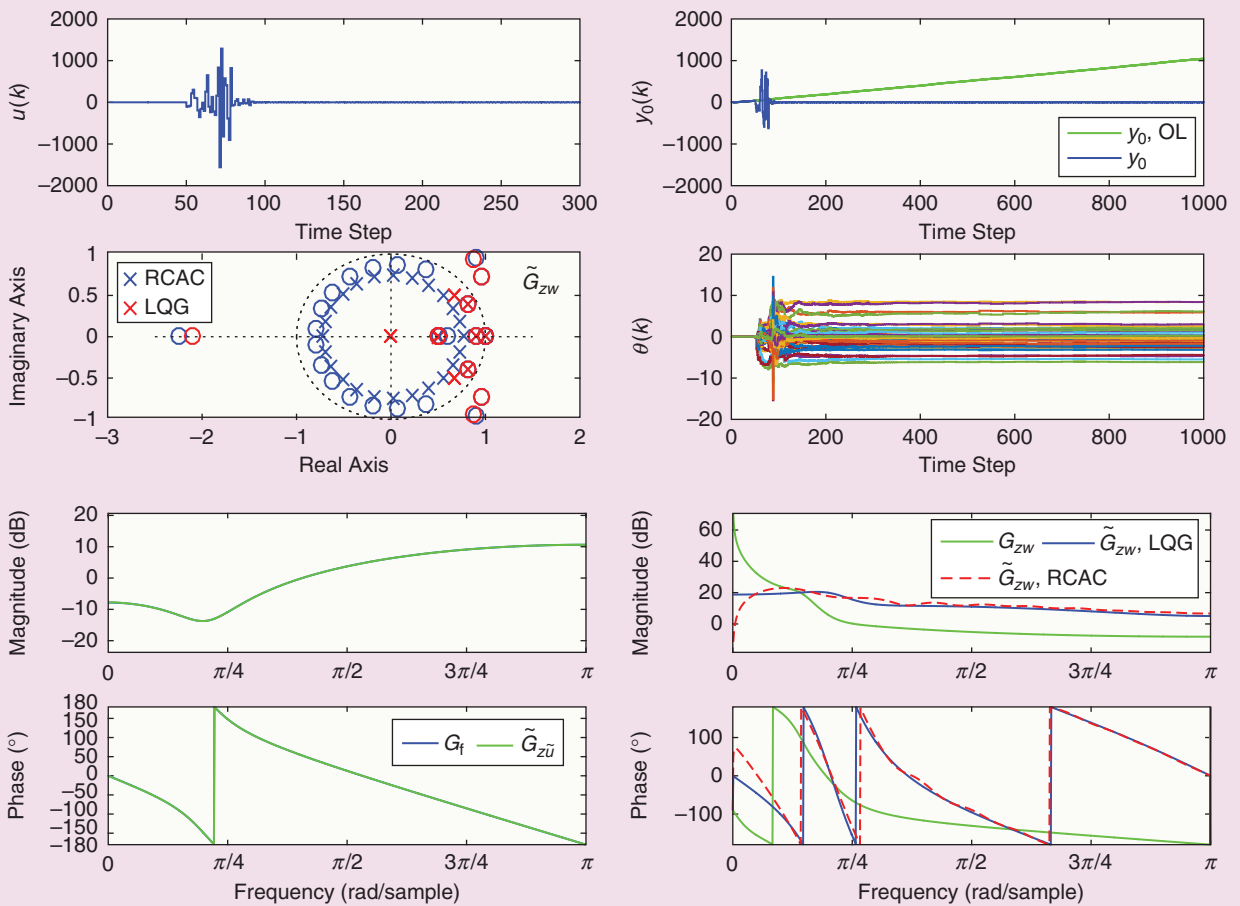


**FIGURE 19** Example SD2: Adaptive standard problem with  $n_c = 5n = 20$ . Retrospective cost adaptive control approximates the closed-loop frequency response of the high-authority linear-quadratic-Gaussian controller except at dc due to the internal model needed to reject the step disturbance. The internal model has the form of a notch at dc corresponding to the closed-loop zero at  $\mathbf{z} = 1$ . In addition, the frequency response of  $\tilde{G}_{z\bar{u},k}$  approximates the frequency response of  $G_f$ . The frequency-response plots and closed-loop poles and zeros are shown at step  $k = 10^5$ .

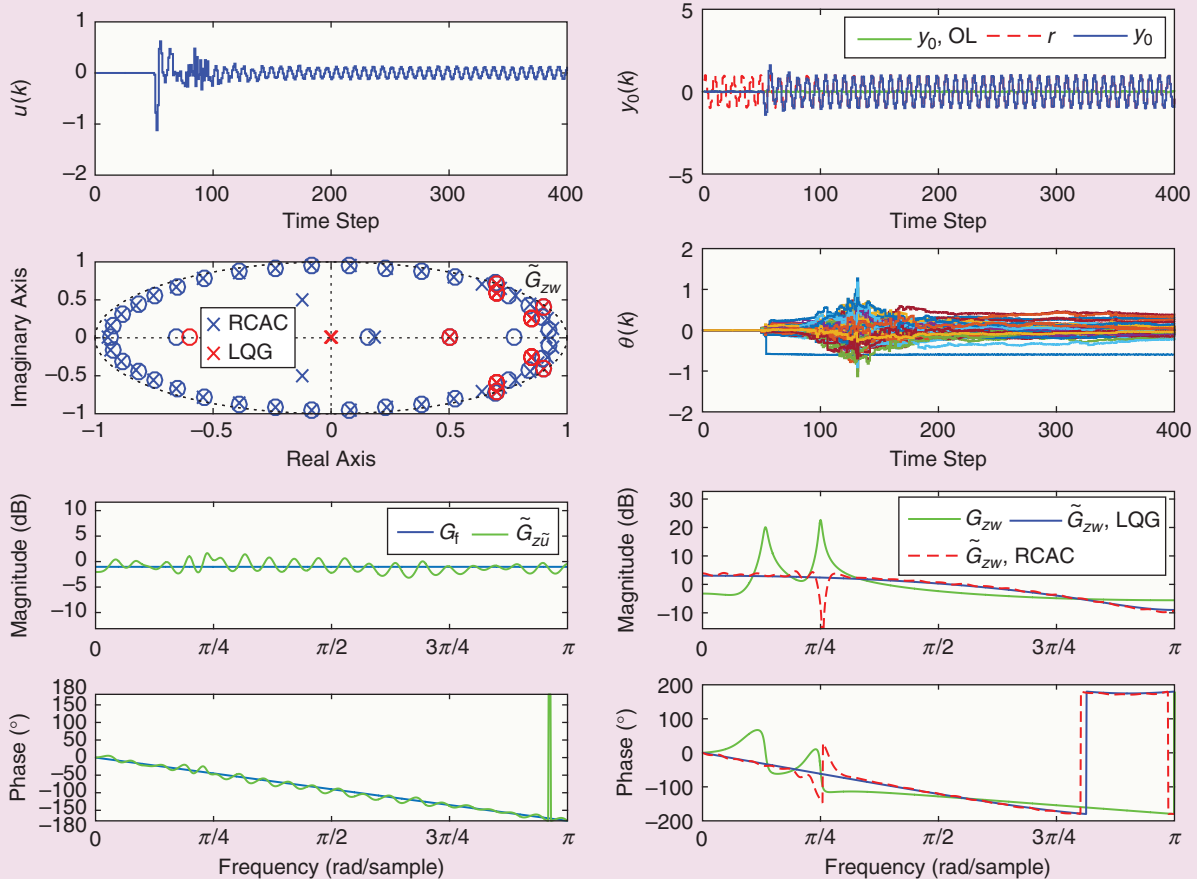


**FIGURE 20** Example SD3: Command following and stochastic disturbance rejection for the adaptive servo problem with  $n_c = 8n = 40$ . Retrospective cost adaptive control approximates the closed-loop frequency response of the high-authority linear-quadratic-Gaussian controller except at the command frequency due to the internal model. The internal model has the form of a notch at the command frequency corresponding to the two closed-loop zeros on the unit circle. The frequency-response plots and closed-loop poles and zeros are shown at step  $k = 10^5$ .

Note that RCAC automatically develops an internal model of the disturbance bias. The  $H_2$  cost of the RCAC controller is 35.79. ■

### Example SD3: Harmonic Command Following and Stochastic Disturbance Rejection for the Adaptive Servo Problem

Consider the asymptotically stable, minimum-phase plant

$$G(\mathbf{q}) = \frac{(\mathbf{q}^2 - 1.7\mathbf{q} + 0.785)(\mathbf{q}^2 - 1.4\mathbf{q} + 0.85)}{(\mathbf{q} - 0.5)(\mathbf{q}^2 - 1.8\mathbf{q} + 0.97)(\mathbf{q}^2 - 1.4\mathbf{q} + 0.98)}. \quad (91)$$

The  $H_2$  cost of the LQG controller is 1.072. Let  $r$  be the harmonic command  $r(k) = \cos \omega k$ , where  $\omega = 0.8$  rad/sample; let  $d$  be zero-mean Gaussian white noise with standard deviation 0.01, and let  $v = 0$ . RCAC is applied with  $n_c = 8n = 40$  and the FIR target model (71), which uses no knowledge of  $\tilde{D}_{\text{HA}}$ . RCAC asymptotically follows the harmonic command and approximates the closed-loop frequency response of high-authority LQG except at the command frequency due to

the internal model of the command, which has the form of a notch at the command frequency, as shown in Figure 20. As in Example SD2, RCAC automatically develops an internal model in response to the harmonic command. The  $H_2$  cost of the RCAC controller is 1.15. ■

The examples in this section show that, as  $G_{c,k}$  adapts, the frequency response of  $\tilde{G}_{z\tilde{u}}$  tends to the frequency response of  $G_f$ . It is also shown that, for sufficiently large  $n_c > n$ , the frequency response of the closed-loop transfer function  $\tilde{G}_{zw}$  obtained from RCAC with the FIR target models (71) and (72) approximates the closed-loop frequency response and  $H_2$  cost of high-authority LQG. In addition, for command following and disturbance rejection, RCAC matches the frequency response of high-authority LQG at nearly all frequencies, apart from the command frequency, where RCAC places an internal model.

### EFFECT OF SENSOR NOISE

In all of the examples considered so far, the measurement  $y$  is not corrupted by noise. In contrast, the examples in this

section consider the adaptive servo problem with stochastic sensor noise  $v$ . Difficulties arising from sensor noise in adaptive control systems are considered in [40] and [75].

### Example SN1: Pole Placement for the Adaptive Servo Problem with Sensor Noise

Consider the unstable, minimum-phase plant

$$G(q) = \frac{q^2 - 1.4q + 0.85}{(q - 1.1)(q^2 - 1.8q + 1.06)}. \quad (92)$$

Let  $r$  be the harmonic command  $r(k) = \cos \omega k$ , where  $\omega = 0.3$  rad/sample, and let  $d = v = 0$ . RCAC is applied with  $R_\theta = 10^{-10} I_{l_\theta}$ ,  $R_u = 0$ , and  $n_c = 6$ . To place four closed-loop poles at  $0, 0.5, \pm 0.1j$ , the IIR target model (73) is used with

$$D_p(q) = q^4 - 0.5q^3 + 0.01q^2 - 0.005q. \quad (93)$$

RCAC places closed-loop poles near the locations of the roots of  $D_p$ , as shown in Figure 21. Now let  $v$  be zero-mean Gaussian white noise with standard deviation  $\sigma$ . For  $\sigma = 0.1$ , RCAC fails to place closed-loop poles near the locations of the roots of  $D_p$  but stabilizes the plant at step  $k = 500$ . For  $\sigma = 0.2$ , RCAC fails to place closed-loop poles near the locations of the roots of  $D_p$ , and the closed-loop system is unstable at step  $k = 500$  (not shown). ■

### Example SN2: Stochastic Disturbance Rejection for the Adaptive Servo Problem with Sensor Noise

Consider the asymptotically stable, minimum-phase plant

$$A = \begin{bmatrix} 0.9 & 1 & 0 & 0 & 0 \\ 0 & 0.95 & -0.1507 & -0.1674 & 0.5189 \\ 0 & 0 & 0.65 & 1 & 0 \\ 0 & 0 & -0.4225 & 0.65 & 0.434 \\ 0 & 0 & 0 & 0 & 0.95 \end{bmatrix}, \quad B = D_1 = \begin{bmatrix} 0 \\ 0 \\ 0 \\ 0 \\ 1 \end{bmatrix}, \quad (94)$$

$$C = E_1 = [0.1596 \quad 0.3991 \quad -0.2405 \quad -0.2672 \quad 0.8283], \\ D_0 = E_0 = E_2 = 0, \quad D_2 = 1. \quad (95)$$

Let  $d$  and  $v$  be zero-mean Gaussian white noise signals with standard deviation  $\sigma = 1$ . RCAC is applied with  $k_w = 50$ ,  $R_\theta = 10^{-20} I_{l_\theta}$ ,  $R_u = 0$ ,  $n_c = 4n = 20$ , and the FIR target model (71). Instead of approximating the closed-loop frequency response of high-authority LQG, RCAC approximates the closed-loop frequency response of the LQG controller designed for the actual sensor noise level, namely,  $V_2 = 1$ , as shown in Figure 22. ■

### Example SN3: Step Command Following and Stochastic Disturbance Rejection for the Adaptive Servo Problem with Sensor Noise

Consider the asymptotically stable, minimum-phase plant

$$A = \begin{bmatrix} 0.8882 & 1 & 0 & 0 & 0 \\ -0.1715 & 0.8882 & -0.3624 & -0.3238 & 0.6679 \\ 0 & 0 & 0.693 & 1 & 0 \\ 0 & 0 & -0.4802 & 0.693 & 0.7276 \\ 0 & 0 & 0 & 0 & 0.5 \end{bmatrix}, \\ B = \begin{bmatrix} 0 \\ 0 \\ 0 \\ 0 \\ 1 \end{bmatrix}, \quad \bar{D}_1 = \begin{bmatrix} 0.5537 \\ 0.0603 \\ -0.5457 \\ 0.5596 \\ -0.2806 \end{bmatrix}, \quad (96)$$

$$\bar{C} = [0.2158 \quad 0.4234 \quad -0.3861 \quad -0.3449 \quad 0.7115], \quad \bar{D}_0 = 0. \quad (97)$$

Let  $r$  be a unit step command, let  $d$  be zero-mean Gaussian white noise with standard deviation 0.05, and let  $v$  be zero-mean Gaussian white noise with standard deviation 0.025. To account for the standard deviation of the sensor noise, it follows from (26) that

$$V_2 = 0.025 D_2 D_2^T = 0.025 [1 \quad 0 \quad -1] [1 \quad 0 \quad -1]^T = 0.05. \quad (98)$$

RCAC is applied with  $R_\theta = 10^{-10} I_{l_\theta}$ ,  $R_u = 0$ ,  $n_c = 8n = 40$ , and the FIR target model (71). RCAC asymptotically follows the step command and approximates the closed-loop frequency response of LQG except at dc due to the internal model of the command, which has the form of a notch at dc, as shown in Figure 23. For this example, RCAC approximates the closed-loop frequency response of the LQG controller designed for the actual sensor noise level, namely,  $V_2 = 0.05$ . ■

The examples in this section investigate the effect of sensor noise on the closed-loop performance of RCAC. Example SN1 shows that, as the level of the sensor noise increases, RCAC fails to place closed-loop poles near the target locations but does stabilize the system. Examples SN2 and SN3 show that RCAC approximates the closed-loop frequency response of LQG in the presence of sensor noise.

## ROBUSTNESS TO ERRONEOUS AND UNMODELED NONMINIMUM-PHASE ZEROS

As shown by the construction of  $G_f$  given by (71)–(74), the modeling information required by RCAC is  $d_{zu}$ ,  $H_{d_{zu}}$ , and the NMP zeros of  $G_{zu}$ . This section investigates the effect of erroneous and unmodeled NMP zeros by considering four examples. The first example considers erroneous estimates of real and complex NMP zeros for the adaptive servo problem. Next, we consider an unmodeled change in the location of the NMP zero during operation. The third example considers unmodeled NMP sampling zeros for a sampled-data system. The final example considers an unstable plant with an unmodeled NMP zero.

### Example NMP1: Erroneous NMP-Zero Estimates for the Adaptive Servo Problem

Consider the unstable, NMP plant

$$G(q) = \frac{(q - 0.95)(q - 0.975)(q - 1.1)}{(q - 0.99)(q - 1.01)(q^2 - 1.4q + 1.13)}. \quad (99)$$

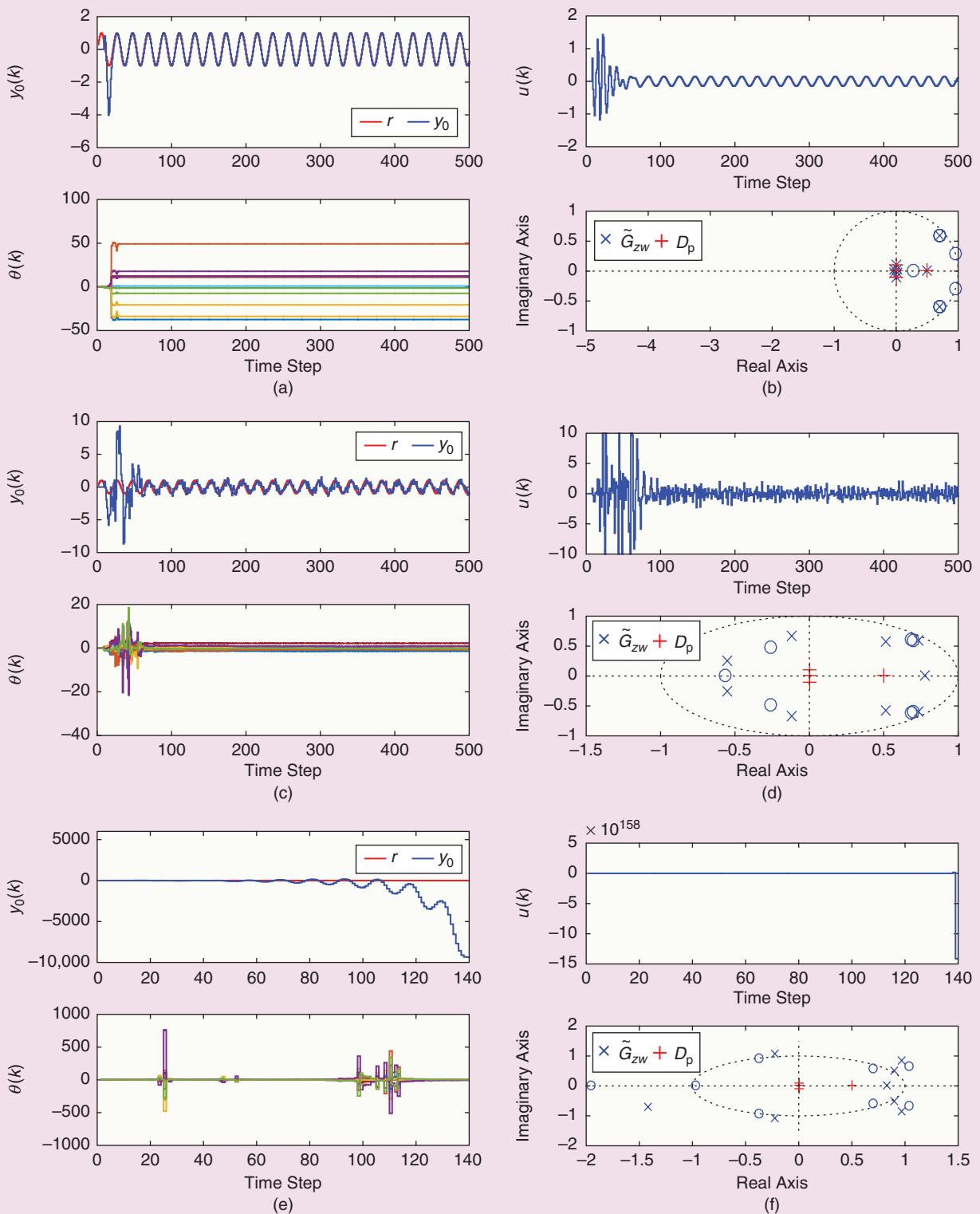


**FIGURE 21** Example SN1: Pole placement for the adaptive servo problem (a) and (b) without sensor noise as well as with zero-mean Gaussian white sensor noise  $v$  with  $\sigma = 0.1$  (c) and (d) and  $\sigma = 0.2$  (e) and (f). In the case where  $v = 0$ , retrospective cost adaptive control (RCAC) places closed-loop poles near the locations of the roots of  $D_p$ . For  $\sigma = 0.1$ , RCAC fails to place closed-loop poles near the locations of the roots of  $D_p$  but stabilizes the plant. For  $\sigma = 0.2$ , RCAC fails to place closed-loop poles near the locations of the roots of  $D_p$ , and the closed-loop system is unstable at step  $k = 500$ . The closed-loop poles and zeros are shown at step  $k = 500$ .

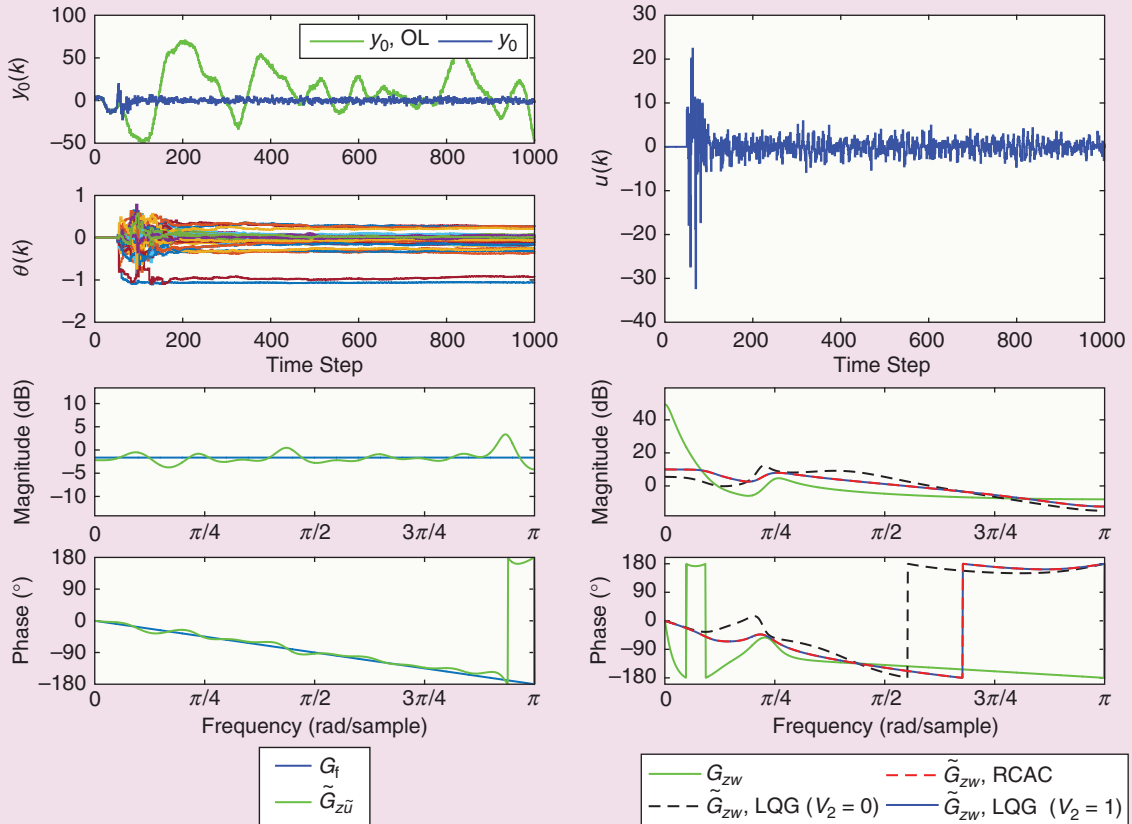


**FIGURE 22** Example SN2: Stochastic disturbance rejection for the adaptive servo problem with zero-mean Gaussian white sensor noise. Retrospective cost adaptive control approximates the closed-loop frequency response of the linear-quadratic-Gaussian controller for  $V_2 = 1$ . In addition, the frequency response of  $\tilde{G}_{z\tilde{u},k}$  approximates the frequency response of  $G_i$ . The frequency-response plots are shown at step  $k = 10^5$ .

Let  $r$  be the harmonic command  $r(k) = \cos \omega k$ , where  $\omega = 0.01$  rad/sample, and let  $d = v = 0$ . The target model  $G_f(\mathbf{q}) = H_{d_{zn}}(\mathbf{q} - 1.265)/\mathbf{q}^2$  is used, where the estimate 1.265 of the NMP zero 1.1 is erroneous by 15%, and set  $R_\theta = 0.1I_{l_\theta}$ ,  $R_u = 0$ , and  $n_c = 12$ . Figure 24 shows the command-following performance. Figure 25 shows the NMP-zero estimates for which RCAC asymptotically follows the harmonic command as well as the NMP-zero estimates for which the closed-loop system becomes unstable. Figure 25 shows that, for the plant (99), RCAC is more robust to overestimation of the NMP zero than underestimation.

Next, let  $d$  be zero-mean Gaussian white noise with standard deviation 0.5. Figure 25 also shows the NMP-zero estimates for which RCAC asymptotically follows the harmonic command as well as the NMP-zero estimates for which the closed-loop system becomes unstable. Figure 25 shows that, for the plant (99), RCAC is less robust to erroneous NMP-zero estimates in the case of stochastic disturbances than in the case of harmonic commands.

Next, consider the asymptotically stable plant with complex NMP zeros given by

$$G(\mathbf{q}) = \frac{\mathbf{q}^2 - 2.1\mathbf{q} + 1.1125}{(\mathbf{q} - 0.999)(\mathbf{q}^2 - 1.9\mathbf{q} + 0.9125)}. \quad (100)$$

Let  $r$  be the harmonic command  $r(k) = \cos \omega k$ , where  $\omega = 0.01$  rad/sample, and let  $d = v = 0$ . The target model  $G_f(\mathbf{q}) = H_{d_{zn}}(\mathbf{q} - \hat{\xi}_1)(\mathbf{q} - \hat{\xi}_2)/\mathbf{q}^2$  is used, where  $\hat{\xi}_1$  and  $\hat{\xi}_2$  are estimates of the NMP zeros  $1.05 \pm 0.1j$ . Figure 26 shows the locations of the NMP-zero estimates for which RCAC asymptotically follows the harmonic command as well as the NMP-zero estimates for which the closed-loop system becomes unstable. ■

#### Example NMP2: Unmodeled Change in the NMP Zeros for the Adaptive Standard Problem

Consider the asymptotically stable, minimum-phase plant

$$G(\mathbf{q}) = \frac{(\mathbf{q} - 0.5)(\mathbf{q}^2 - 1.92\mathbf{q} + 1.44)}{(\mathbf{q} - 0.35)(\mathbf{q} - 0.6)(\mathbf{q}^2 - 0.8\mathbf{q} + 0.32)}, \quad (101)$$

and let  $w$  be zero-mean Gaussian white noise with standard deviation 0.01. RCAC is applied with  $R_\theta = 10^{-5}I_{l_\theta}$ ,

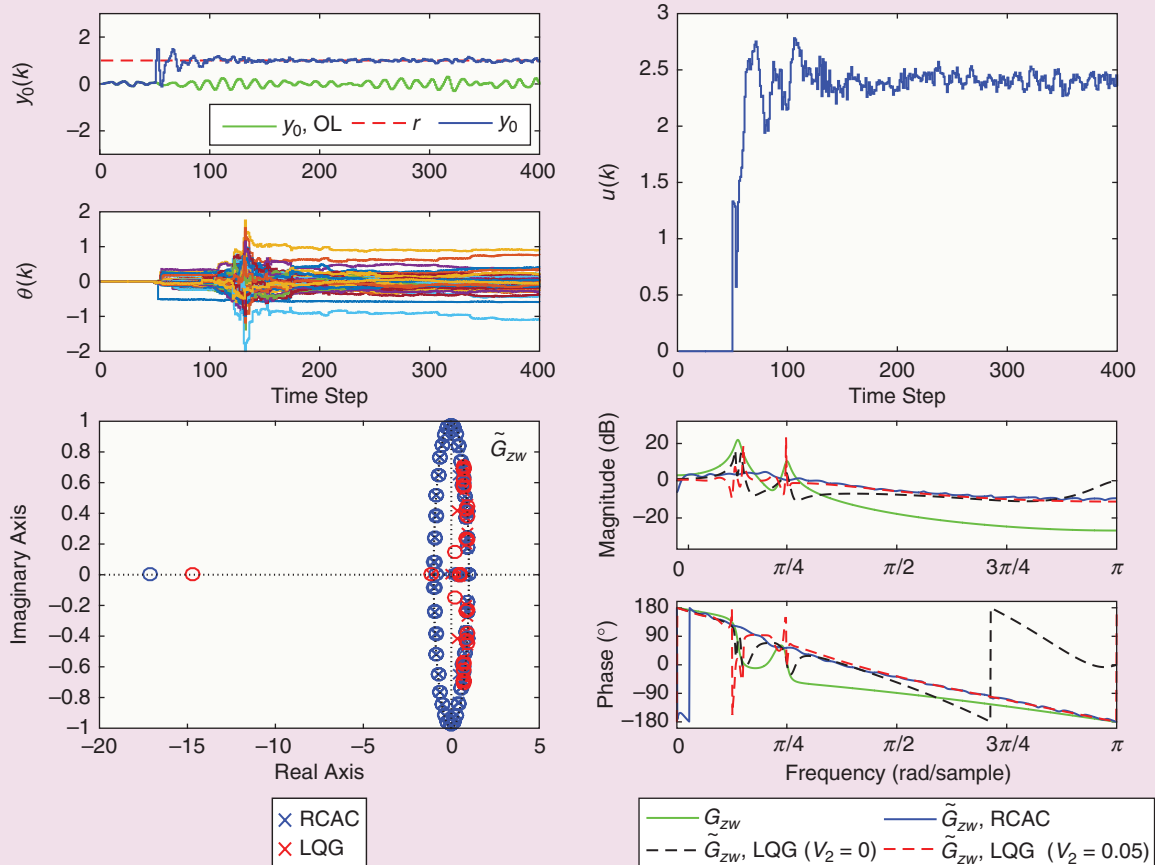


**FIGURE 23** Example SN3: Command following and stochastic disturbance rejection for the adaptive servo problem with zero-mean Gaussian white sensor noise. Retrospective cost adaptive control (RCAC) approximates the closed-loop frequency response of linear-quadratic Gaussian (LQG) for  $V_2 = 2$  except at dc due to the internal model. The internal model has the form of a notch at dc corresponding to the closed-loop zero at  $z = 1$ . For this example, RCAC approximates the closed-loop frequency response of LQG in the presence of sensor noise. The frequency-response plots and closed-loop poles and zeros are shown at step  $k = 10^5$ .

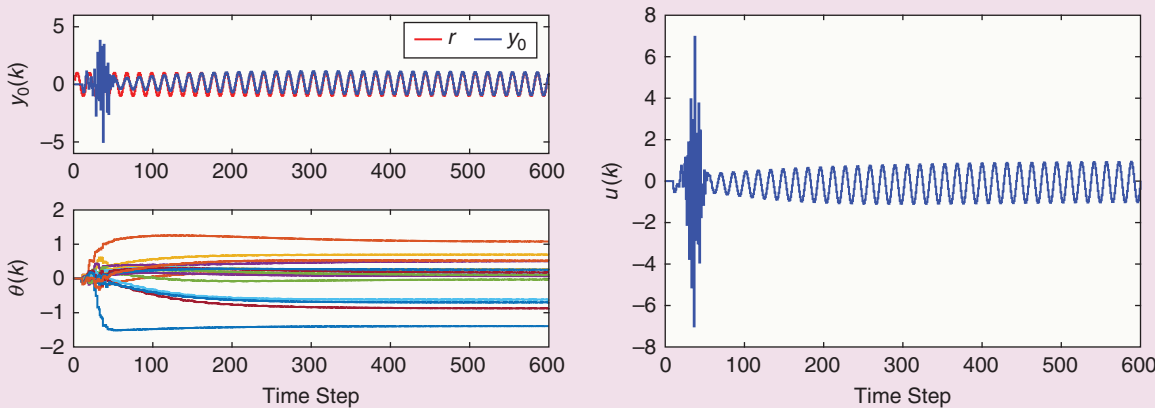


**FIGURE 24** Example NMP1: Erroneous nonminimum-phase (NMP)-zero estimates for the adaptive servo problem. Retrospective cost adaptive control automatically develops an internal model of the command and asymptotically follows the command despite a 15% error in the estimate of the NMP zero used by  $G_f$ .

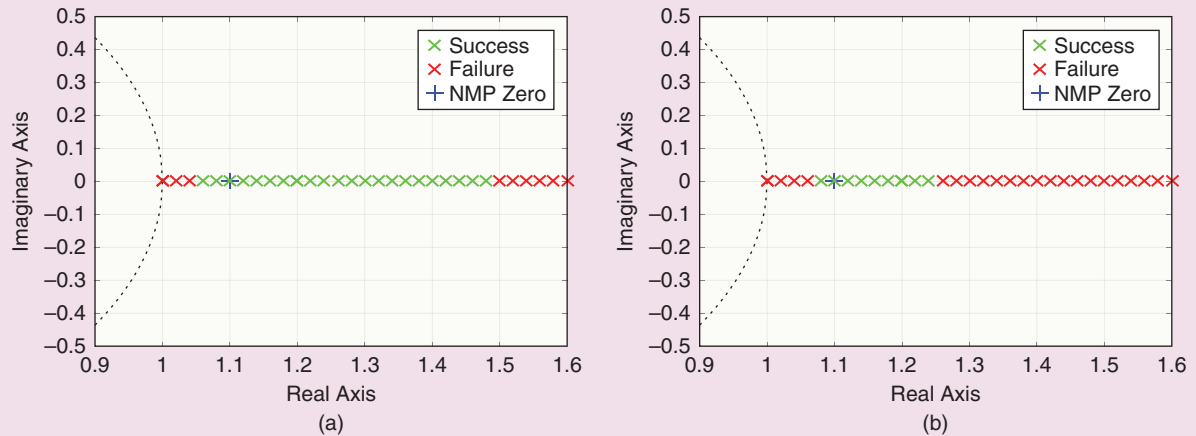


**FIGURE 25** Example NMP1: Erroneous nonminimum-phase (NMP)-zero estimates for the adaptive servo problem. In the case where  $d = 0$  and the command is harmonic, (a) shows the NMP-zero estimates for which retrospective cost adaptive control (RCAC) asymptotically follows the harmonic command as well as the NMP-zero estimates for which the closed-loop system becomes unstable. In the case where the command is harmonic and  $d$  is zero-mean Gaussian white noise with standard deviation 0.5, (b) shows the NMP-zero estimates for which RCAC asymptotically follows the harmonic command as well as the NMP-zero estimates for which the closed-loop system becomes unstable. Note that RCAC is less robust to erroneous NMP-zero estimates in the case of stochastic disturbance rejection than in the case of harmonic commands following. For this example, RCAC is more robust to overestimation of the NMP zero than it is to underestimation.

$R_u = 0.1z^2$ ,  $n_c = 4$ , and the IIR target model (74) with the roots of  $D_p(\mathbf{q})$  chosen as the closed-loop poles of high-authority LQG. RCAC approximates the closed-loop frequency response of high-authority LQG, as shown in Figure 27. At step  $k = 5000$ , the plant dynamics change so that the NMP zeros move from  $0.96 \pm 0.72j$  to  $0.99 \pm 1.38j$ . If  $G_{c,k}$  is fixed to be  $G_{c,5000}$ , then the closed-loop system becomes unstable. However, under continued adaptation, the plant is restabilized, and RCAC approximates the closed-loop frequency response of high-authority LQG for the modified plant, as shown in Figure 27. ■

### Example NMP3: Unmodeled NMP Sampling Zero for the Adaptive Servo Problem

Consider the asymptotically stable, continuous-time plant  $T(s) = \Lambda(s)T_0(s)$ , where

$$\Lambda(s) = \frac{229}{(s - 15 + 2j)(s - 15 - 2j)}, \quad T_0(s) = \frac{2}{s + 1}, \quad (102)$$

where  $\Lambda(s)$  represents unmodeled high-frequency dynamics [40]. Since the relative degree of  $T_0(s)$  is one, the discrete-time sampled-data plant  $G_0(z)$  obtained by discretizing  $T_0(s)$  does not yield any sampling zeros [76]. However, since the relative degree of  $T(s)$  is three, the discrete-time, sampled-data plant  $G(z)$  obtained by discretizing  $T(s)$  possesses two sampling zeros due to  $\Lambda(s)$ . It is shown in [41] that, if the sampling period  $h \leq 0.2$ , then one of the sampling zeros is NMP. Since  $\Lambda(s)$  represents unmodeled dynamics, neither the presence nor the location of this NMP zero can be assumed to be known. The parameter choice  $h = 0.1$  results in  $G$  having an NMP sampling

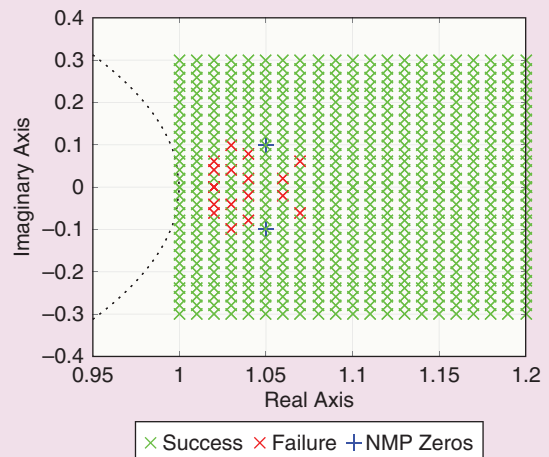


**FIGURE 26** Example NMP1: Erroneous nonminimum-phase (NMP)-zero estimates for the adaptive servo problem. In the case where the NMP zeros are complex, this plot shows the NMP-zero estimates for which retrospective cost adaptive control (RCAC) asymptotically follows the harmonic command as well as the NMP-zero estimates for which the closed-loop system becomes unstable. For this example, RCAC is more robust to overestimation of the NMP zeros than underestimation.

zero at  $-2.1481$  and a minimum-phase sampling zero at  $-0.0672$ . Let  $r$  be the harmonic command  $r(k) = \cos \omega k$ , where  $\omega = 0.2$  rad/sample, and let  $d = v = 0$ . RCAC is applied with  $R_\theta = 10I_{10}$ ,  $R_u = 0.1z^2$ ,  $n_c = 10$ , and the minimum-phase FIR target model (71). RCAC avoids unstable pole-zero cancellation and asymptotically follows the

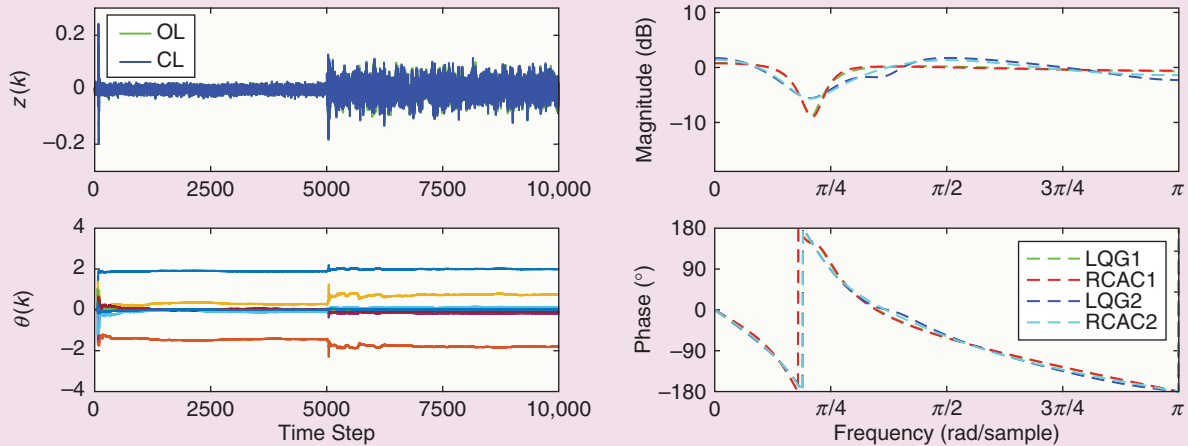


**FIGURE 27** Example NMP2: Unmodeled change in the nonminimum-phase (NMP) zeros for the adaptive standard problem. At step  $k = 5000$ , the NMP zeros move to  $0.99 \pm 1.38j$ . If  $G_{c,k}$  is fixed to be  $G_{c,5000}$ , then the closed-loop system becomes unstable. With continued adaptation, however, the plant is restabilized. LQG1 is the high-authority linear-quadratic-Gaussian (LQG) controller for  $G$  with NMP zeros at  $0.96 \pm 0.72j$  whereas LQG2 is the high-authority LQG controller for  $G$  with NMP zeros at  $0.99 \pm 1.38j$ . RCAC1 and RCAC2 are the corresponding retrospective cost adaptive control (RCAC) controllers.

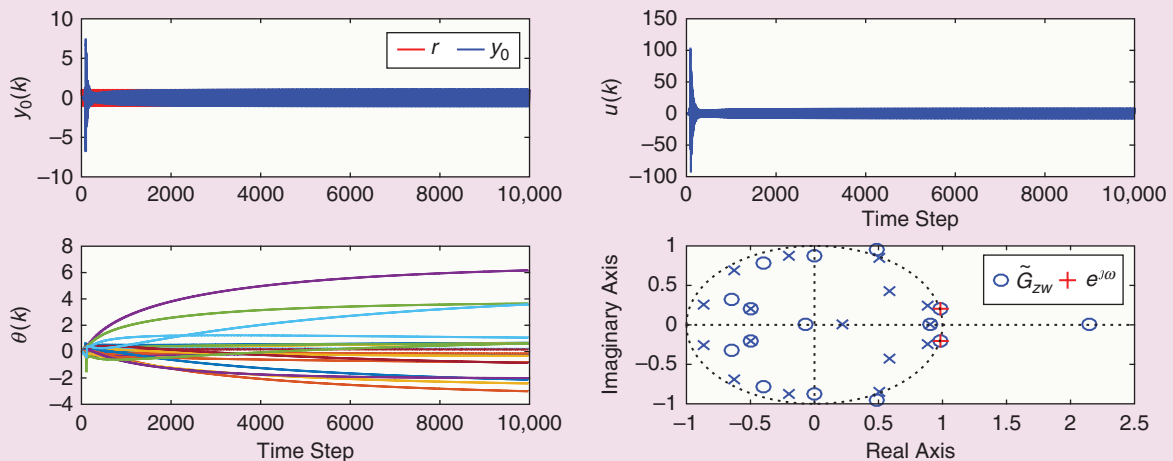


**FIGURE 28** Example NMP3: Unmodeled nonminimum-phase (NMP) sampling zero for the adaptive servo problem. Retrospective cost adaptive control (RCAC) automatically develops an internal model of the harmonic command signal by placing controller poles at the command frequency, and  $\tilde{G}_{zw}$  is asymptotically stable at step  $k = 10,000$ . The internal-model poles of the controller are evident in the form of two closed-loop zeros on the unit circle at the command frequency, which are shown by the red plus signs. For this example, the performance-dependent control weighting  $R_u$  allows RCAC to asymptotically follow the command for a sampled-data plant with an unmodeled NMP zero. The closed-loop poles and zeros are shown at step  $k = 10^4$ .

command without knowledge of the unmodeled NMP zero, as shown in Figure 28. ■

#### Example NMP4: Unmodeled NMP Zero for the Adaptive Servo Problem

Consider the unstable, NMP double integrator

$$G(q) = \frac{q - 1.15}{(q - 1)^2}. \quad (103)$$

Let  $r$  be the harmonic command  $r(k) = \cos \omega k$ , where  $\omega = 0.55$  rad/sample, and let  $d = v = 0$ . RCAC is applied

with  $R_\theta = 10^4 I_{l_\theta}$ ,  $R_u = z^2$ , and  $n_c = 6$ . Assuming that the NMP zero of  $G$  is unmodeled, the FIR target model (71) is used. Figure 29 shows the command-following performance. As  $z$  becomes unbounded, the term  $\sum_{i=1}^k \lambda^{k-i} \hat{\theta}^T \Phi_i^T(i) R_u(i) \Phi_i(i) \hat{\theta}$  in (42) dominates the remaining terms, and  $u$  converges to zero. Therefore, the closed-loop system reverts to the unstable open-loop plant, and RCAC does not follow the harmonic command. For this unstable plant, RCAC is not robust to unmodeled NMP zeros, despite using the performance-dependent control weighting  $R_u = z^2$ . ■

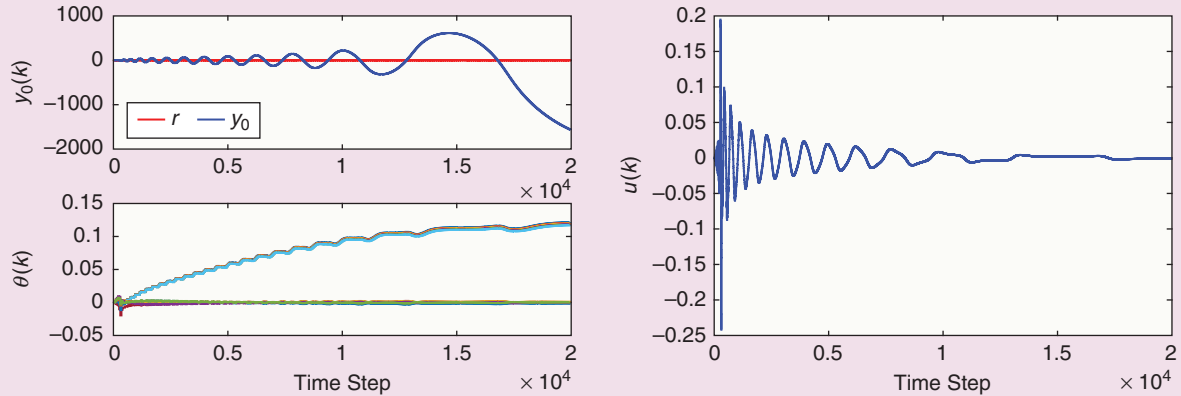


**FIGURE 29** Example NMP4: Unmodeled nonminimum-phase (NMP) zero for the adaptive servo problem. Retrospective cost adaptive control (RCAC) does not follow the harmonic command, and, as  $z$  becomes unbounded, the closed-loop system tends to the unstable open-loop plant. For this unstable example, RCAC is not robust to unmodeled NMP zeros, despite using the performance-dependent control weighting  $R_u = z^2$ .

The examples in this section investigate the robustness of RCAC to modeling errors in the target model. For Example NMP1, RCAC is less robust to erroneous NMP-zero estimates in the case of stochastic disturbance rejection than in the case of harmonic command following. For Example NMP2, where the NMP zeros are uncertain, performance-dependent cost regularization, that is, choosing  $R_u$  to be a function of  $z$ , improves the robustness of RCAC to uncertainty in the location of the NMP zero. For Rohrs's counterexample involving unmodeled dynamics [40], Example NMP3 shows that, with performance-dependent regularization, RCAC stabilizes the closed-loop system. Example NMP4 shows that unstable plants with uncertain NMP zeros are difficult for RCAC to control.

### ROBUSTNESS TO ERRONEOUS RELATIVE DEGREE AND UNMODELED DELAY

This section investigates the effect of erroneous relative degree and unmodeled delays by considering three examples that involve critical changes in the plant during operation. The first example considers the effect of erroneous estimates of the relative degree of  $G_{zu}$ . The next example considers unmodeled time delays both in the initial modeling of the system and during operation. Finally, RCAC is applied to a plant with limited achievable delay margin, and the effect of unmodeled time delays exceeding the delay margin is investigated. In all cases, design guidelines for each type of modeling error are provided.

#### Example DM1: Erroneous $d_{zu}$ for the Adaptive Servo Problem

Consider the asymptotically stable, minimum-phase plant

$$G(\mathbf{q}) = \frac{\mathbf{q} - 0.95}{(\mathbf{q} - 0.85)(\mathbf{q}^2 - 1.5\mathbf{q} + 0.985)}. \quad (104)$$

Let  $r$  be the harmonic command  $r(k) = \cos \omega k$ , where  $\omega = 0.15$  rad/sample, and let  $d = v = 0$ . RCAC is applied with  $R_\theta = 10I_{l_\theta}$ ,  $R_u = 0$ , and  $n_c = 6$ . For  $G$  given by (104),  $d_{zu} = 2$ . The FIR target model (71) is used, but with  $d_{zu}$  replaced by  $\hat{d}_{zu}$ , where  $\hat{d}_{zu}$  is an estimate of  $d_{zu}$ . Figure 30 shows the command-following performance for  $\hat{d}_{zu} = 1$ ,  $\hat{d}_{zu} = 3$ , and  $\hat{d}_{zu} = 4$ . For  $\hat{d}_{zu} = 3$  and  $\hat{d}_{zu} = 4$ , RCAC asymptotically follows the harmonic command. For  $\hat{d}_{zu} = 1$ , however, RCAC does not follow the harmonic command, and the plant output  $y_0$  diverges. RCAC asymptotically follows the command for  $2 \leq \hat{d}_{zu} \leq 4$ . Moreover, by using  $R_u = z^2$ , RCAC asymptotically follows the command for  $1 \leq \hat{d}_{zu} \leq 10$ . For this example, RCAC is more robust to overestimation of  $d_{zu}$  than underestimation of  $d_{zu}$ . Note that  $\hat{d}_{zu} > d_{zu}$  accounts for an unmodeled time delay of  $\hat{d}_{zu} - d_{zu}$  steps in the sense that, if the plant experiences an unmodeled time delay of  $\hat{d}_{zu} - d_{zu}$  steps, then  $\hat{d}_{zu}$  is the true relative degree. The next example considers time delay directly. ■

#### Example DM2: Unmodeled Time Delay for the Adaptive Servo Problem

Consider the asymptotically stable, minimum-phase plant  $G = G_{TD}G_0$ , where

$$G_{TD}(\mathbf{q}) \triangleq \mathbf{q}^{-k_d}, \quad G_0(\mathbf{q}) = \frac{\mathbf{q} - 0.9}{(\mathbf{q} - 0.95)(\mathbf{q}^2 - 1.6\mathbf{q} + 0.89)}, \quad (105)$$

and  $G_{TD}$  represents an unmodeled time delay of  $k_d$  steps. Let  $r$  be the harmonic command  $r(k) = \cos \omega k$ , where  $\omega = 0.1$  rad/sample, and let  $d = v = 0$ . RCAC is applied with  $R_\theta = 100I_{l_\theta}$ ,  $R_u = 0.1z^2$ , and  $n_c = 10$ . Since  $G_{TD}$  is unmodeled, the FIR target model (71) based on  $G_0$  is used. Figure 31 shows the command-following error  $e_0$  for  $k_d = 1$ ,  $k_d = 2$ ,  $k_d = 3$ , and  $k_d = 4$ . RCAC asymptotically follows the harmonic command in each case.

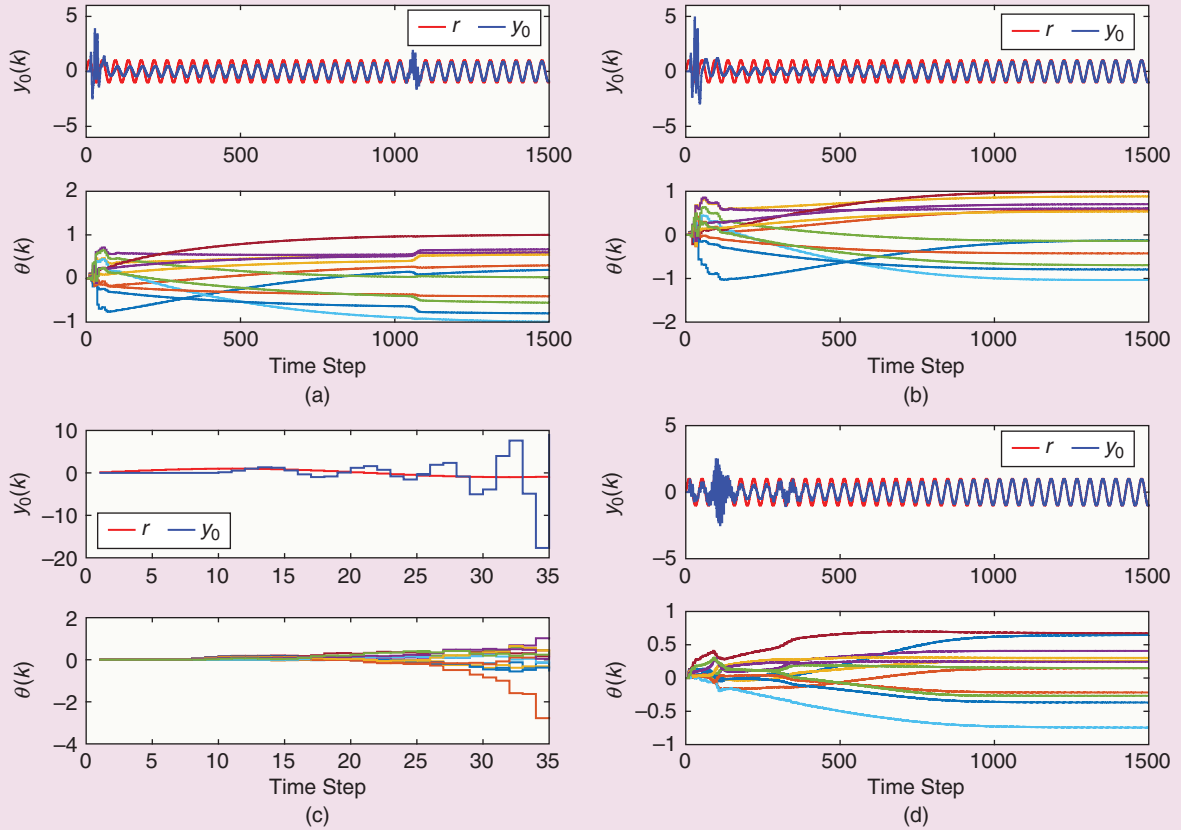


**FIGURE 30** Example DM1: Effect of erroneous relative degree on command-following performance for the adaptive servo problem. For (a)  $\hat{d}_{zu} = 3$  and (b)  $\hat{d}_{zu} = 4$ , retrospective cost adaptive control (RCAC) asymptotically follows the harmonic command. For (c)  $\hat{d}_{zu} = 1$ , RCAC does not follow the harmonic command, and the plant output  $y_0$  diverges. However, by using the performance-dependent control weighting (d)  $R_u = z^2$ , RCAC asymptotically follows the harmonic command, although the transient response is poor. For this example, RCAC is robust to overestimation of  $\hat{d}_{zu}$  but is less robust to underestimation of  $\hat{d}_{zu}$ .

Next, let  $r(k) = \cos \omega k$ , where  $\omega = 0.5$  rad/sample, and let  $\hat{d} = v = 0$ . RCAC is applied with  $R_\theta = 0.1I_{l_\theta}$ ,  $R_u = 0.1z^2$ ,  $n_c = 15$ , and the FIR target model (71). At step  $k = 15,000$ , an unmodeled one-step time delay is inserted into the loop. At step  $k = 30,000$ , an additional unmodeled two-step time delay is inserted, and, at step  $k = 60,000$ , an additional unmodeled six-step time delay is inserted. Table 1 shows the magnitude crossover frequency  $\omega_{mco}$ , the phase margin (PM), and the delay margin (DM) prior to each insertion of additional delays, where

$$DM = \frac{PM}{\omega_{mco}} \frac{\pi}{180}, \quad (106)$$

where the units of PM are degrees and the units of  $\omega_{mco}$  are rad/sample. Note that each time delay exceeds the delay margin at the time step of insertion. In each case, RCAC readapts and restabilizes the closed-loop system, as shown in Figure 32. After the third time delay is inserted into the loop at  $k = 60,000$ , RCAC restabilizes the closed-loop system at step  $k = 100,000$  (not shown). ■

### Example DM3: Limited Delay Margin for the Adaptive Standard Problem

Consider the unstable, minimum-phase, continuous-time plant given by [77]

$$A = \begin{bmatrix} -0.08 & -0.03 & 0.2 \\ 0.2 & -0.04 & -0.005 \\ -0.06 & 0.2 & -0.07 \end{bmatrix}, B = D_1 = \begin{bmatrix} -0.1 \\ -0.2 \\ 0.1 \end{bmatrix}, \quad (107)$$

$$C = E_1 = [0 \ -1 \ 0], \quad D_2 = 0. \quad (108)$$

This plant has an unstable pole at 0.1081. It is shown in [77] that the maximum achievable delay margin for this plant is 18.51 s. For the standard problem, (107) and (108) are discretized with the sampling period  $h = 0.1$  s. Using the controller given by (23) in [77] and discretizing the continuous-time plant with the sampling period  $h = 0.1$  s, the delay margin of the discrete-time closed-loop system is 6.07 steps.

Next, RCAC is used with the adaptive standard problem to stabilize (107) and (108). RCAC is applied with

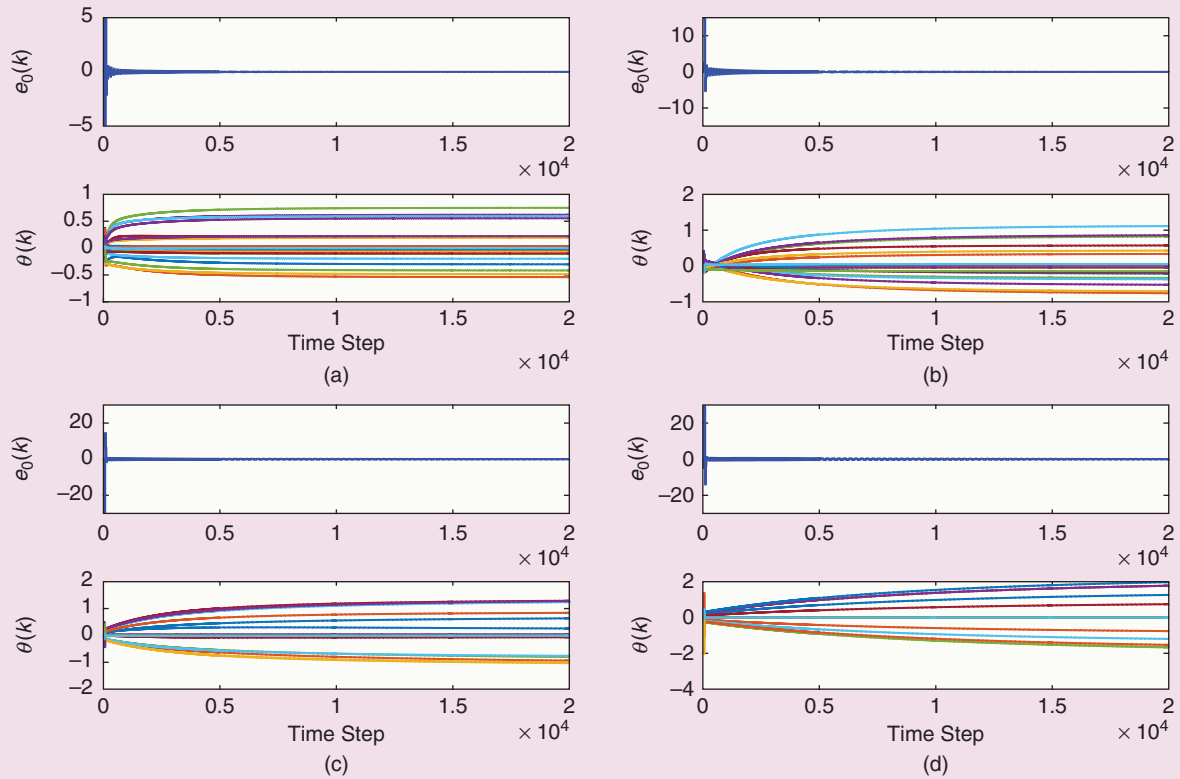


**FIGURE 31** Example DM2: Unmodeled time delay for the adaptive servo problem. For (a)  $k_d = 1$ , (b)  $k_d = 2$ , (c)  $k_d = 3$ , and (d)  $k_d = 4$ , retrospective cost adaptive control asymptotically follows the harmonic command.

$R_\theta = 100I_{10}$ ,  $R_u = 0.1z^2$ ,  $n_c = 3$ , and the FIR target model (71). The delay margin of the closed-loop system at step  $k = 3000$  using RCAC is 0.31 steps, as shown by Table 2. Figure 33 shows the closed-loop responses for the initial condition  $x(0) = [0.1 \ 0.1 \ 0.1]^T$  for both RCAC and the controller given by [77] discretized with the sampling period  $h = 0.1$  s. At step  $k = 3000$ , an unmodeled seven-step time delay is inserted into the loop, which destabilizes both closed-loop systems. Under continued adaptation, RCAC restabilizes the closed-loop system at time step  $k = 11,800$ . ■

### ROBUSTNESS TO ERRONEOUS PLANT GAIN

This section investigates the effect of the estimate of the plant gain as determined by the leading numerator coefficient by considering three examples that involve either erroneous estimates of the plant gain or unmodeled changes in the plant gain. The first example considers erroneous estimates of  $H_{dzu}$  for the adaptive servo problem. The gain margin of RCAC is compared to high-authority LQG, and an unmodeled change in the plant gain is considered. Finally, a plant with limited achievable gain margin is considered for both high-authority LQG and RCAC, and the effect of unmodeled changes in the plant gain for this system is investigated.

**TABLE 1** Example DM2: Unmodeled time-varying time delay for the adaptive servo problem. The values of magnitude crossover frequency ( $\omega_{mco}$ ), phase margin (PM), and delay margin (DM) are determined prior to the insertion of additional time delays into the loop. Each additional time delay inserted at time step  $k$  exceeds the DM at time step  $k$ .

$k$	$\omega_{mco}$ (rad/sample)	PM (°)	DM (steps)	Additional Unmodeled Delay Inserted (steps)
15,000	1.8872	19.0799	0.1765	1
30,000	1.4003	86.1123	1.0733	2
60,000	0.5742	181.7065	5.5233	6

### Example GM1: Erroneous $H_{dzu}$ for the Adaptive Servo Problem

Consider the asymptotically stable, minimum-phase plant (104), let  $r$  be a unit step command, and let  $d = v = 0$ . RCAC is applied with  $R_\theta = 10I_{10}$ ,  $R_u = 0$ , and  $n_c = 5$ . The FIR target model (71) is used with  $H_{dzu}$  replaced by  $\hat{H}_{dzu}$ , where  $\hat{H}_{dzu}$  is an estimate of the true value  $H_{dzu} = 1$ . Figure 34 shows the command-following performance for  $\hat{H}_{dzu} = -1$ ,  $\hat{H}_{dzu} = 0.1$ , and  $\hat{H}_{dzu} = 10$ . RCAC asymptotically follows the command for  $\hat{H}_{dzu} = 0.1$  and  $\hat{H}_{dzu} = 10$ , but not for  $\hat{H}_{dzu} = -1$ . For this

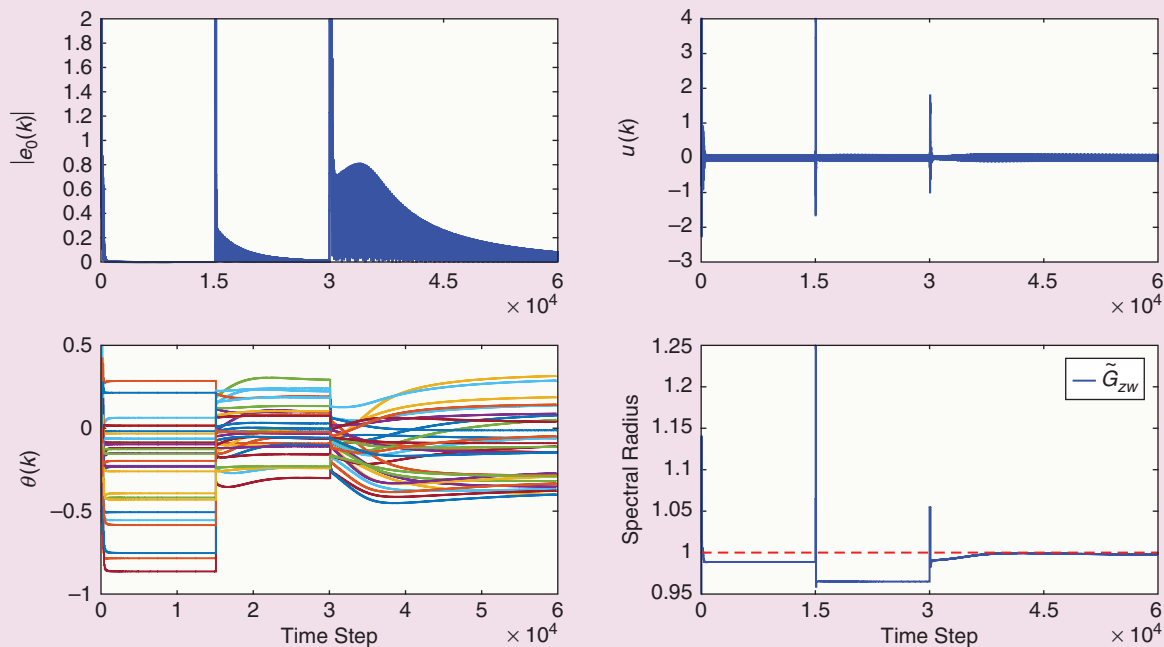


**FIGURE 32** Example DM2: Unmodeled time-varying time delay for the adaptive servo problem. At step  $k = 15,000$ , an unmodeled one-step time delay is inserted into the loop. At step  $k = 30,000$ , an additional unmodeled two-step time delay is inserted, and at step  $k = 60,000$ , an additional unmodeled six-step time delay is inserted. With  $G_{c,k}$  fixed, each inserted time delay is destabilizing. Under continued adaptation, however, retrospective cost adaptive control readapts and restabilizes the closed-loop system.

**TABLE 2** Margins for the controller from [77] and the retrospective cost adaptive control (RCAC) controller at step  $k = 3000$ . Note that the RCAC controller has significantly smaller phase margin (PM) and delay margin (DM) than the optimized controller given in [77].

Controller	$\omega_{mco}$ (rad/s)	PM ( $^\circ$ )	DM (steps)
[77]	0.3708	129.12	6.07
RCAC	2.1834	38.83	0.31

example, RCAC is robust to errors in the magnitude of the estimate of  $H_{dzw}$ , but is not robust to errors in the sign of  $H_{dzw}$ .

### Example GM2: Unmodeled Change in the Static Gain for the Adaptive Standard Problem

Consider the asymptotically stable, NMP plant

$$G(q) = \frac{(q^2 - 1.7q + 0.785)(q^2 - 1.4q + 0.85)}{(q - 0.5)(q^2 - 1.8q + 0.97)(q^2 - 1.4q + 0.98)}, \quad (109)$$

and let  $w$  be zero-mean Gaussian white noise with standard deviation 0.01. RCAC is applied with  $R_\theta = 10^{-5}I_{10}$ ,  $R_u = 0$ ,  $n_c = 10$ , and the FIR target model (72). Figure 35 shows that RCAC approximates the closed-loop frequency

response of high-authority LQG. At step  $k = 5000$ , the closed-loop system has a gain margin of 1.8105 at the phase crossover frequency  $\omega_{pco} = 0$  rad/sample. At step  $k = 5000$ ,  $G$  is replaced by  $2.9G$ , where the additional gain 2.9 is unmodeled. If  $G_{c,k}$  is fixed to be  $G_{c,5000}$ , then the closed-loop system becomes unstable. However, under continued adaptation, the plant is restabilized, and RCAC approximates the closed-loop frequency response of LQG for the modified plant, as shown in Figure 35. ■

### Example GM3: Severely Limited Gain Margin for the Adaptive Standard Problem

Consider the unstable, minimum-phase, continuous-time plant from [9] given by

$$A = \begin{bmatrix} 1 & 1 \\ 0 & 1 \end{bmatrix}, \quad B = \begin{bmatrix} 0 \\ 1 \end{bmatrix}, \quad D_1 = \begin{bmatrix} 1 \\ 1 \end{bmatrix}, \quad (110)$$

$$C = E_1 = [1 \quad 1], \quad D_2 = 1. \quad (111)$$

For the standard problem, (110) and (111) are discretized with the sampling period  $h = 0.1$  s. RCAC is applied with  $R_\theta = 10^{-10}I_{10}$ ,  $R_u = 0$ ,  $n_c = 6$ , and the FIR target model (72). Figure 36 shows that RCAC approximates the closed-loop frequency response of high-authority LQG. The LQG controller yields a gain margin of 0.04, and the RCAC controller yields a gain margin of 0.0012. Hence both controllers yield small gain margins. At step  $k = 10,000$ ,  $G$  is

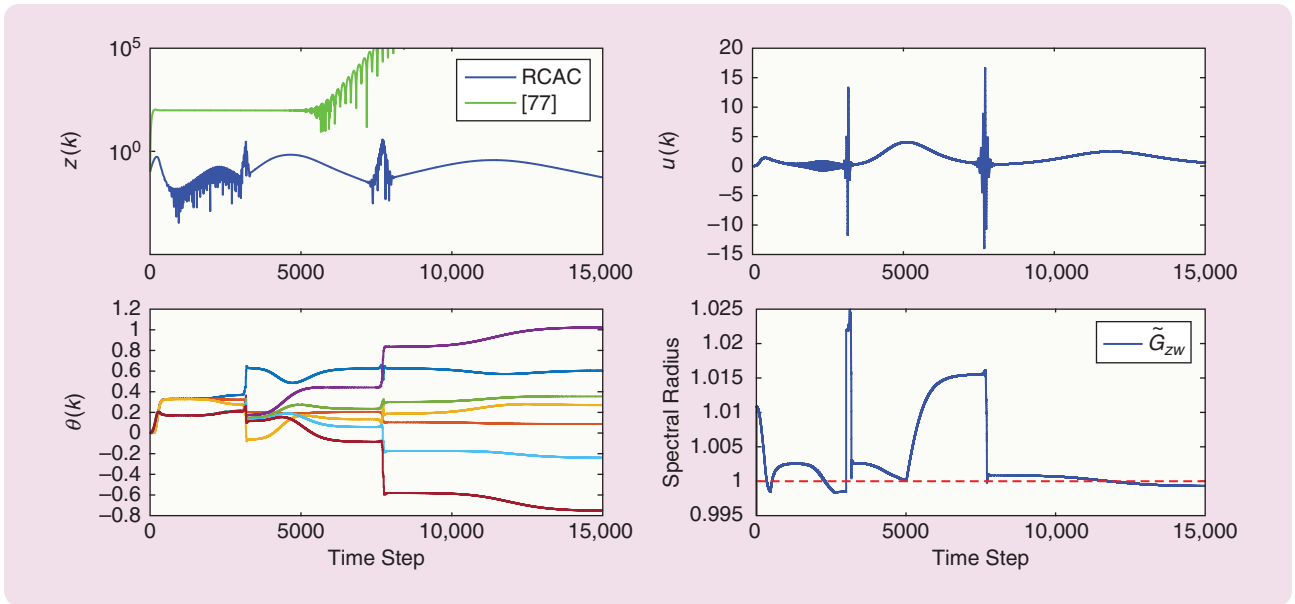


**FIGURE 33** Example DM3: Limited delay margin for the adaptive standard problem. These plots show the closed-loop responses with the initial condition  $x(0) = [0.1 \ 0.1 \ 0.1]^T$  for the controller given by [77] as well as for retrospective cost adaptive control (RCAC). At step  $k = 3000$ , an unmodeled seven-step time delay is inserted into the loop, which destabilizes both closed-loop systems. Under continued adaptation, RCAC restabilizes the closed-loop system.

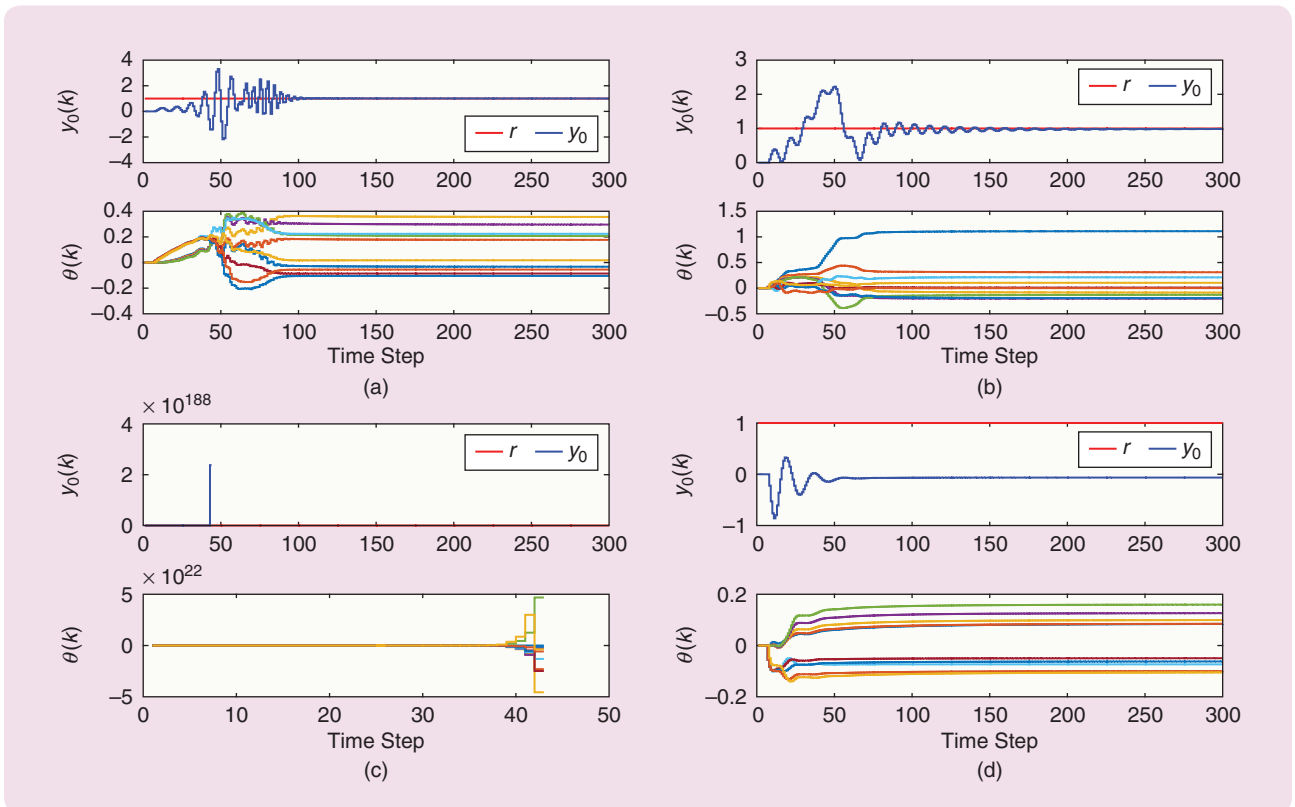


**FIGURE 34** Example GM1: Effect of erroneous  $H_d$  on command-following performance for the adaptive servo problem. Command-following performance for (a)  $\hat{H}_{dzw} = 0.1$ , (b)  $\hat{H}_{dzw} = 10$ , (c)  $\hat{H}_{dzw} = -1$ , and (d)  $\hat{H}_{dzw} = -1$  with performance-dependent control weighting  $R_u = z^2$ . Retrospective cost adaptive control (RCAC) asymptotically follows the command for  $\hat{H}_{dzw} = 0.1$  and  $\hat{H}_{dzw} = 10$ . For  $\hat{H}_{dzw} = -1$ , RCAC causes instability in the case where  $R_u = 0$ , but the closed-loop system remains asymptotically stable at step  $k = 5000$  by using  $R_u$  (not shown). For this example, RCAC is robust to errors in the magnitude of the estimate of  $H_{dzw}$  but is not robust to errors in the sign of the estimate of  $H_{dzw}$ .

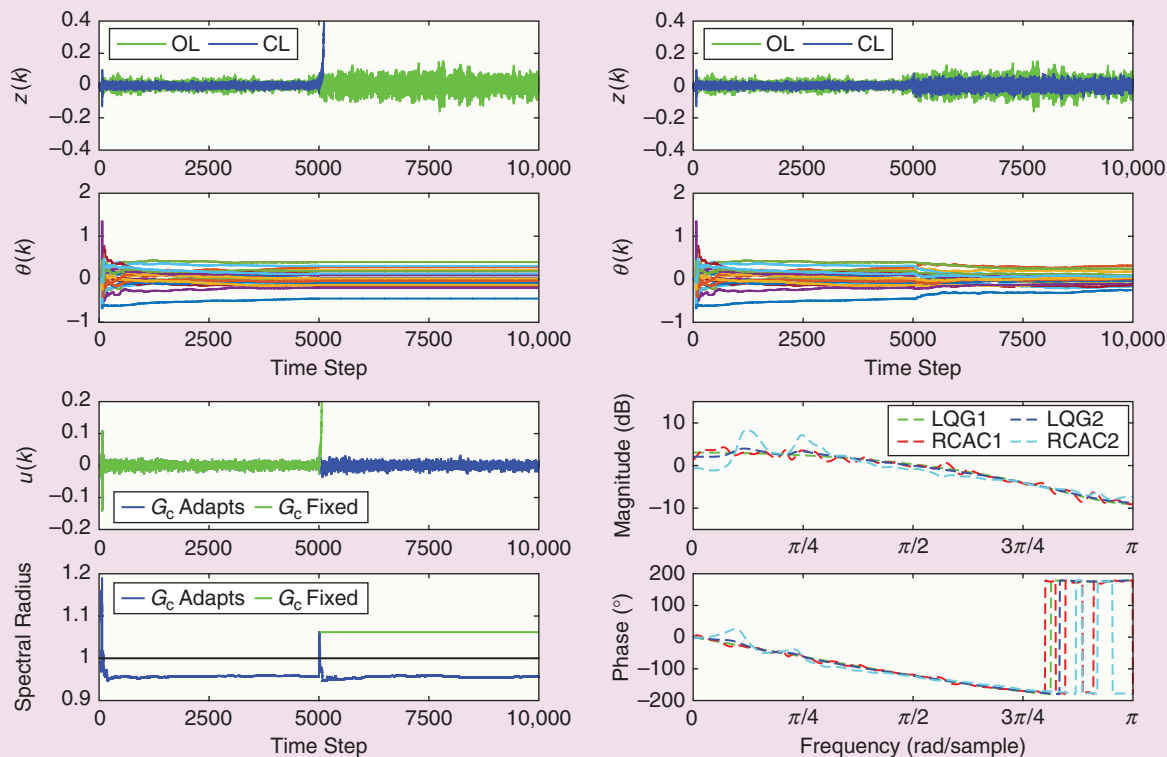


**FIGURE 35** Example GM2: Unmodeled change in the static gain for the adaptive standard problem. At step  $k = 5000$ , the gain margin is 1.8105, and  $G$  is replaced by  $2.9G$ , where the gain 2.9 is unmodeled. If  $G_{c,k}$  is fixed to be  $G_{c,5000}$ , then the closed-loop system becomes unstable. Under continued adaptation, however, retrospective cost adaptive control (RCAC) restabilizes the closed-loop system. LQG1 is the high-authority linear-quadratic-Gaussian (LQG) controller for  $G$ , and LQG2 is the high-authority LQG controller for  $2.9G$ . RCAC1 and RCAC2 are the corresponding RCAC controllers.

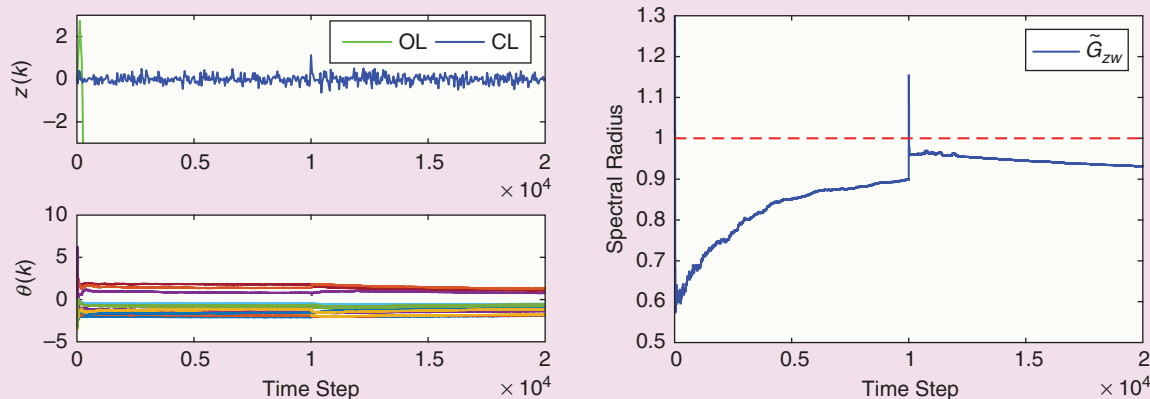


**FIGURE 36** Example GM3: Discretized plant from [9] with severely limited gain margin. At step  $k = 10,000$ , the gain margin is 1.0034, and  $G$  is replaced by  $1.1G$ , where the gain 1.1 is unmodeled. If  $G_{c,k}$  is fixed to be  $G_{c,10,000}$ , then the closed-loop system becomes unstable. Under continued adaptation, however, retrospective cost adaptive control restabilizes the closed-loop system.

replaced by  $1.1G$ , where the additional gain 1.1 is unmodeled. If  $G_{c,k}$  is fixed to be  $G_{c,10,000}$ , then the closed-loop system becomes unstable. However, under continued adaptation, the plant is restabilized, as shown in Figure 36. ■

In this section and the previous section, RCAC was applied to a collection of examples involving plants that are practically impossible to control using fixed-gain controllers due to extremely small gain and PMs. Plants of this type are

## Application to Control Saturation

The most common nonlinearity encountered in practice is control saturation, which can lead to integrator windup and possibly instability. Since control magnitude and rate saturation affect all real-world control systems, it is not surprising that an extensive literature is devoted to this problem [S9]–[S14].

The performance of RCAC is now investigated in the presence of control magnitude and rate saturation, as shown in Figure S8. The output of RCAC is the requested control  $u(k)$ , and the input to the plant is the actual control  $u_a(k)$ . In all examples, the regressor  $\Phi(k)$  contains  $u_a(k)$ . This means that either the nonlinearity is known or its output is measured. The case where the nonlinearity is unknown and its output is not measured is considered in [46].

### Example SAT1: Control Magnitude and Rate Saturation for the Adaptive Servo Problem

Consider the unstable, NMP triple integrator

$$G(\mathbf{q}) = \frac{(\mathbf{q} - 1.075)(\mathbf{q} - 0.95)}{(\mathbf{q} - 1)^3}. \quad (\text{S36})$$

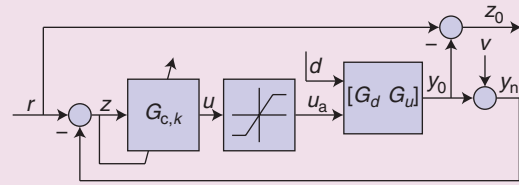


**FIGURE S8** Adaptive servo problem with control magnitude and rate saturation, where  $u$  is the requested control and  $u_a$  is the actual control.

Let  $r$  be the ramp command  $r(k) = k$ . RCAC is applied with and  $R_\theta = 10^3 I_\theta$ ,  $R_u = 0$ ,  $n_c = 10$ , and the FIR target model (72). The control  $u$  is magnitude-saturated at  $\pm 50$ , and rate-saturated (that is, control-change-saturated) at  $\pm 60$ . The rate-saturation limit of  $\pm 60$  prevents bang-bang behavior but allows the control  $u$  to change sign when it reaches the magnitude limit. Despite the magnitude and rate saturation, Figure S9 shows that RCAC asymptotically follows the command. Stabilization and tracking for a chain of integrators in the presence of control saturation is considered in [S15] and [S16] under full-state feedback. ■

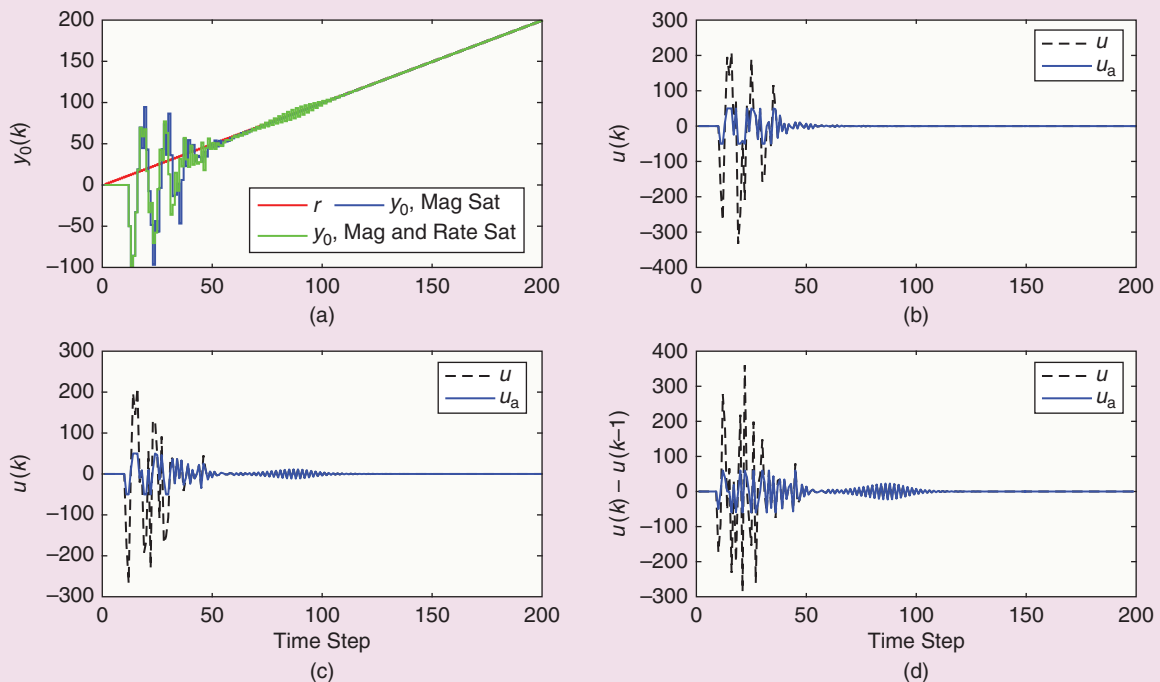


**FIGURE S9** Example SAT1: Control magnitude and rate saturation for the adaptive servo problem. (a) shows the closed-loop response, where the green line shows the response in the presence of magnitude saturation and the blue line shows the response in the presence of magnitude and rate saturation. (b) shows the requested and actual control signals in the presence of magnitude saturation. (c) shows the requested and actual control signals in the presence of magnitude and rate saturation. (d) shows the requested and actual control-change signals in the presence of magnitude and rate saturation. Despite the control magnitude and rate saturation, retrospective cost adaptive control asymptotically follows the command.

(continued)

## Application to Control Saturation (Continued)

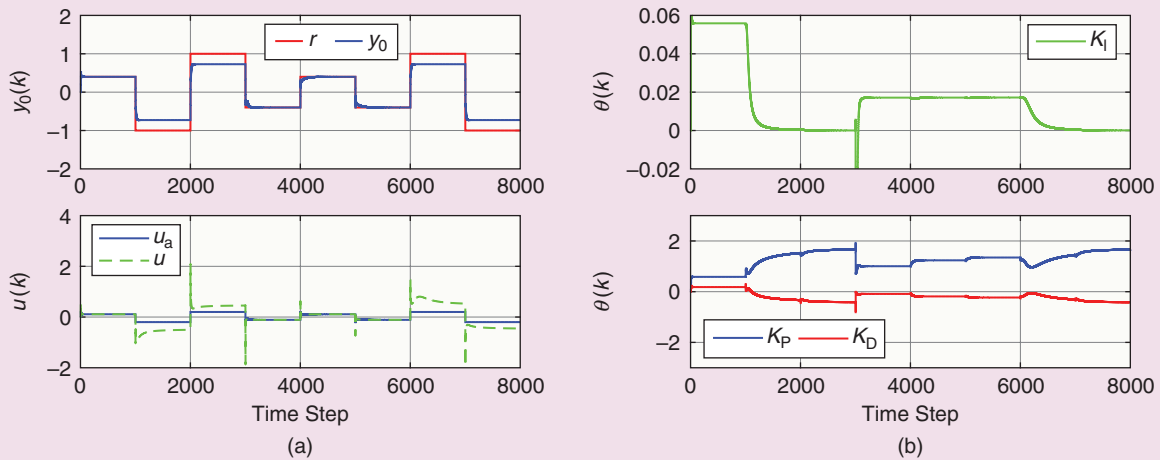


**FIGURE S10** Example SAT2: Control magnitude saturation for the adaptive servo problem with adaptive proportional-integral-derivative (PID) control. For step commands with height  $\pm 0.4$ , the adaptive PID controller uses integral action to follow the step command. However, for step commands with height  $\pm 1$ , which cannot be followed due to the magnitude saturation, the adaptive PID controller automatically reduces the integral gain  $K_I$  to zero, which avoids integrator windup.

### Example SAT2: Control Magnitude Saturation for the Adaptive Servo Problem with Adaptive PID Control

Consider the asymptotically stable, minimum-phase plant

$$G(\mathbf{q}) = \frac{(\mathbf{q} - 0.09)(\mathbf{q} - 0.8)}{(\mathbf{q}^2 - \mathbf{q} + 0.5)(\mathbf{q} - 0.9)}. \quad (\text{S37})$$

Let  $r$  be a sequence of step commands with heights  $\pm 0.4$  and  $\pm 1$ , and let  $d = v = 0$ . The PID controller structure (S1) is used with  $R_\theta = 0.1I_\theta$  and  $R_u = 0$ . The control  $u$  is saturated at  $\pm 0.2$ . This saturation level allows the controller to follow step commands with height  $\pm 0.4$  but not with height  $\pm 1$ . Figure S10 shows the response of the adaptive PID controller. For step commands with height  $\pm 0.4$ , the adaptive PID controller uses integral action to follow the step command. However, for step commands with height  $\pm 1$ , the adaptive PID controller drives the integral gain  $K_I$  to zero. The reduction in  $K_I$  allows RCAC to avoid integrator windup. ■

### REFERENCES

- [S9] D. S. Bernstein and A. N. Michel, "A chronological bibliography on saturating actuators," *Int. J. Robust Nonlinear Control*, vol. 5, pp. 375–580, 1995.
- [S10] N. Kapoor, A. R. Teel, and P. Daoutidis, "An anti-windup design for linear systems with input saturation," *Automatica*, vol. 34, pp. 559–574, 1998.
- [S11] A. H. Glattfelder and W. Schaufelberger, *Control Systems with Input and Output Constraints*. New York: Springer-Verlag, 2003.
- [S12] P. Hippe, *Windup in Control: Its Effects and Their Prevention*. New York: Springer-Verlag, 2006.
- [S13] L. Zaccarian and A. R. Teel, *Modern Anti-Windup Synthesis: Control Augmentation for Actuator Saturation*. Princeton, NJ: Princeton Univ. Press, 2011.
- [S14] S. Tarbouriech, G. Garcia, J. M. G. da Silva, and I. Queinnec, *Stability and Stabilization of Linear Systems with Saturating Actuators*. New York: Springer-Verlag, 2011.
- [S15] A. R. Teel, "Global stabilization and restricted tracking for multiple integrators with bounded controls," *Syst. Control Lett.*, vol. 18, pp. 165–171, 1992.
- [S16] T. Lauvdal, R. M. Murray, and T. I. Fossen, "Stabilization of integrator chains in the presence of magnitude and rate saturations: A gain scheduling approach," in *Proc. Conf. Dec. Control*, San Diego, CA, pp. 4004–4005, 1997.

viewed in [8] as potentially problematic for adaptive control as well. At convergence, the closed-loop systems possess small gain or PM, as expected, and thus the insertion of additional gain or time delay caused instability. For these examples, however, RCAC was able to restabilize the closed-loop system.

### DISCUSSION

This expository article presented a self-contained description of the RCAC algorithm for adaptive control. Control

objectives include stabilization, command following, and disturbance rejection. RCAC is based on a recursive least-squares procedure for updating the coefficients of a linear controller for feedback or feedforward control, where all signals are vectors.

A key contribution of this article is the demonstration that retrospective cost optimization updates the controller coefficients so as to match the intercalated closed-loop transfer function  $\tilde{G}_{z\tilde{u},k}$  to the target model  $G_f$ . It was shown

## Application to Nonlinear Oscillators

Aside from nonlinearity due to control saturation, it is interesting to apply RCAC to plants with nonlinear dynamics and observe the resulting response. For illustration, consider the Van der Pol and Duffing oscillators, which possess limit-cycle and bistable dynamics, respectively.

### Example NLO1: Harmonic Command Following for the Van der Pol Oscillator

Consider the discretized Van der Pol oscillator

$$x_1(k) = x_1(k-1) + hx_2(k-1), \quad (\text{S38})$$

$$x_2(k) = x_2(k-1) + h[(1 - x_1(k-1)^2)x_2(k-1) - x_1(k-1) + u(k-1)], \quad (\text{S39})$$

where  $h = 0.01$  s,  $y_0(k) = x_2(k)$ , and  $z(k) = r(k) - y_0(k)$ . Let  $r$  be the harmonic command  $r(k) = \cos \omega k$ , where  $\omega = 0.002$  rad/sample, and let  $d = v = 0$ . RCAC is applied with  $R_\theta = 1I_{l_\theta}$ ,  $R_u = 0$ ,  $n_c = 10$ , and the FIR target model (71). Figure S11 shows the command-following performance.

Next, consider the harmonic command  $r(k) = 10 \cos \omega k$ , where  $\omega = 0.0008$  rad/sample, and let  $d = v = 0$ . RCAC is applied with  $R_\theta = 100I_{l_\theta}$ ,  $R_u = 0$ ,  $n_c = 20$ , and the FIR target model (71). Figure S12 shows the command-following performance. Note that, in both cases, the resulting trajectory is harmonic in both states despite the nonlinearities. ■

### Example NLO2: Harmonic Command Following for the Duffing Oscillator

Consider the discretized Duffing oscillator with constant disturbance

$$x_1(k) = x_1(k-1) + hx_2(k-1), \quad (\text{S40})$$

$$x_2(k) = x_2(k-1) + h\left[-\frac{1}{4}x_2(k-1) + 4x_1(k-1) - x_1^3(k-1) + u(k-1) + 1\right], \quad (\text{S41})$$

where  $h = 0.01$  s. The open-loop plant has asymptotically stable equilibria  $(-1.86, 0)$  and  $(2.11, 0)$ . Let  $y_0(k) = x_2(k)$ ,  $z(k) = r(k) - y_0(k)$ , let  $r$  be a unit-amplitude harmonic command with frequency  $\omega = 0.0025$  rad/sample, and let  $v = 0$ . The plant is linearized about the equilibrium  $x_e = [0 \ 0]^T$ , and ten Markov parameters of the linearized model are used to construct the FIR target model. RCAC is applied with  $R_\theta = 10I_{l_\theta}$ ,  $R_u = 0$ , and  $n_c = 10$ . Figure S13 shows the harmonic command-following performance for the initial condition  $x(0) = [0.1 \ 0.1]^T$ . In the open-loop case with zero command, the open-loop plant approaches the equilibrium  $(2.11, 0)$ . The state  $x_2$  of the closed-loop system asymptotically follows the harmonic command. ■

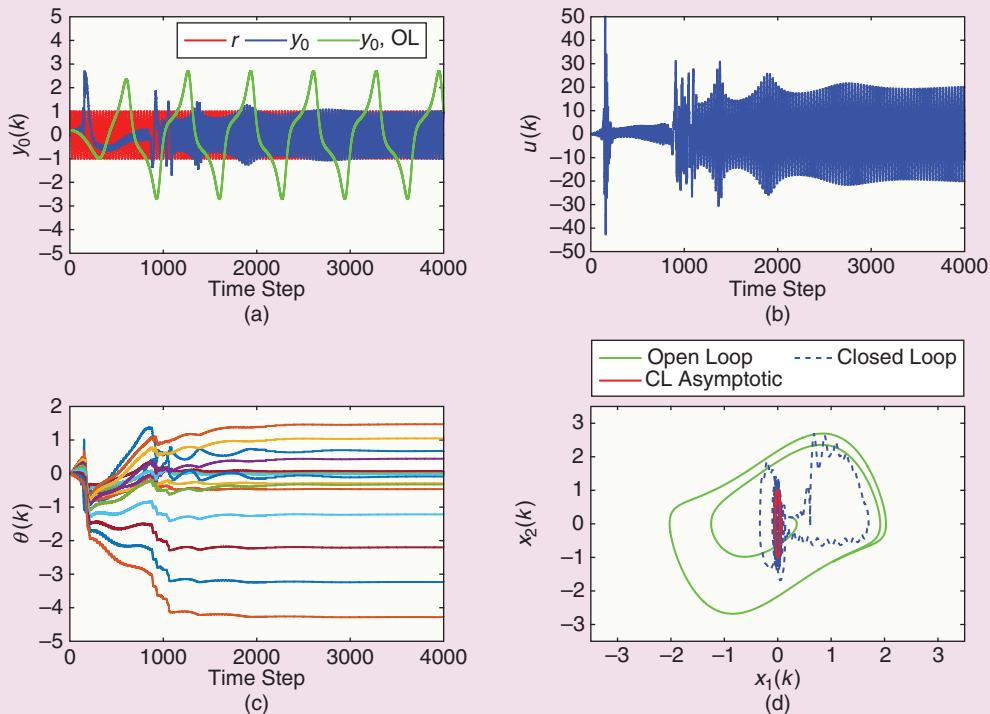


**FIGURE S11** Example NLO1: Harmonic command following for the Van der Pol oscillator (S38)–(S39) with a harmonic command whose phase portrait is inside the limit cycle. The open-loop plant approaches the limit cycle, and retrospective cost adaptive control asymptotically follows the harmonic command.

(continued)

## Application to Nonlinear Oscillators (*Continued*)

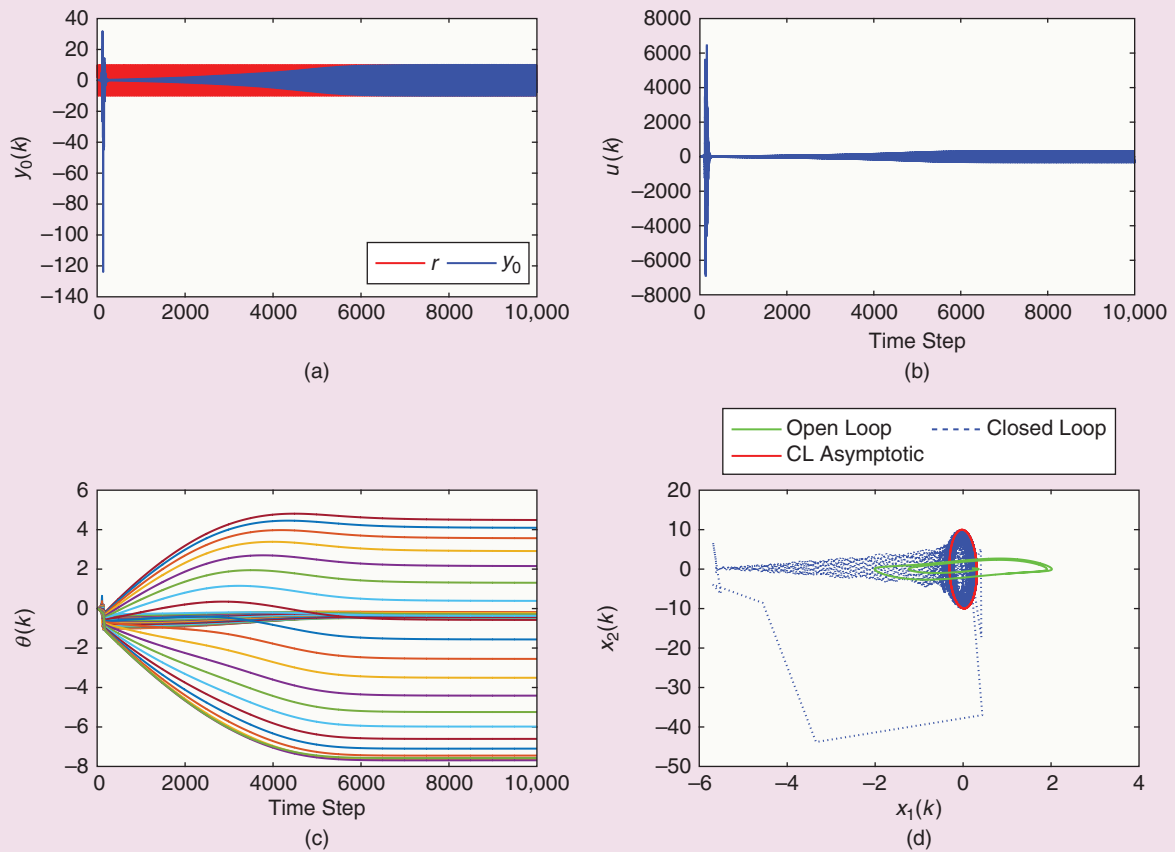


**FIGURE S12** Example NLO1: Harmonic command following for the Van der Pol oscillator (S38)–(S39) with a harmonic command whose phase portrait is outside the limit cycle. The open-loop plant approaches the limit cycle, and retrospective cost adaptive control asymptotically follows the harmonic command.

that  $\tilde{G}_{z\tilde{u},k}$  is the transfer function from the virtual external controller perturbation  $\tilde{u}$  to the performance variable  $z$ . The special nature of  $\tilde{G}_{z\tilde{u},k}$  is due to the fact that  $\tilde{u}$  enters the feedback loop through intercalated injection, which means that  $\tilde{u}$  is injected internally to the controller as opposed to being added to the control input.

The target model  $G_f$  is selected by the user, and the choice of  $G_f$  is guided by its role in the controller adaptation. In particular, since RCAC tends to match  $\tilde{G}_{z\tilde{u},k}$  to the target model and, since the target model possesses the NMP zeros of  $G_{zu}$ , the NMP zeros must be reproduced in the target model; otherwise, RCAC may cancel them, resulting in a hidden instability. This modeling information, along with the relative degree of  $G_{zu}$  and its leading numerator coefficient, constitutes the basic modeling information required by RCAC. These statements apply to the case where  $G_{zu}$  is SISO.

The role of the target model was examined from various angles. First, it was shown that, in the absence of sensor noise and control weighting  $R_u$ , RCAC tends to match the closed-loop frequency response of the high-authority LQG controller. This connection is surprising in view of the fact that RCAC uses extremely limited modeling information relative to LQG. In effect, RCAC uses data to compensate for missing or erroneous modeling information. In addition to matching closed-loop properties of the LQG controller, RCAC can be used for adaptive pole placement by choosing the poles of the target model as the desired closed-loop spectrum. For the adaptive servo problem, RCAC is used to follow step and harmonic commands as well as to reject step, harmonic, and broadband disturbances.

For some adaptive control algorithms, sensor noise may produce bursting and gain divergence [75]. To assess the performance of RCAC in the presence of sensor noise, it was

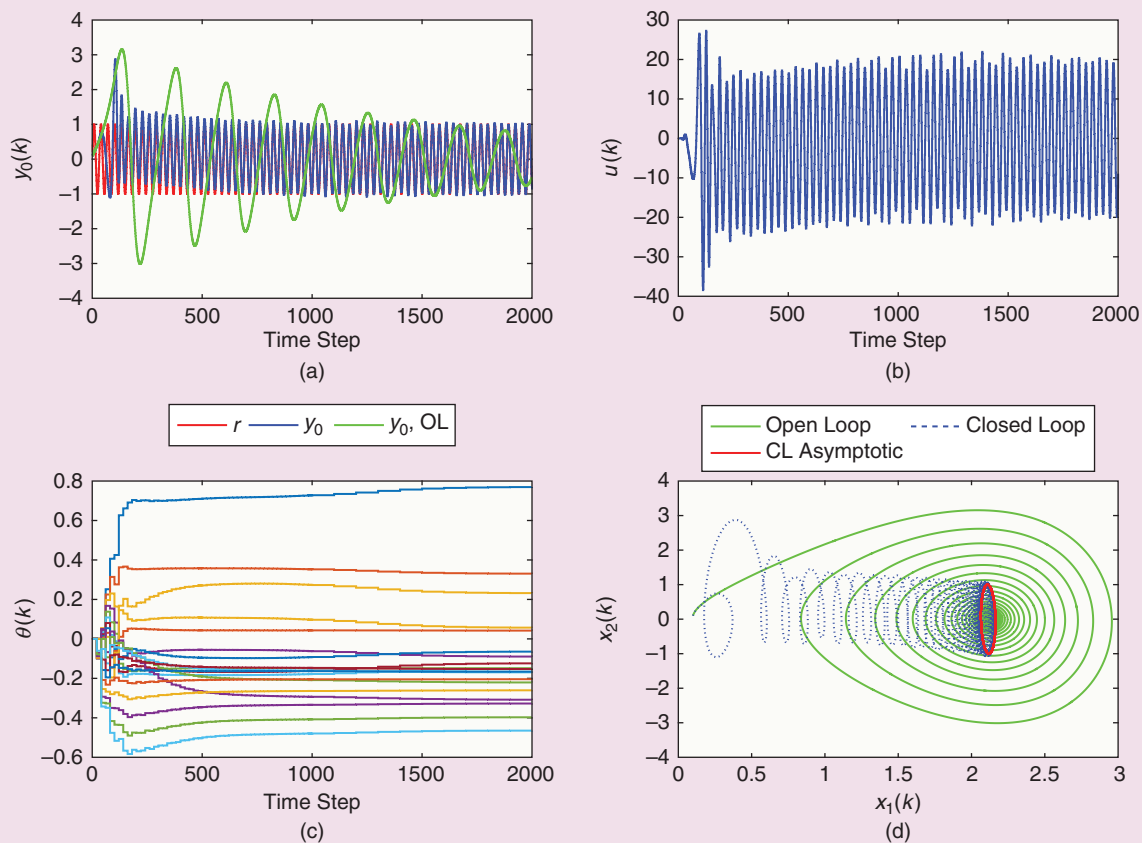


**FIGURE S13** Example NLO2: Harmonic command following for the Duffing oscillator (S40)–(S41). (d) shows the phase portraits of the open-loop limit cycle and the closed-loop response. The open-loop plant approaches the equilibrium (2.11, 0), and retrospective cost adaptive control asymptotically follows the harmonic command.

shown that RCAC matches the closed-loop frequency response of the LQG controller synthesized for the actual sensor-noise variance. Stabilization, command-following, and disturbance-rejection problems were also considered with broadband sensor noise with and without bias. For several examples, especially involving plants that are not asymptotically stable, the level of sensor noise was increased until RCAC failed to either follow the command or stabilize the plant. In all examples, no bursting was observed.

The performance of RCAC was then examined in the case where the NMP zeros, relative degree, or leading numerator coefficient are uncertain. In the case where the NMP zeros are uncertain, it was shown that performance-dependent cost regularization, that is, choosing  $R_u$  to be a function of  $z$ , improves the robustness of RCAC to uncertainty in the location of the NMP zero. Likewise, in the case where the relative degree is uncertain, it was

shown that performance-dependent cost regularization improves the robustness of RCAC. This uncertainty was related to uncertain time delay, that is, unknown latency in the feedback loop. Additional numerical examples given in “Application to Control Saturation” investigate the performance of RCAC under saturation, while examples given in “Application to Nonlinear Oscillators” investigate the performance of RCAC for classical nonlinear plants.

The examples in this article provide insight and guidelines for the application of RCAC. In particular, Example PP1 shows that RCAC can be used to assign a subset of the closed-loop poles and that the remaining closed-loop poles may cancel unmodeled minimum-phase zeros. This example also shows that the accuracy of pole placement depends on the choice of  $R_\theta$ , which initializes the RLS covariance. Example H2 shows that, for harmonic command following and harmonic disturbance rejection, RCAC can develop an

internal model of the command and disturbance without knowledge of the spectrum of the exogenous dynamics. Under stochastic disturbances, Example SD1 shows that, by choosing  $n_c \gg n$ , RCAC tends to match the closed-loop frequency response of high-authority LQG. For Example NMP1, RCAC is less robust to erroneous NMP-zero estimates in the case of stochastic disturbance rejection than in the case of harmonic command following. For Example NMP3, which is a counterexample involving unmodeled dynamics [40], RCAC with performance-dependent cost regularization stabilizes the closed-loop system. Example NMP4 shows that unstable plants with uncertain NMP zeros are especially difficult for RCAC to control. For a plant with severely limited delay margin, Example DM3 illustrates the ability of RCAC to readapt in the case where the margin is exceeded due to the introduction of an unmodeled time delay. Example GM3 illustrates the corresponding property in the case of limited gain margin. The ability of RCAC to restabilize the plant after unmodeled destabilizing time delays and gains are inserted into the loop suggests that the views expressed in [8] quoted in the opening section of this article may be unduly pessimistic.

## AUTHOR INFORMATION

**Yousaf Rahman** received the B.E. degree in aerospace engineering from the National University of Sciences and Technology in Pakistan and the Ph.D. degree in aerospace engineering from the University of Michigan, Ann Arbor. He is currently at the Ford Motor Company. His research interests include adaptive control and model refinement for aerospace and automotive applications.

**Antai Xie** received the Sc.B. degree in aerospace engineering from the University of Michigan, Ann Arbor, in 2008 and is currently in the aerospace engineering Ph.D. program at the University of Michigan. The focus of his studies is in adaptive control for spacecraft and acoustic control applications.

**Dennis S. Bernstein** (dsbaero@umich.edu) received the Sc.B. degree in applied mathematics from Brown University in 1977 and the Ph.D. degree in control engineering from the University of Michigan in Ann Arbor, Michigan, in 1982, where he is currently professor in the Aerospace Engineering Department. His interests are in estimation and control for aerospace applications. He is the author of *Matrix Mathematics* (Princeton University Press).

## REFERENCES

- [1] K. J. Astrom and P. R. Kumar, "Control: A perspective," *Automatica*, vol. 50, no. 1, pp. 3–43, 2014.
- [2] J. Hathout, M. Fleifel, A. Annaswamy, and A. Ghoniem, "Role of actuation in combustion control," *Comb. Sci. Tech.*, vol. 167, no. 1, pp. 57–82, 2001.
- [3] M. Pastoor, L. Henning, B. R. Noack, R. King, and G. Tadmor, "Feedback shear layer control for bluff body drag reduction," *J. Fluid Mech.*, vol. 608, pp. 161–196, 2008.
- [4] N. Gautier, J.-L. Aider, T. Duriez, B. R. Noack, M. Segond, and M. Abel, "Closed-loop separation control using machine learning," *J. Fluid Mech.*, vol. 770, pp. 442–457, 2015.
- [5] S. L. Brunton and B. R. Noack, "Closed-loop turbulence control: Progress and challenges," *Appl. Mech. Rev.*, vol. 67, pp. 050 801–1–050 801–48, 2015.

- [6] G. Ambrosino, M. Ariola, G. De Tommasi, and A. Pironti, "Plasma vertical stabilization in the ITER Tokamak via constrained static output feedback," *IEEE Trans. Control Syst. Tech.*, vol. 19, pp. 376–381, 2011.
- [7] M. M. Seron, J. H. Braslavsky, and G. C. Goodwin, *Fundamental Limitations in Filtering and Control*. New York: Springer-Verlag, 1997.
- [8] B. D. O. Anderson and A. Dehghani, "Challenges of adaptive control—past, permanent and future," *Ann. Rev. Control*, vol. 32, pp. 123–135, 2008.
- [9] J. C. Doyle, "Guaranteed margins for LQG regulators," *IEEE Trans. Automat. Control*, vol. 23, pp. 756–757, 1978.
- [10] K. Narendra and A. Annaswamy, "A new adaptive law for robust adaptive control without persistent excitation," *IEEE Trans. Automat. Control*, vol. AC-32, pp. 134–145, 1987.
- [11] P. A. Ioannou and J. Sun, *Robust Adaptive Control*. Englewood Cliffs, NJ: Prentice Hall, 1996.
- [12] A. M. Annaswamy and J. Wong, "Adaptive control in the presence of saturation non-linearity," *Int. J. Adapt. Control Signal Proc.*, vol. 11, no. 1, pp. 3–19, 1997.
- [13] K. S. Narendra and J. Balakrishnan, "Adaptive control using multiple models," *IEEE Trans. Automat. Control*, vol. 42, no. 2, pp. 171–187, 1997.
- [14] G. Tao, *Adaptive Control Design and Analysis*. New York: Wiley, 2003.
- [15] N. T. Nguyen, K. S. Krishnakumar, and J. D. Boskovic, "An optimal control modification to model-reference adaptive control for fast adaptation," in *Proc. AIAA Guidance Navigation Control Conf.*, Honolulu, HI, Aug. 2008, AIAA-2008-7283.
- [16] E. Lavretsky, "Combined/composite model reference adaptive control," in *Proc. AIAA Guidance Navigation Control Conf.*, Chicago, IL, Aug. 2009, AIAA-2009-6065.
- [17] N. Hovakimyan and C. Cao, *L1 Adaptive Control Theory: Guaranteed Robustness with Fast Adaptation*. Philadelphia, PA: SIAM, 2010.
- [18] G. Chowdhary, T. Yucelen, M. Mühlegg, and E. N. Johnson, "Concurrent learning adaptive control of linear systems with exponentially convergent bounds," *Int. J. Adapt. Control Signal Proc.*, vol. 27, no. 4, pp. 280–301, 2013.
- [19] G. C. Goodwin, P. J. Ramadge, and P. E. Caines, "Discrete-time multi-variable adaptive control," *IEEE Trans. Automat. Control*, vol. 25, pp. 449–456, 1980.
- [20] K. J. Åström, "Direct methods for nonminimum phase systems," in *Proc. Conf. Decision Control*, Albuquerque, NM, Dec. 1980, pp. 611–615.
- [21] G. C. Goodwin and K. S. Sin, "Adaptive control of nonminimum phase systems," *IEEE Trans. Automat. Control*, vol. 26, pp. 478–483, 1981.
- [22] R. Johansson, "Parametric models of linear multivariable systems for adaptive control," *IEEE Trans. Automat. Control*, vol. 32, pp. 303–313, 1987.
- [23] L. Praly, S. T. Hung, and D. S. Rhode, "Towards a direct adaptive scheme for a discrete-time control of a minimum phase continuous-time system," in *Proc. Conf. Decision Control*, Fort Lauderdale, FL, Dec. 1989, pp. 1188–1191.
- [24] R. Venugopal, V. G. Rao, and D. S. Bernstein, "Lyapunov-based backward-horizon discrete-time adaptive control," *Adapt. Control Signal Proc.*, vol. 17, pp. 67–84, 2003.
- [25] T. Hayakawa, W. M. Haddad, and A. Leonessa, "A Lyapunov-based adaptive control framework for discrete-time non-linear systems with exogenous disturbances," *Int. J. Control*, vol. 77, pp. 250–263, 2004.
- [26] S. Akhtar, R. Venugopal, and D. S. Bernstein, "Logarithmic Lyapunov functions for direct adaptive stabilization with normalized adaptive laws," *Int. J. Control*, vol. 77, pp. 630–638, 2004.
- [27] J. B. Hoagg, M. A. Santillo, and D. S. Bernstein, "Discrete-time adaptive command following and disturbance rejection with unknown exogenous dynamics," *IEEE Trans. Automat. Control*, vol. 53, pp. 912–928, 2008.
- [28] C.-C. Cheng and S. H.-S. Fu, "On trajectory-dependent direct adaptive control for a class of uncertain linear discrete-time systems," *Int. J. Adapt. Control Signal Proc.*, vol. 23, pp. 1014–1030, 2009.
- [29] C. Li and J. Lam, "Stabilization of discrete-time nonlinear uncertain systems by feedback based on LS algorithm," *SIAM J. Control Optim.*, vol. 51, pp. 1128–1151, 2013.
- [30] M. Yu, J.-X. Xu, and D. Huang, "Discrete-time periodic adaptive control for parametric systems with non-sector nonlinearities," *Int. J. Adapt. Control Signal Proc.*, vol. 28, pp. 987–1001, 2014.
- [31] M. C. Campi, A. Lecchini, and S. M. Savaresi, "Virtual reference feedback tuning (VRFT): A new direct approach to the design of feedback controllers," in *Proc. Conf. Decision Control*, Sydney, Australia, 2000, pp. 623–629.
- [32] M. C. Campi and S. M. Savaresi, "Direct nonlinear control design: The virtual reference feedback tuning (VRFT) approach," *IEEE Trans. Automat. Control*, vol. 51, no. 1, pp. 14–27, 2006.

- [33] Z. Hou and S. Jin, "A novel data-driven control approach for a class of discrete-time nonlinear systems," *IEEE Trans. Control Syst. Tech.*, vol. 19, no. 6, pp. 1549–1558, 2011.
- [34] A. S. Bazanella, L. Campestrini, and D. Eckhard, *Data-Driven Controller Design: The H2 Approach*. New York: Springer-Verlag, 2011.
- [35] S. S. Ge, Z. Li, and H. Yang, "Data driven adaptive predictive control for holonomic constrained under-actuated biped robots," *IEEE Trans. Control Syst. Tech.*, vol. 20, no. 3, pp. 787–795, 2012.
- [36] Z. S. Hou and Z. Wang, "From model-based control to data-driven control: survey, classification and perspective," *Inform. Sci.*, vol. 235, pp. 3–35, 2013.
- [37] R. Venugopal and D. S. Bernstein, "Adaptive disturbance rejection using ARMARKOV system representations," *IEEE Trans. Contr. Syst. Tech.*, vol. 8, pp. 257–269, 2000.
- [38] M. A. Santillo and D. S. Bernstein, "Adaptive control based on retrospective cost optimization," *J. Guid. Control Dyn.*, vol. 33, pp. 289–304, 2010.
- [39] J. B. Hoagg and D. S. Bernstein, "Retrospective cost model reference adaptive control for nonminimum-phase systems," *J. Guid. Control Dyn.*, vol. 35, pp. 1767–1786, 2012.
- [40] C. E. Rohrs, L. Velavani, M. Athans, and G. Stein, "Robustness of continuous-time adaptive control algorithms in the presence of unmodeled dynamics," *IEEE Trans. Autom. Control*, vol. AC-30, pp. 881–889, 1985.
- [41] E. D. Sumer and D. S. Bernstein, "Robust sampled-data adaptive control of the Rohrs counterexamples," in *Proc. Conf. Decision Control*, Maui, HI, Dec. 2012, pp. 7273–7278.
- [42] E. D. Sumer, J. B. Hoagg, and D. S. Bernstein, "Broadband disturbance rejection using retrospective cost adaptive control," in *Proc. Dynamic System Control Conf.*, Fort Lauderdale, FL, Oct. 2012, pp. 1–10.
- [43] E. D. Sumer and D. S. Bernstein, "Adaptive decentralized noise and vibration control with conflicting performance objectives," in *Proc. Dynamic System Control Conf.*, Fort Lauderdale, FL, Oct. 2012, pp. 1–10.
- [44] E. D. Sumer and D. S. Bernstein, "Aliasing effects in direct digital adaptive control of plants with high-frequency dynamics and disturbances," in *Proc. American Control Conf.*, Washington, D.C., June 2013, pp. 4934–4939.
- [45] E. D. Sumer and D. S. Bernstein, "On the role of subspace zeros in retrospective cost adaptive control of nonsquare plants," *Int. J. Control*, vol. 88, pp. 295–323, 2015.
- [46] J. Yan and D. S. Bernstein, "Minimal modeling retrospective cost adaptive control of uncertain Hammerstein systems using auxiliary nonlinearities," *Int. J. Control*, vol. 87, pp. 483–505, 2014.
- [47] B. C. Coffey, J. B. Hoagg, and D. S. Bernstein, "Cumulative retrospective cost adaptive control with amplitude and rate saturation," in *Proc. American Control Conf.*, San Francisco, CA, June 2011, pp. 2344–2349.
- [48] M. Al Janaideh and D. S. Bernstein, "Adaptive control of Hammerstein systems with unknown Prandtl-Ishlinskii hysteresis," *Proc. Inst. Mech. Eng., Part I: J. Syst. Contr. Eng.*, vol. 229, no. 2, pp. 149–157, 2015.
- [49] M. Rizzo, M. A. Santillo, A. Padthe, J. B. Hoagg, S. Akhtar, D. S. Bernstein, and K. G. Powell, "CFD-based identification for adaptive flow control using ARMARKOV disturbance rejection," in *Proc. American Control Conf.*, Minneapolis, MN, June 2006, pp. 3783–3788.
- [50] Y.-C. Cho, J. B. Hoagg, D. S. Bernstein, and W. Shyy, "Retrospective cost adaptive flow control of low-Reynolds number aerodynamics using a dielectric barrier discharge actuator," in *Proc. 5th AIAA Flow Control Conf.*, Chicago, IL, Aug. 2010, AIAA-2010-4841.
- [51] M. Isaacs, J. B. Hoagg, A. V. Morozov, and D. S. Bernstein, "A numerical study on controlling a nonlinear multilink arm using a retrospective cost model reference adaptive controller," in *Proc. Conf. Decision Control*, Orlando, FL, Dec. 2011, pp. 8008–8013.
- [52] E. D. Sumer and D. S. Bernstein, "Adaptive control of flexible structures with uncertain dynamics and uncertain disturbance spectra," in *Proc. AIAA Guidance Navigation Control Conf.*, Minneapolis, MN, Aug. 2012, AIAA-2012-4437-323.
- [53] A. K. Padthe, P. P. Friedmann, and D. S. Bernstein, "Retrospective cost adaptive control for helicopter vibration reduction," in *Proc. AHS 69th Annu. Forum*, Phoenix, AZ, May 2013, AHS2013-000179.
- [54] J. Yan, A. M. D'Amato, K. Butts, I. Kolmanovsky, and D. S. Bernstein, "Adaptive control of the air flow system in a diesel engine," in *Proc. Dynamic Systems Control Conf.*, Fort Lauderdale, FL, Oct. 2012, pp. 1–9.
- [55] M. J. Yu, Y. Rahman, E. M. Atkins, I. Kolmanovsky, and D. S. Bernstein, "Minimal modeling adaptive control of the NASA generic transport model with unknown control-surface faults," in *Proc. AIAA Guidance Navigation Control Conf.*, Boston, MA, Aug. 2013, AIAA-2013-4693.
- [56] F. Sobolic and D. S. Bernstein, "Aerodynamic-free adaptive control of the NASA generic transport model," in *Proc. AIAA Guidance Navigation Control Conf.*, Boston, MA, Aug. 2013, AIAA-2013-4999.
- [57] M. J. Yu, J. Zhong, E. M. Atkins, I. V. Kolmanovsky, and D. S. Bernstein, "Trim-commanded adaptive control for waypoint-defined trajectory following," in *Proc. AIAA Guidance Navigation Control Conf.*, Boston, MA, Aug. 2013, AIAA-2013-4999.
- [58] A. Ansari and D. S. Bernstein, "Adaptive control of an aircraft with uncertain nonminimum-phase dynamics," in *Proc. American Control Conf.*, Chicago, IL, July 2015, pp. 844–849.
- [59] A. Ansari and D. S. Bernstein, "Retrospective cost adaptive control of the generic transport model under uncertainty and failure," *AIAA J. Aerospace Inform. Syst.*, vol. 14, pp. 123–174, 2017.
- [60] M. Cambor, G. Cruz, S. Esteban, F. A. Leve, and D. S. Bernstein, "Retrospective cost adaptive spacecraft attitude control using control moment gyros," in *Proc. American Control Conf.*, Portland, OR, June 2014, pp. 2492–2497.
- [61] S. Dai, T. Lee, and D. S. Bernstein, "Adaptive control of a quadrotor UAV transporting a cable-suspended load with unknown mass," in *Proc. Conf. Decision Control*, Los Angeles, CA, Dec. 2014, pp. 6149–6154.
- [62] F. Sobolic and D. S. Bernstein, "An inner-loop/outer-loop architecture for an adaptive missile autopilot," in *Proc. American Control Conf.*, Chicago, IL, July 2015, pp. 850–855.
- [63] A. Goel, A. Xie, K. Duraisamy, and D. S. Bernstein, "Retrospective cost adaptive thrust control of a 1D scramjet with mach number disturbance," in *Proc. American Control Conf.*, Chicago, IL, July 2015, pp. 5551–5556.
- [64] M. Al Janaideh and D. S. Bernstein, "Adaptive control of Hammerstein systems with unknown Prandtl-Ishlinskii hysteresis," *Proc. I Mech E Part 1: J. Syst. Contr. Eng.*, pp. 1–9, 2014. doi: 10.1177/0959651814551660.
- [65] M. Al Janaideh and D. S. Bernstein, "Adaptive control of mass-spring systems with unknown hysteretic contact friction," in *Proc. American Control Conf.*, Boston, MA, July 2016, pp. 667–672.
- [66] H. Sane and D. S. Bernstein, "Active noise control using an acoustic Servovalve," in *Proc. American Control Conf.*, Philadelphia, PA, June 1998, pp. 2621–2625.
- [67] H. Sane, R. Venugopal, and D. S. Bernstein, "Disturbance rejection using self-tuning ARMARKOV adaptive control with simultaneous identification," *IEEE Trans. Control Syst. Tech.*, vol. 19, pp. 101–106, 2001.
- [68] S. L. Lacy, R. Venugopal, and D. S. Bernstein, "ARMARKOV adaptive control of self-excited oscillations of a ducted flame," in *Proc. Conf. Decision Control*, Tampa, FL, Dec. 1998, pp. 4527–4528.
- [69] B. L. Pence, M. A. Santillo, and D. S. Bernstein, "Markov-parameter-based adaptive control of 3-axis angular velocity in a 6DOF Stewart platform," in *Proc. American Control Conf.*, Seattle, WA, June 2008, pp. 4767–4772.
- [70] E. D. Sumer and D. S. Bernstein, "Retrospective cost adaptive control with error-dependent regularization for MIMO systems with uncertain nonminimum-phase transmission zeros," in *Proc. AIAA Guidance Navigation Control Conf.*, Minneapolis, MN, Aug. 2012, AIAA-2012-4670-123.
- [71] K. J. Astrom and B. Wittenmark, *Adaptive Control*, 2nd ed. Reading, MA: Addison-Wesley, 1995.
- [72] G. C. Goodwin and K. S. Sin, *Adaptive Filtering, Prediction, and Control*. Englewood Cliffs, NJ: Prentice Hall, 1984.
- [73] B. Teixeira, "Kalman filters," *IEEE Contr. Syst. Mag.*, vol. 28, no. 2, pp. 16–18, 2008.
- [74] M. Vidyasagar, *Control System Synthesis: A Factorization Approach*. Cambridge, MA: MIT Press, 1985.
- [75] B. D. Anderson, "Adaptive systems, lack of persistency of excitation and bursting phenomena," *Automatica*, vol. 21, no. 3, pp. 247–258, 1985.
- [76] K. J. Astrom, P. Hagander, and J. Sternby, "Zeros of sampled systems," *Automatica*, vol. 20, pp. 31–38, 1984.
- [77] R. H. Middleton and D. E. Miller, "On the achievable delay margin using LTI control for unstable plants," *IEEE Trans. Automat. Control*, vol. 52, no. 7, pp. 1194–1207, 2007.
- [78] E. Lavretsky and K. Wise, *Robust and Adaptive Control: With Aerospace Applications*. New York: Springer-Verlag, 2012.
- [79] D. S. Bernstein, *Matrix Mathematics*, 2nd ed. Princeton, NJ: Princeton Univ. Press, 2009.

